Investigation of the Thermal Parameters of Reclaimed Asphalt Materials with Applications to Asphalt Recycling

A THESIS

SUBMITTED TO THE FACULTY OF THE GRADUATE SCHOOL

OF THE UNIVERSITY OF MINNESOTA

BY

Christopher Daniel DeDene

IN PARTIAL FULFILLMENT OF THE REQUIREMENTS

FOR THE DEGREE OF

DOCTOR OF PHILOSOPHY

Faculty Advisors

Mihai O. Marasteanu

Eshan V. Dave

August

2014

To the love of my life, my soul mate, and team partner

ACKNOWLEDGEMENTS

First and foremost, I would like to thank my advisors, Mihai Marasteanu and Eshan Dave, for their guidance on how to pursue my research. I would also like to thank Adam Rothman, Eph Sparrow, and Vaughn Voller for serving on my committee and offering their input on my thesis. In addition to reviewing my thesis, countless thanks are due to Eph Sparrow for the use of his laboratory, and for the many good conversations over countless cups of coffee. For John Gorman, who went above and beyond in teaching and troubleshooting my ANSYS simulations, thank you. To Mugurel Turos, for thank you for your help, wisdom, expertise, and friendship. Last but not least, I would like to thank my wife for all of her love, support, and encouragement.

Much thanks to the NSF for their financial support and bestowing the title of NSF fellow on me. This material is based upon work supported by the National Science Foundation Graduate Research Fellowship under Grant No. DGE-105103. I would also like to acknowledge the Minnesota Department of Transportation for donating materials used in this research.

ABSTRACT

Asphalt concrete is the third most widely used resource in the world, next to Portland Cement Concrete and water. In the United States alone, over 550 million tons of hot mix asphalt (HMA) are produced at more than 4,000 asphalt plants across the country. With over 94% of the paved roads in the United States surfaces with asphalt concrete, it's safe to say asphalt pavement is what America drives on. However, a majority of today's pavement projects are geared towards rehabilitation and reconstruction of existing pavements, rather than construction of new roads. While it is true that asphalt pavement is 100% recyclable and it is the most recycled material in America, the reality is most roads contain no more than 20% recycled material. There are many factors that prohibit new road construction in excess of 20% recycled content, and this thesis aims to explore just one of those factors - the thermodynamics of hot mix asphalt pavement recycling.

Most research that is investigating the use of high amounts of Reclaimed Asphalt Pavement (RAP) have been based on empirical trials. This work has approached the issue of pavement recycling by measuring the thermal properties of recycled asphalt, examining the thermodynamic limits of asphalt drum mixing, and by modeling asphalt mixing drums using finite element techniques to determine the amount of time required to achieve full melting inside of asphalt drums. It was found that for many different drum configurations, there is insufficient retention time for RAP to reheat. This insufficient heating could cause premature failures in asphalt pavements using high percentages of RAP.

A secondary goal of this thesis is to explore the benefits of using the waste mining material, taconite tailings, in new asphalt pavements. This research shows there is thermodynamic benefit gained by using taconite tailings because they can be heated faster than traditional aggregates. This heating supplies more heat to RAP, which in turn, may allow for more of the recycled asphalt pavement to be incorporated into new asphalt pavements.

Contents

List of Tables

List of Figures

1.0 INTRODUCTION

Recycling asphalt pavement has become commonplace within the asphalt pavement industry. It is not uncommon for new asphalt mixtures to contain as much as 20% reclaimed asphalt pavement (RAP). However, there are some barriers that exist to increasing the percentage of RAP included in new pavements. One barrier is the need for the asphalt binder contained within the RAP to melt and incorporate inside of new Hot-Mix Asphalt (HMA) while inside of an asphalt mixing drum. The blending of the aged binder into the new mix is crucial if the full value of the RAP is going to be utilized, since the asphalt binder is the most expensive part of the asphalt pavement. This research was conducted to investigate the limit of asphalt recycling inside of a typical asphalt mixing drums to determine how much RAP can be successfully reheated.

With the goal of improving asphalt pavement recycling, this research sets out to model the recycling process of asphalt materials inside of a rotary asphalt mixing drum. In researching the thermal parameters of aged asphalt materials, it was discovered there was a literature gap on such properties. Therefore, investigation of the thermal conductivity of RAP and aged asphalt binder became necessary. Laboratory measurements of the thermal conductivity of RAP, aggregates, aged asphalt binder, and virgin asphalt binder were then taken using a parallel-plate heating apparatus. To process the results of the parallel-plate testing and obtain the thermal properties of the aged asphalt materials, it was necessary to perform a finite element simulation.

A simple model was then created to estimate the time needed for a spherical particle of RAP to become heated to the point where the asphalt binder contained within would reach a melting temperature. Building off of the simple model and incorporating the new thermal properties, an asphalt mixing drum was simulated using finite elements.

1.1 Thesis Objectives

There are three main objectives of this research on asphalt pavement recycling. The first objective is to investigate the thermal properties of reclaimed asphaltic materials. Current research on asphalt recycling assumes the properties of virgin asphalt and aged asphalt are the same. The implementation of the objective will check that assumption by comparing the thermal properties of aged asphalt to virgin binder.

The second objective is to develop a model to predict the time it would take a homogeneous sphere to reach a desired temperature at its center when exposed to constant heat. The application of this model is for drum recycling. It was developed as a quick method to check

to if reclaimed asphalt particles spend enough time inside of an asphalt mixing drum to become heated enough to where the reclaimed binder will reach the recommended mixing temperature.

The final objective is to simulate asphalt drum recycling using finite element techniques to create a virtual asphalt mixing drum. Those simulations were then used to explore the factors that most directly affect asphalt recycling. The drum simulations are then expanded to analyze alternative aggregates, and explore how alternative aggregates could be used to improve the recycling of asphalt materials.

1.2 Content

Chapter two presents a review of the existing literature pertaining to this thesis. One important contribution of this thesis is the presentation of measured thermal parameters of aged asphalt material. Based on a review of the existing literature, it was found that no thermal properties of aged asphalt have been reported to date; however, several authors have presented thermal properties for virgin materials. The literature review also introduces different types of asphalt mixing drums and presents research in which previous authors have attempted to model those drums.

Chapter three details the laboratory testing of asphalt pavement, asphalt binder, and aggregates. The first phase of this research is to investigate the thermal properties of RAP material. RAP is known to be a stiffer material than virgin asphalt materials. The reason for this increased stiffness is because RAP has undergone significant aging in service. The thermal parameters of RAP have gone untested, despite a well known change to mechanical properties. To investigate the thermal properties of RAP, a series of laboratory tests is proposed and implemented.

Chapter four presents the derivation of a simple algebraic equation that can be used to estimate the amount of heating time required at an asphalt recycling plant. Also contained in Chapter Four are simple applications for the derived equation. Lastly, Chapter Four presents two validations for the proposed algebraic equation.

In Chapter five, finite-difference modeling software was employed to process the laboratory work presented in Chapter Three. First, a packed bed of homogenous asphalt particles was modeled to simulate the parallel plate testing from Chapter Three. Then, the temperatures measured during the laboratory testing were applied to the model in order to gain insight into the thermal conductivity of the individual particles. Using those results, the thermal properties of the

individual particles could be better estimated, rather than measuring bulk properties. This back calculation was also done for the asphalt aggregates after the binder was removed. Lastly, a composite RAP particle consisting of a solid aggregate sphere surrounded by a thin layer of RAP was simulated so that the thermal properties of the RAP layer could be back calculated.

Chapter six is on modeling of the asphalt recycling process. Using thermal properties measured and derived from previous chapters, a virtual asphalt drum was constructed using finite element techniques. The simulated drum was used to predict the amount of time required to heat particles, and the degree as to which the particles are heated after their short journey inside the drum.

2.0 LITERATURE REVIEW

First, a summary of the basics of asphalt materials and asphalt testing are presented. Next, a review of existing literature on thermal properties of asphalt is performed to establish the existing knowledge base. A brief overview on the various methods used to determine the thermal properties of granular materials and asphalt concrete follows. A review of existing models for rotating drum heaters is included as a basis for developing a model in which reclaimed asphalt pavement (RAP) is heated inside of an asphalt drum.

2.1 Asphalt Pavement

Asphalt pavements represent 94% of the nearly 200 million miles of roads in the United States. Asphalt pavement is generally constructed in layers of thickness varying from 4-12 inches and is often optimized to be as thin as possible. Each layer of asphalt pavement is made of a different blend of asphalt mixture which serves a different purpose in the pavement system. Asphalt mixtures are created at asphalt plants and transported hot to the construction site, where it is spread and compacted. Upon cooling, the asphalt road is ready for traffic [1, 2]. Asphalt mixtures are comprised of three materials: aggregate, asphalt binder, and air. Although a majority of asphalt pavement is aggregate (about 90%), the two remaining components play a vital role in the stability of the pavement. The level of air voids in the pavement designed to be 4% by volume, and is intended to accommodate thermal expansion of the asphalt binder. The last component, asphalt binder, is the "glue" that holds the pavement together. The binder is by far the most complex component of the pavement system, in terms of both chemical structure and material response. Even though the binder accounts for only five percent of the total weight of an asphalt mixture, its contribution to the system is integral to the success of the pavement system.

2.2 Asphalt Binder

Asphalt binder is a coproduct of petroleum distillation. Asphalt binder is a black, sticky, odoriferous, viscoelastic substance which is semi-solid at ambient temperatures. Since asphalt binder has excellent waterproofing properties and chemical resistance to corrosion from acids and salts, it has been used as an industrial sealant; however, the main use of asphalt binder is in the construction of asphalt pavements. Upon heating, asphalt binder becomes less viscous and easily flows. At elevated temperatures (around 160°C, 320°F), the heated binder is mixed with aggregates to form asphalt concrete. Upon cooling, the binder will return to its semisolid state with the aggregates contained within the pavement matrix [1].

2.3 Superpave

In the United States, the most current materials characterization system is the Superior Performing Asphalt Pavements system, or Superpave system. The Superpave system classifies asphalt binder based on its rheological properties at different temperatures. The system specifies temperature ranges within the rheological properties must fall in order to achieve a particular performance grading. The performance grade (PG) of asphalt binder is based on two temperatures, a high temperature and a low temperature. The high temperature refers to the maximum seven-day average temperature that the pavement will experience during its design life. The low temperature is the lowest single-day temperature the pavement will experience during its design life. This range is denoted by a binder classification of PG XX-YY, where XX is the rated high temperature (°C), and YY is the low temperature rating of the binder (-°C).

Several tests have been developed to determine the performance grade (PG) temperature of asphalt binder. The dynamic shear rheometer (DSR) and bending beam rheometer (BBR) are the standard tests used in the Superpave system to classify binder. Two methods of simulating the aging of asphalt binder have also been adopted by Superpave. The rolling thin film oven is used to simulate short-term aging, and the pressure aging vessel simulates long term aging.

2.4 Dynamic Shear Rheometer

In this dissertation, the DSR was used to compare the different asphalt binders tested. The Dynamic Shear Rheometer (DSR) is used to measure asphalt binder's rheological properties when subjected to a sinusoidal load. The testing is best described by AASHTO T 315-10. The DSR test involves a sample of asphalt binder placed between horizontal circular parallel plates that have a sinusoidal load applied, and the response of the binder is then measured. For typical binders at moderate to high temperatures, plates measuring 25 mm in diameter and spaced a distance of 1000 microns apart are used for DSR testing. Depending on whether the binder is aged or unaged, variants of the test are performed. Since asphalt binder has a temperature-dependent response to loading at lower temperatures, a smaller plate is utilized in the DSR to account for this stiffness. The smaller sample size is used on aged binder because of a mechanical limitation of the DSR being unable to accurately shear the stiffened binder. For cold temperatures, the plates are 8 mm in diameter and set 2000 microns apart.

To conduct the test, the binder is tested at a fixed temperature equal to the proposed PG high temperature grade. After temperature acclimation, the binder is loaded, and the DSR applies

a sinusoidal load to the asphalt binder. The total resistance to shearing is recorded as the Complex Modulus (G*). The lag between the shearing from the DSR and the response in the asphalt binder is known as the phase angle (δ). The Superpave system uses the parameter G*/Sin (δ) as an indication of the rutting or permanent deformation standard performance criterion and G*·Sin(δ) as an indication of the resistance to cracking for the low temperatures.

When the G*/Sin (δ) parameter is greater than 1.00 kPa for unaged binder or greater than 2.2 kPa for RTFO-aged binder at a given PG temperature, the binder meets the rutting criterion for performance. Binder is tested at progressively higher temperatures until it exceeds the test parameter, or fails. For Pressure Aging Vessel (PAV) aged binder, G*·Sin(δ) has a ceiling of 5,000 kPa, and if the binder exceeds that limit, it fails specification.

A variation on the standard DSR test is often used for characterizing different asphalt binders. This variation involves changing the testing frequency at every temperature and measuring the response of the binder to the changes in both frequency and temperature. This practice of testing an asphalt binder at different temperatures and frequencies is often referred to as a "frequency sweep" of the asphalt binder. Using the results obtained at different temperatures, a curve unique to the asphalt binder can be generated. The curve uses the principles of time-temperature superposition to transform the frequencies tested at different temperatures into a unique reduced frequency. The reduced frequency permits the results from different testing temperatures to be plotted on a single curve. This curve, known as a master curve, contains information about the response of the asphalt binder at every testing temperature and every load rate. Since the master curve characterizes an asphalt binders' response across a wide range of temperatures, it can be used as a method for comparing two or more different specimens.

2.5 Laboratory Aging of Asphalt Binder

Laboratory aging of the binders are also specified under the Superpave system. The system uses two machines, the rolling thin film oven (RTFO) and pressure aging vessel (PAV) to simulate different periods of aging for asphalt binder. The RTFO testing procedure is described by AASHTO T 240. In this test, glass bottles are filled with 35 grams of asphalt binder and freely spun in a 163°C oven for 75 minutes. This process is often referred to as short-term aging, as it is meant to simulate the aging that binder undergoes during mixing and transporting to the construction site.

The pressure aging vessel (PAV) is used to simulate long-term aging. AASHTO R 28 outlines the procedures for obtaining PAV-aged asphalt binder [3]. To perform this test, RTFO-aged binder is poured into shallow steel pans at a weight of 50 grams of binder per pan. The PAV is then loaded with the pans and sealed. The sealed chamber is heated to 100°C and a pressure of 2.10 MPa (305 psi). The accelerated aging occurs in an oxygen-rich environment in which the high pressure forces oxygen into the asphalt binder to simulate field oxidation. Even though the sample is held under heat and pressure for only 20 hours, the end result is binder that has a simulated field age of 5 to 10 years.

2.6 Reclaimed Asphalt Pavement (RAP)

Reclaimed asphalt pavement (RAP) is the material produced from the removal of old asphalt pavement material from roads and highways. When a roadway is in need of maintenance, the old road can either be completely removed or have only the top few inches ground off, a procedure called milling. In either case, this waste material, called RAP, is typically ground into particles, which are inherently coated with aged asphalt binder. This ground material can be added into new roads at the asphalt plant, to reduce the amount of virgin aggregates and virgin binder needed. The primary benefit of using RAP is a direct cost savings due to the reduction in virgin materials. The aggregate in RAP replaces some of the aggregate in new asphalt pavement, and the aged binder coating the RAP aggregates is assumed to replace a portion of virgin binder required for new road construction [4]. The price of asphalt binder is significantly greater than the price of aggregates; therefore, when recycling asphalt pavement, it is most beneficial to try to maximize the reuse of the RAP binder.

Although many DOTs have adopted the practice of using RAP in their pavements, the quantity at which it is added is fairly low; 10-15% in the wearing course per Superpave specifications with only few state agencies allowing for high RAP contents [5, 6]. There are several issues with using RAP to replace some virgin materials. Most notably, there is an increased stiffness associated with using RAP, which may improve rutting resistance, but causes premature failure in low temperature cracking [5]. There is also debate about how much of the asphalt binder contained in the RAP contributes to the new asphalt mixture, since some of the aged binder may be trapped inside of the pores of the RAP aggregates [4]. It is this uncertainty in performance that contributes to the reluctance of using higher RAP pavements.

Another problem with using RAP as an engineering material is the variability between RAP sources and stockpiles. Depending on where the RAP originated, there could be different

source binder PGs, different degrees and types of aging, and different binder additives. This variability is the main reason that DOTs will only allow RAP to be added in small percentages, because small percentages of recycled binder have little effect on the overall pavement performance. Ultimately, to use high percentages of RAP as standard practice, one solution may be to thoroughly test and classify each stockpile before it can be incorporated into high-percentage recycled roads.

Within the asphalt industry, there are three primary ways RAP is introduced into the mixing process: center entry in a mixing drum (typically using RAP collar), adding a secondary mixer, or Drum Mix Coater (DMC), after the drum mixer to mix RAP with superheated aggregates, or adding the RAP into the outer shell of a double-barrel drum configuration. According to Federal Highway Administration (FHWA), the most efficient system, the double-barrel drum mixer, allows for 1 ½ minutes of mixing time in the external shell. Less efficient drum configurations using a RAP collar allow for significantly less mixing time, around 10-12 seconds [7]. Most of the existing hot-mix drum plants utilize the center entry with RAP collar method to manufacture mixes containing RAP. The most common asphalt drum configurations are depicted in Figure 2.1.

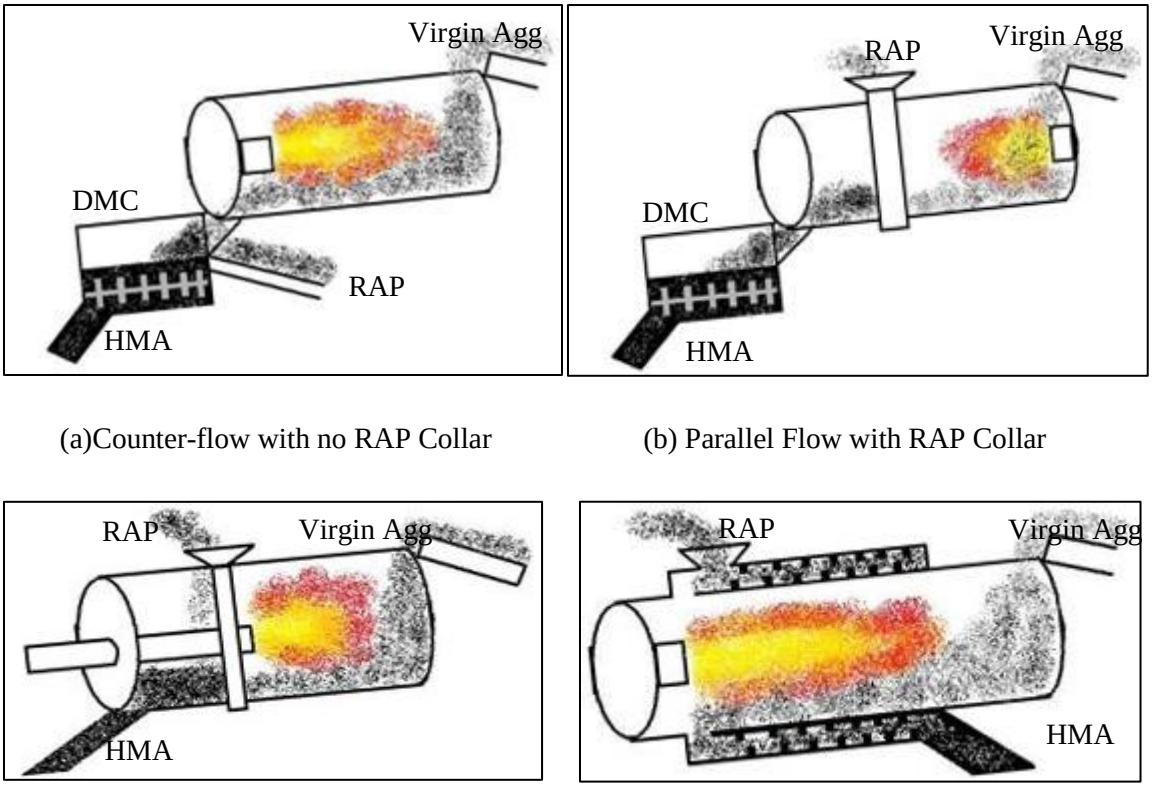

(a)Counter-flow with no RAP Collar (b) Parallel Flow with RAP Collar

(c) Counter-flow with RAP Collar (d) Double Barrel™ Drum Mixer

Figure 2.1 Various Mixing Drum Configurations for use with RAP

To reach the desired output temperatures of the HMA, the virgin aggregates are often superheated before being mixed with RAP and new asphalt binder. During superheating, the virgin aggregates can reach temperatures between 260°C (500°F) and 315°C (600°F) [7, 8]. Although the RAP is not directly exposed to these hot temperatures, it is estimated 90% of the RAP is heated by the virgin aggregates, while the remainder is heated from the hot gasses inside the drum [8]. This means the heat used to melt the RAP is coming from a source in the range of 260°C (500°F) to 315°C (600°F).

2.7 Thermal Properties of Asphalt Materials

Some of the earliest work looking at asphalt pavement thermal conductivity was conducted by O'Blenis in 1940 [9]. O'Blenis outfitted several different asphalt pavements with thermocouples at varying depths and looked at the diurnal fluctuations of pavement temperature. Using those diurnal changes, the conductivity between layers in the asphalt pavement could be calculated. He also reports calculated thermal diffusivities of 0.0278 ft^2/hr – 0.0466 ft^2/hr.

Since asphalt concrete is comprised of three different material phases, it is a heterogeneous composite. These three materials should be considered when investigating the thermal properties of the composite: asphalt binder, which is a viscous liquid, aggregates, a solid, and the air contained within the air voids that comprises 4% of the total volume. However, previous research by Highter and Wall concludes that using average thermal properties is suitable for asphalt concrete, even though it is a heterogeneous mixture [10]. Highter and Wall also conclude that specific heat and thermal diffusivity depend on gradation, while thermal conductivity is a function of gradation and asphalt content. In general, aggregates were reported to be more conductive than binder, which was more conductive than air voids.

Building on Highter and Wall's conclusions, there have been several studies that aim to define the thermal properties of hot mix asphalt concrete (HMA). Mamlouk et al. used a hollow HMA core with a probe thermometer inserted inside to measure the change in temperature of a core at thermal equilibrium after being placed inside an oven of known temperature. In their experiments, the temperature of the HMA core was recorded as a transient until reaching steady state. Then, the paper employed a curve-fitting algorithm to determine the values of heat capacity and thermal conductivity and suggested an empirical relationship that relates thermal conductivity to heat capacity [11].

The work by Mallick et al. examined the effects of moisture content on the thermal conductivity of asphalt samples. Their method involved imbedding thermocouples into compacted HMA cores, then using a heat lamp to introduce heat to one side of the well-insulated specimen. After the experimentation, back calculation of the thermal properties was achieved with FEM software to determine the thermal properties [12].

Solaimanian et al. evaluated the Integrated Climatic Model (ICM) as a part of the Strategic Highway Research Plan (SHRP). The ICM predicts pavement temperatures as a function of air temperature, sunshine, and wind velocity [13]. The report concludes that air temperature is the most influential factor in temperature prediction of in-place HMA. It was also found that the thermal properties of the aggregate, which is the predominant component of the mix, significantly influence thermal conductivity of the asphalt concrete.

Tan et al. describes the methods for calculating thermal conductivity, k, diffusivity, α, and heat transfer convection coefficient, h [14]. The method is for one-dimensional heat transfer using plate theory. The dimensions of the plate or the unbounded aggregate bed must satisfy a depth to length ratio of 0.2. The method involves two thermocouples placed under a well-

insulated section of pavement or granular media, shown in Figure 2.2. The results from the tests were then curve fit to determine the thermal properties of asphalt, and wet or dry unbounded aggregates.

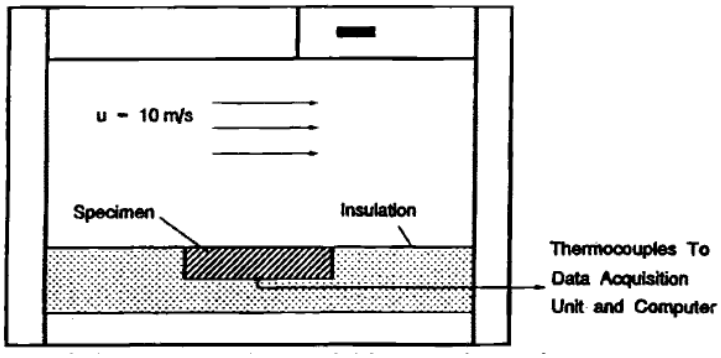

Figure 2.2 Experimental Set-up from Tan et al. (1997)

Luca and Mrawira proposed a new method for determining properties of Superpave asphalt concrete using a guarded thermocouple setup shown in Figure 2.3. The paper supplies a range of referenced thermal properties for various mixtures and concludes that mechanical properties, such as resilient modulus and density, were not correlated to thermal properties[15].

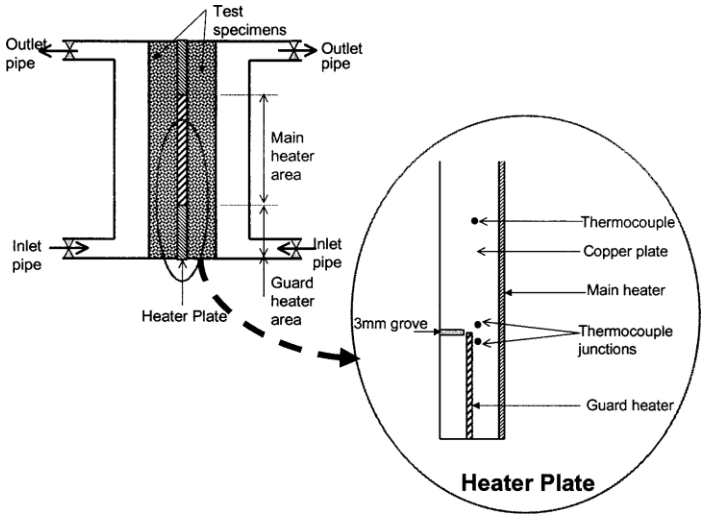

Figure 2.3 Guarded thermocouple set-up from Luca and Mrawira (2005)

The following tables contain a comprehensive list of published thermal conductivity and heat capacity values for asphalt pavement and asphalt binder. The published thermal conductivities range from 0.85 – 3.97 (W/m°C), depending on the mixture. A notable thermal conductivity comes from a textbook published in the 1920s, which was heavily referenced by the

other sources. The reference provides an empirical equation rather than a range for thermal conductivity, and is used only for asphalt binder.

Table 2.1 Published Thermal Conductivity Values of HMA

Thermal Conductivity, K	Notes	Source
2.28 (W/m°C)		[16]
3.97 (W/m°C)		[1]
2.4-2.5 (W/m°C)		[17]
1220-1280 (Cal/h.m.C)		[18]
1250(Cal/h.m.C)		[19]
0.6 – 1.2 BTU/ft hr F		[20]
1.45 – 1.81(W/m°C)		[15]
0.85-2.32 (W/m°C) 0.58 – 1.3 BTU/ft/hr/°F		[9]
1.05 – 1.52 (W/m°C)		[21]
1.33 – 1.49 (W/m°C)		[14]
=0.813/SG*[1-.0003(Temp-32)]	BTU/hr.ft^2.F/in	[22] *For bitumen only
1-1.3(W/m°C)		[12]

Table 2.2 features the ranges of heat capacities found in the literature. Again, the textbook from the 1920's provides an empirical equation, which can be used to calculate the heat capacity of asphalt binder.

Table 2.2 Published Heat Capacity Values of HMA

C, Heat Capacity	Notes	Source
464543-510997 (Cal/m^3)		[18]
336393 (Cal/m^3)		[19]
600702 (Cal/m^3)		[21]
1.12-1.368 (kJ/kg K)	Unguarded	[15]
1.475-1.835 (kJ/kg K)	Guarded	[15]
=1/SQRT(SG)*(0.388+0.00045*TEMP)	Cal/g.C	[22]
1.10-1.25 (kJ/kg K)		[12]

2.8 Existing Specifications Involving the Calculation of Thermal Properties

There are several ASTM specifications which cover methods for determining various thermal properties of materials. ASTM C 1045 contains general procedures for reporting thermal properties. ASTM C 1058 includes specifications for selecting temperatures and reporting values of thermal properties. Neither of the ASTM specifications listed above contain testing procedures

for determining thermal properties; however, they are referenced by all of the following specifications.

The ASTM C518 specification covers Steady-State Thermal Transmission Properties by Means of the Heat Flow Meter Apparatus. This method needs a sample of known thermal conductivity to calibrate the testing equipment. The heat flow meter apparatus establishes steady-state one-dimensional heat flux through a test specimen between two parallel plates at constant but different temperatures, shown in Figure 2.4. By appropriate calibration of the heat flux transducer(s) with calibration standards and by measurement of the plate temperatures and plate separation, Fourier's law of heat conduction is used to calculate thermal conductivity, thermal resistivity or thermal resistance, and thermal conductance. This specification is used in conjunction with ASTM C1045 for data processing of results. One drawback of this method is it will only yield thermal conductivity. Specific heat and density must then be calculated to get thermal diffusivity, α.

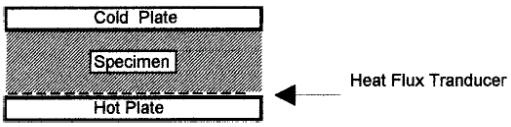

FIG. 1 Apparatus with One Heat Flux Transducer and One Specimen

Figure 2.4 ASTM C 518 Apparatus

The ASTM E 1530 specification pertains to Evaluating the Resistance to Thermal Transmission of Materials by the Guarded Heat Flow Meter Technique. This is a modified ASTM C 518 for smaller particles with higher thermal conductivities. This procedure uses a heat flux transducer (HFT) in combination with an insulated system. The HFT is sandwiched between a sample and that is between two plates. The plates are loaded to maintain a constant pressure in the system. Heat is passed between the top plate into the bottom plate through the specimen and HFT. A highly conductive heat transfer compound is also spread onto either side of the specimen to minimize thermal resistance at the interfaces. Since this method requires full contact with the HFT plates, it only suitable for measuring pavement sections, not unbound aggregates.

Another specification, ASTM C 177 - Steady-State Heat Flux Measurements and Thermal Transmission Properties by Means of the Guarded-Hot-Plate Apparatus, pertains to determining thermal conductivity. This specification uses a guarded hot plate, shown in Figure 2.5, and follows a similar theory as ASTM C 518, but with a different testing apparatus.

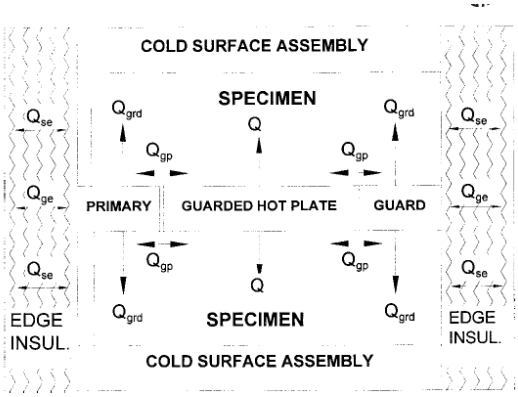

FIG. 2 Illustration of Idealized Heat Flow in a Guarded-Hot-Plate Apparatus

Figure 2.5 ASTM C 177 Set-up

ASTM E2584 describes a procedure for measuring thermal conductivity of materials using a thermal capacitance (Slug) calorimeter. This procedure measures the thermal conductivity of a specimen that has a metal slug calorimeter inserted into the sample. A schematic of the test apparatus can be seen in Figure 2.6. During testing, contact between the specimen and the slug must be maintained. This test may be difficult if not impossible to perform on granular media; however, it would work for a compacted HMA core with a hole drilled in the sample.

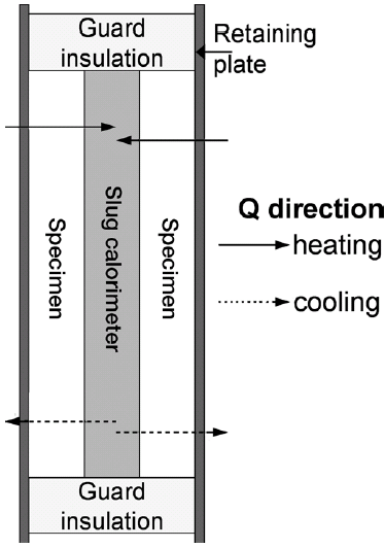

Figure 2.6: ASTM E 2584 Slug Diagram

Another relevant specification, ASTM C 1113 that specifies a method for determining thermal conductivity with a hot wire (Platinum Resistance Thermometer Technique), involves passing electric current though a pure platinum wire, which is in contact with the test specimen. The wire heats up as a function of the heat being transferred out of the wire from the specimen.

This test is intended for isotropic materials, and only yields thermal conductivity. Figure 2.7 and Figure 2.8 show diagrams of the experimental setup required for testing.

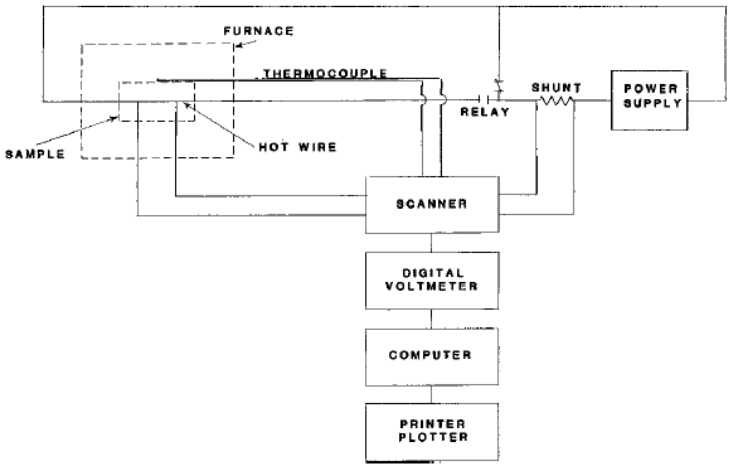

Figure 2.7 Diagram of ASTM C 1113 Apparatus

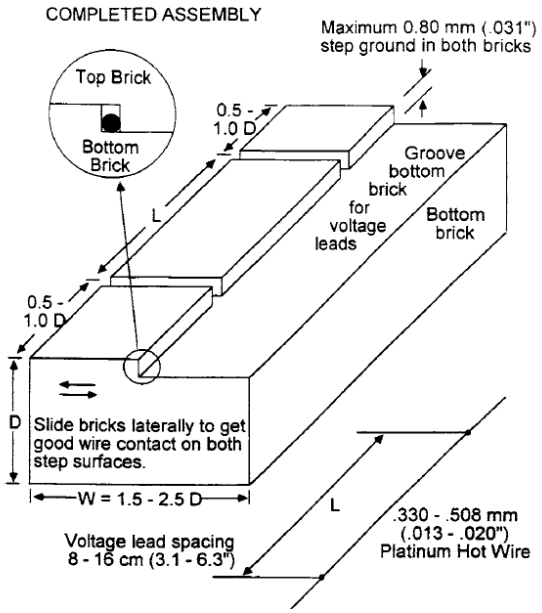

Figure 2.8 ASTM C 1113 Experimental Set-up

The last ASTM specification pertaining to thermal properties is ASTM E 1952, which employs Differential Scanning Calorimetry (DSC) to obtain thermal conductivity and thermal diffusivity by means of modulated temperature. This test is specified for a homogeneous solid and provides thermal conductivity and thermal diffusivity of the homogeneous solid. This test could be used for testing pure binder; however, the challenge would be the requirement of having a DSC for testing.

2.9 Modelling the Heating of Asphaltic Materials

Most models for granular motion in a rotating drum are built upon the work of Henein, who defined the six phases of motion of granular media in a rotating cylinder [23]. This research was built upon by Ding, who provides equations for the two most common forms of particle motion: slumping and rolling. Both slumping and rolling occur at low drum speeds when the drum is less than 50% filled with material. Ding also provides equations to determine thermal relaxation time for the granular media, assuming the heating is occurring at the drum wall [24]. Thermal relaxation time is the time that it takes for a particle to reach thermal equilibrium with the surrounding environment. Mellmann further builds on the work of Henein when, in 2001, a seventh phase of motion for granular media in a rotating drum is proposed [25]. Chen and Louge explain the theory of heat transfer of homogeneous spheres where the heat transfer takes place while a particle is suspended in a fluid (such as air). Chen and Louge's model ignores particle-to-particle contact, since the magnitude of the difference in temperatures between particles and the gas will drive heat exchange. This statement is based on the assumption that particles are colliding too fast to transfer heat between each other and is valid when collision times are significantly smaller than the time spent inside the mixing drum [26].

Early work with rotating drums assumes a smooth-walled drum; however, modern asphalt plants employ baffles inside the drums to cascade aggregates through the heated air flowing through the middle of the drum. One such modeling approach using baffles involves a discrete element model (DEM) simulation. Chaudhuri, Muzzio, and Tomassone developed a DEM which, through focusing on particle-to-particle contact heat transfer, can account for the uniform heating of individual particles [27]. Chaudhuri concludes that baffles increase the temperature rise within the granular medium, based on the assumption that the medium is thermally thin (has a Biot number well below one), and the ratio of the thermal conductivity of the granular medium to the conductivity of the air is much greater than one (which ignores heating from interstitial gasses inside the drum). The Biot number is a dimensionless number used to identify thermally thin or thermally thick bodies. A thermally thin body does not experience spatial thermal gradients within its bounds.If the Biot number is less than 0.1, it can be classified as thermally thin. Lisboa researched the effects that baffles and drum speed have on drying time and particle time spent in a drum. Even though Lisboa's research focused on granular media drying, knowing the dimensions of a drum could allow the model developed in this research to be tailored to specific asphalt plants [28].

The modeling of asphalt heating has been researched previously; however, many of these heating models focus on heating pavement in place, not heating of asphalt particles inside a mixing drum [13, 24, 29]. To date, little research has been published on asphalt particle heating inside of a rotary drum, and incorporating RAP into the model has yet to be documented. LeGuen, Huchet, and Tamagny focused on modeling a co-current asphalt drum with the aid of a 1/3-scale model; however, their work focused on energy balance for particles as a one-dimensional mass, not accounting for individual particle heating [30].

2.10 Summary

The most current methods for measuring the thermal properties of asphalt pavements rely on a curve fitting technique of time series data [11, 12, 14, 15]. This technique was noted in several of the more recent publications on asphalt thermal properties. Using data for the heating of an asphalt specimen over time, one practice back calculates both thermal conductivity and thermal diffusivity of a specimen by comparing simulation results to laboratory data. These techniques essentially solve for two, or more, unknowns using one equation, which relies on probability to arrive at a solution. This author believes more accurate experimental technique can be employed to directly measure one variable in lieu of back calculation.

Based on a review of the literature, hot mix asphalt has a range of thermal conductivities from 0.85 – 3.97 W/m°C. The explanation given for the large variation was seen in the thermal conductivities was attributed to the differences in aggregates; however these references do not take into account potential changes in thermal conductivity that may be caused by aging of the asphalt binder. Even current models for asphalt pavement recycling assume the thermal properties of reclaimed asphalt to be the same as virgin asphalt, however there is a known stiffening that occurs when asphalt binder ages.

3.0 LABORATORY TESTING

In order to effectively predict the amount of time aged asphalt particles will take to heat to a reasonable mixing temperature, it is important to know the thermal parameters of the particles in question. Since a literature gap exists in the thermal properties of aged asphalt binder, the values must be measured directly in the laboratory. Direct measurement of the thermal conductivity of asphaltic material was achieved by use of a parallel plate heating apparatus outfitted with temperature thermocouples and heat flux gages. With this parameter, in conjunction with particle density, and an assumed heat capacity, it is possible to fully characterize aged asphalt binder for comparison to its virgin counterpart.

Three parameters are required for fully characterizing the thermal properties of any material: the thermal conductivity, heat capacity, and density. Finding the density of an object is commonplace for civil engineers; however, measuring the thermal conductivity and heat capacity are more challenging. With density accounted for, the thermal conductivity and heat capacity remain as necessary inputs in modeling the recycling process of asphalt pavements if one wishes to analyze the heat required in mobilizing, or softening, the binder contained within RAP. Due to time constraints, only procedures for measuring thermal conductivity are to be presented in this thesis. To measure the thermal conductivity of aged asphalt materials, two laboratory testing approaches were taken. First, RAP samples were recovered from the field and then sieved to sort the particles into their respective sieve sizes. Those sieved RAP particles were then tested for thermal conductivity at each respective sieve size to obtain the bulk thermal properties at each particle size. In order to test pure asphalt binder, a slightly different approach was used. For pure asphalt binder testing, an unmodified, or neat binder was chosen. To simulate aged binder, laboratory aging was performed on the neat binder. The laboratory aged binder was then substituted for RAP binder in subsequent tests. With the use of simulated RAP binder and virgin binder, the thermal conductivities were measured following the same principles of the particle testing.

3.1 RAP Stockpile

In order to test the effect of aging on the thermal properties of RAP, a RAP stockpile was sourced from a rehabilitation project on County-State-Aid-Highway #21 (CSAH-21) near Babbitt Minnesota. The stockpiles was constructed with an unknown base binder and contained at least 15% taconite tailings. The RAP stockpile was sieved into different particle sizes, ranging from the ½-inch sieve to the #16 sieve which has a particle diameter of 0.05 inches. Since the finer

particles of RAP are a conglomeration of asphalt binder and small particles, there were few particles smaller than the #16 sieve, therefore the #16 sieve was chosen as the smallest sieve to include.

To facilitate the sieving of the RAP ASTM C 136 was followed. After the shaking was finished, the sorted RAP particles were stored inside containers for future testing. Large particles of RAP, having a diameter greater than half an inch, were weighed and placed in the ignition oven to determine the asphalt binder content of the RAP.

3.2 Specific Gravity Testing

Once the aggregates were sieved, it was necessary to determine the bulk specific gravity of each sieve size. For this purpose, ASTM D 2041was performed. For this test, 1000 grams of the stockpile of interest was weighed inside of a tared pycnometer. Then, water was added to the specimen and a vacuum of 27.75 mm Hg (3.7 kPa) was applied to remove the air inside the specimen. The specimen was weighed after 10 minutes of agitation under vacuum to obtain the maximum density (G_{mm}) of each sieve size. The volume and mass of the samples tested in thermal conductivity were treated as a bulk density (G_{mb}). The G_{mm} and G_{mb} were then used to calculate the amount of air present in the samples.

3.3 Binder Preparation

Since the RAP stockpiles had unknown base asphalts, testing with virgin binder and laboratory aged binder was conducted to measure the differences in thermal properties between new binder and highly aged binder. Traditionally, laboratory aged binder is used to simulate seven to ten years of aging in the field. This laboratory-aged binder can then be used to simulate field-recovered RAP binder. With the use of the laboratory aged binder, two sets of tests were run: one on virgin binder and one on simulated RAP binder. It is then assumed that the differences in the virgin binder and PAV binder will represent the differences in thermal properties between new asphalt binder and RAP binder.

3.4 Virgin Binder

A PG 58-34 base binder, original binder (OB), was selected for asphalt binder testing because it was readily available in the laboratory. The binder was aged in the rolling thin film oven (RTFO) and in the pressure aging vessel (PAV) to simulate short and long term aging, respectively. At each stage of aging, including the virgin state, a frequency sweep of Dynamic

Shear Rheometer (DSR) testing was performed at several temperatures to generate a master curve. With a common reference temperature of 22°C, the master curve for the three levels of aging can be seen in Figure 3.1 and Figure 3.2. Figure 3.1 shows the characteristic leftward shift from OB to RTFO to PAV as the binders become increasingly aged. Figure 3.2 has a similar shift in phase angle; it can be seen that the phase angle is decreasing as the binder is increasingly aged. These curves provide a practical way for comparing the levels of aging on the oven aged binder and on subsequent PAV aged binders to the source binder depicted. Generating a new master curve for any aged binder originating from the same source binder and plotting the curve against the three known levels of aging will allow for a visual comparison to be made on the level of aging.

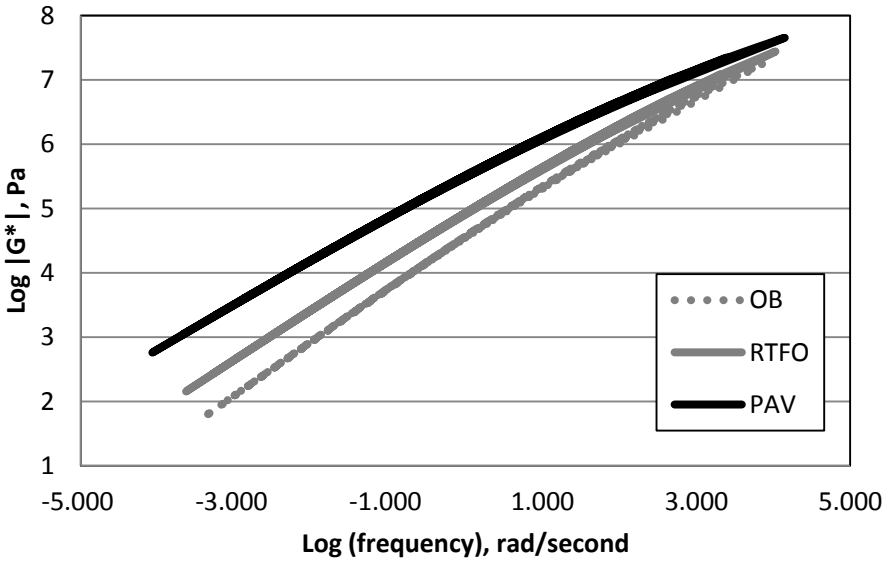

Figure 3.1: Master Curves of Original Binder (OB), Rolling-Thin-Film Oven (RTFO) and Pressure Aging Vessel (PAV) Aged Binders

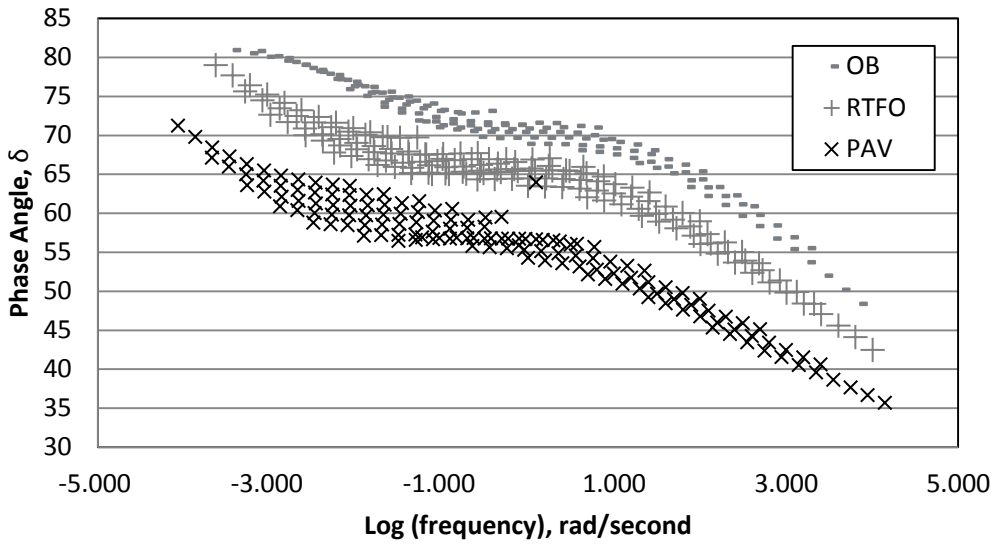

Figure 3.2: Phase Angles of Original Binder (OB), Rolling-Thin-Film Oven (RTFO) and Pressure Aging Vessel (PAV) Aged Binders

3.5 Laboratory-aged RAP Binder

Since the thermal conductivity and heat capacity testing requires a significant amount of asphalt binder to test, it was decided that PAV binder was unfeasible to use as simulated RAP binder. The PAV generates 400 grams of binder in 20 hours; however, the thermal conductivity testing requires 3,500 grams of asphalt binder to perform the test. Therefore, traditional PAV aging was a last resort, since it would have taken 10 PAV cycles to prepare the necessary amount of binder needed for the thermal conductivity testing. Using a reliably available stockpile of PG 58-34 3M binder, a unique aging process was chosen to simulate RAP binder that was more feasible than PAV testing.

Simulated RAP binder was created using AASHTO R 30 specifications, which call for oven aging in a forced air oven for 80 hours at a moderate temperature. The one notable difference between AASHTO R 30 and the procedures followed is that AASHTO R 30 calls for loose mix fresh HMA to be long-term aged, while this laboratory setup omitted aggregates, as interest was only in testing aged binder. The PG 58-34 binder was heated in an oven to aid in pouring. Then, the heated binder was poured into shallow pans and placed inside an 85°C forced-draft oven to simulate long term aging. After 120 hours of conditioning in a shallow pan, the

binder was considered to be aged. The new oven-aged (OA) binder was removed from the oven and poured into air-tight containers for further testing.

3.6 Comparison of Binders

Based on a master curve comparison of OA binder and OB, it became apparent that PAV aging was necessary to achieve a binder that could be substituted for RAP binder. Using the OB, OA, RTFO, and PAV binders, four different master curves were generated to compare the levels of aging on the different binders. Shown in Figure 3.3 and Figure 3.4 are the four different master curves and phase angle plots generated from the above-mentioned binders. Again, the reference temperature is 22°C. Based on the four master curve plots, it can be seen that the effect of oven aging on creating RAP binder was minimal. The OA master curve is only slightly shifted towards the more-aged PAV curve, while the phase angles have a similar trend.

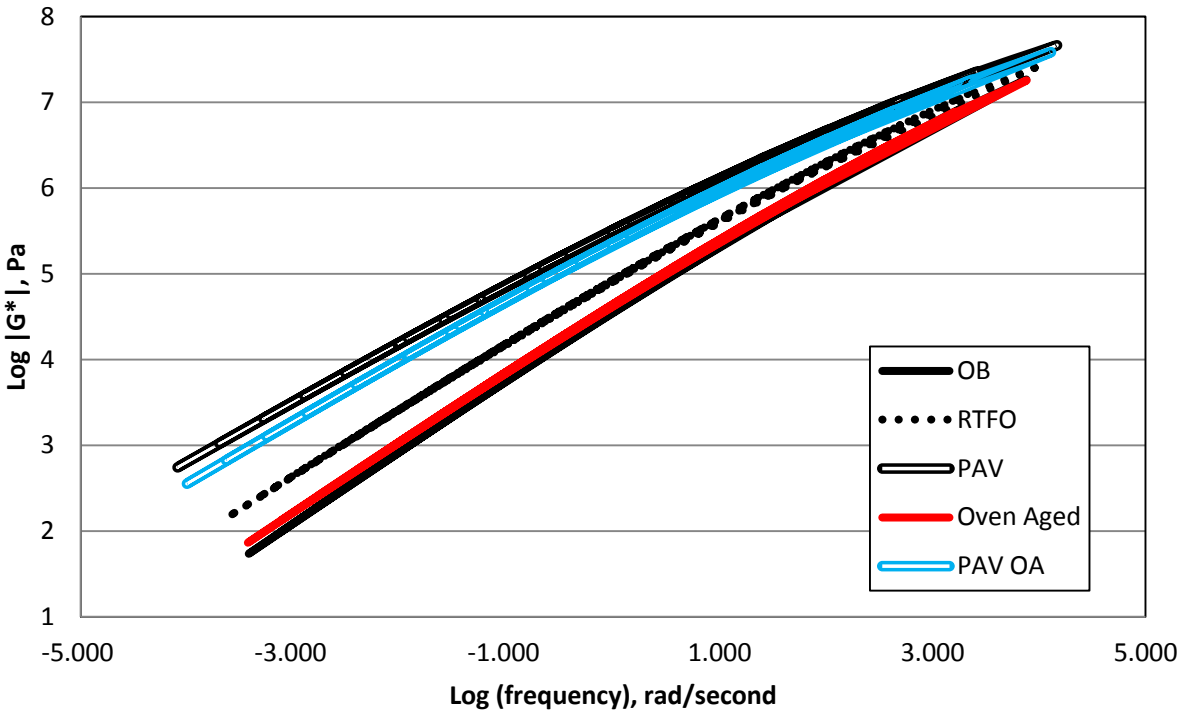

Figure 3.3: Master Curves of All Binders Tested

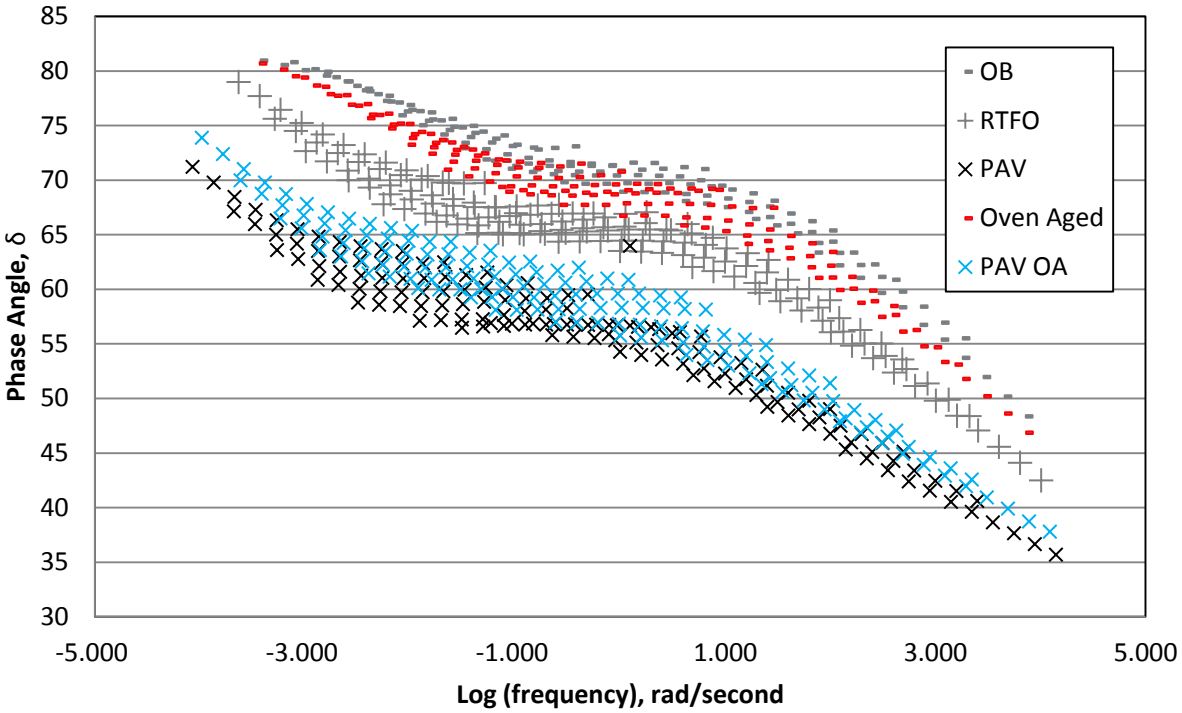

Figure 3.4: Phase Angles of All Binders Tested

3.7 Thermal Conductivity Testing

Using a parallel-plate heating setup, it is possible to measure the temperature and heat flowing into and out of a specimen in order to directly calculate the thermal conductivity. By the use of the experimental techniques pioneered by Sparrow, such a parallel-plate heating setup was created and instrumented [31]. The equation used to calculate thermal conductivity is as follows:

$$k = S \cdot E(L/\Delta T) \qquad (1)$$

Where:

k = Thermal Conductivity (W/(m·K)

S = Calibration factor of the heat flux transducer ($(W/m^2)/V$)

E = Heat flux transducer output (V)

L = Distance between the heat flux transducers (m)

ΔT = Temperature difference between the two plates (°C)

The parallel plate test employed involves two heated plates on either side of a specimen. Each plate is equipped with a heat flux transducer to measure the heat leaving one plate and arriving at the other plate. Thermocouples installed in each plate measured the temperature difference across the test specimen. The specimen is wide enough to make edge losses negligible, so that the experiment is one-dimensional.

3.8 Experimental Set-up

Thermal conductivity testing utilizes a parallel-plate heating apparatus, similar to the one shown in Figure 3.5 (figure reproduced from [31]). The testing apparatus consists of a sheet heater adhered to the top of a thick aluminum plate which is in full contact with the specimen being tested. A mirrored setup is on the other side of the specimen. The entire testing apparatus is then wrapped in insulation to limit the heat loss throughout the testing. Affixed centrally toeach plate are a heat flux sensor and a thermocouple. Aluminum was chosen as the plate material for its ability to evenly distribute the heat from the sheet heater throughout the volume of the plate so as to achieve a uniform temperature at the specimen surfaces. Each sheet heaters was connected to a DC power supply. The DC power supplies are designed to permit independent variation of the voltage and current. The constant internal resistance of the heater allowed for a desired temperature to be achieved simply by increasing or decreasing the voltage from the DC source. The aluminum plates and sheet heaters measured 10 inches x 10 inches. The thermocouples measure the temperatures at either side of the specimen, while the heat flux gauges measure the energy flowing through the specimen.

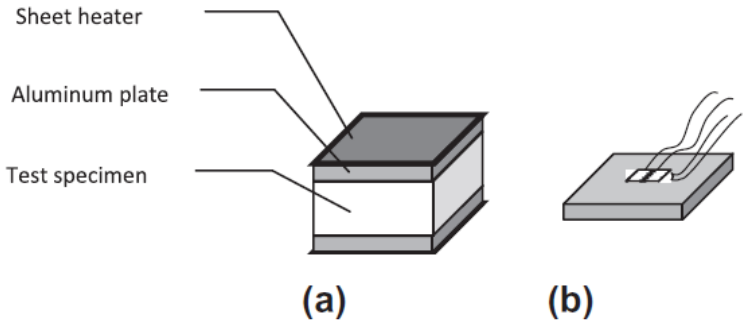

Figure 3.5 (a) Thermal Conductivity Experimental Schematic (b) Close-up of Aluminum Plate with Embeded Sensors (From [32])

Two different testing apparatuses were used for the thermal conductivity testing. When testing with granular media, such as RAP particles or aggregates, a 9.5 inch x 9.5 inch x 1.5 inch, a Styrofoam insulation mold with ¼ inch-thick walls was placed on top of the bottom plate and

filled with the loose granules. Saran plastic wrap was laid on either side of the Styrofoam to protect the sensors from asphalt binder contained in the RAP. After the granular media was loaded into the Styrofoam mold, a straight-edge was used to doctor the surface of the granules. The weight of each specimen inside of the mold was recorded for volumetric calculations. Then, the upper plate and heater were placed on top of the specimen, and insulation was placed around the specimen. A schematic of the granular setup can be seen in Figure 3.3.6 (borrowed from [33]). In the schematic, the green line represents the thermocouple, while the blue lines are heat flux transducers. The DC power supplies were turned on, and the specimen was allowed to reach steady state for a period of at least 12 hours.

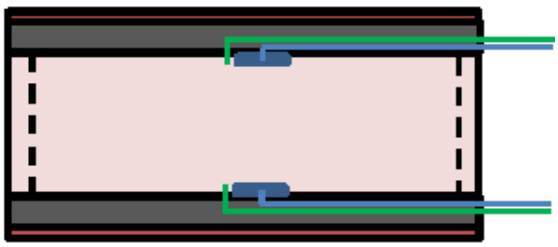

Figure 3.3.6 Diagram of Thermal Conductivity Testing with Granular Media (From [33])

For asphalt binder thermal conductivity testing, the Styrofoam insulation mold was unsuitable because the high temperatures of asphalt binder caused the mold to melt. To improvise a better way to measure pure asphalt binder, a wooden frame, with dimensions larger than the aluminum plate (12inch x 12 inch x1.5inch) was filled with hot, liquid asphalt binder. The asphalt binder was poured onto a sheet of tempered glass lined with parchment paper to aid in the release once the binder had cooled. The frame used can be seen in Figure 3.7.

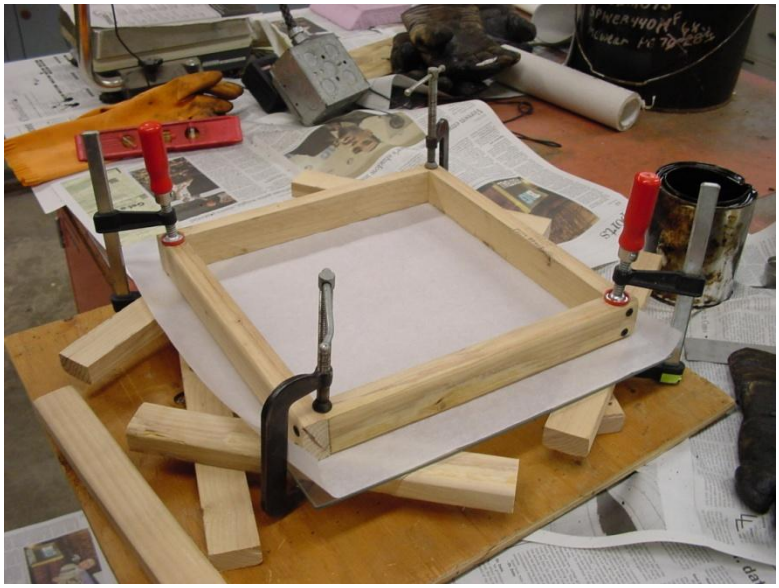

Figure 3.7 Picture of Wooden Frame Used in Asphalt Binder Thermal Conductivity Testing

The asphalt binder was heated to 150°C for several hours before pouring into the wooden frame. Once heated, the binder was stirred to achieve homogeneity. The hot binder was then poured into the frame and allowed to cool at room temperature overnight. Next, the frame was set inside of a refrigerator, then transferred to a freezer to freeze the binder and make it more manageable to work with. The binder was cooled in this fashion to alleviate possibility of developing thermal cracks from the extreme temperature changes. Once frozen, the binder was demolded from the parchment paper and sealed inside of Saran plastic, as shown in Figure 3.8 (A). As with the granular media testing, the prepared asphalt binder specimen was loaded into the testing apparatus with the aluminum plate on top of the specimen, then the sheet heater and lastly insulation. The assembly of the asphalt specimen testing apparatus can be seen in Figure 3.8. In addition to the insulation shown on top of the specimen in Figure 3.8 (D), fiberglass insulation was wrapped around the sides of the wooden frame to further insulate the experiment. Then, the DC power supplies were turned on and the asphalt was allowed to reach thermal equilibrium to achieve a steady-state test condition.

(A)

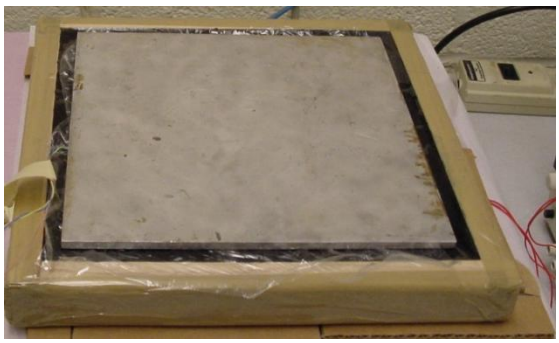

(B)

(C)

(D)

Figure 3.8 Asphalt Binder Specimen (A) Wrapped in Plastic (B) Between the Aluminum Plates (C) With the Sheet Heater (D) Insulated

Once a specimen had reached thermal equilibrium between the two heater plates, a data logger was set to record the heat fluxes and temperatures from the sensors embedded in both aluminum plates. Data were recorded at a rate of one data point per minute in the equilibrium state. An averaged value of the final 500 data points recorded was reported as the values obtained from the test. From those averaged values, the thermal conductivity was directly calculated using $k = S \cdot E(L/\Delta T)$ (1).

3.9 Results

The largest particle size in each specimen tested was plotted against the measured thermal conductivity, for the granular specimens. This plot, shown in Figure 3.9, shows an increasing trend in conductivity as the particle size increases. The scatter shown in the figure is due in part to the use of the largest particle to characterize the bed. The density and distribution of the particle bed are not taken into account when viewing only the largest particle size, therefore this plot only represents one variable from testing.

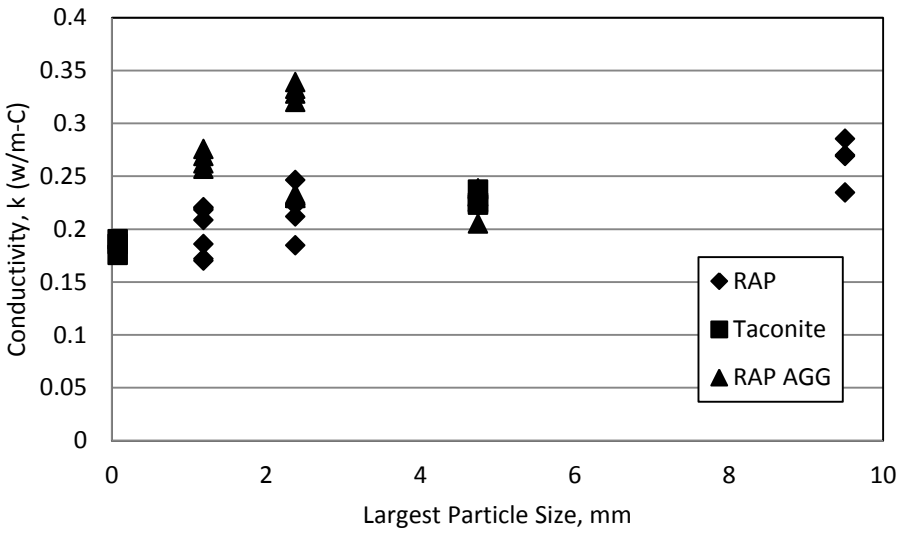

Figure 3.9 Granular Particle Size vs. Thermal Conductivity

However, particle size is only one metric for which the data can be analyzed. With the use of the recorded weights of the samples inside of the conductivity molds, plots of the bulk density versus conductivity can be generated, as in Figure 3.10. For data points where the density is the same, multiple readings were taken with the same specimen and plotted. This plot shows a direct relationship between particle density and thermal conductivity; however, it would appear that each source tested has a unique trend line. This suggests thermal conductivity is specific to the material tested and not just on density.

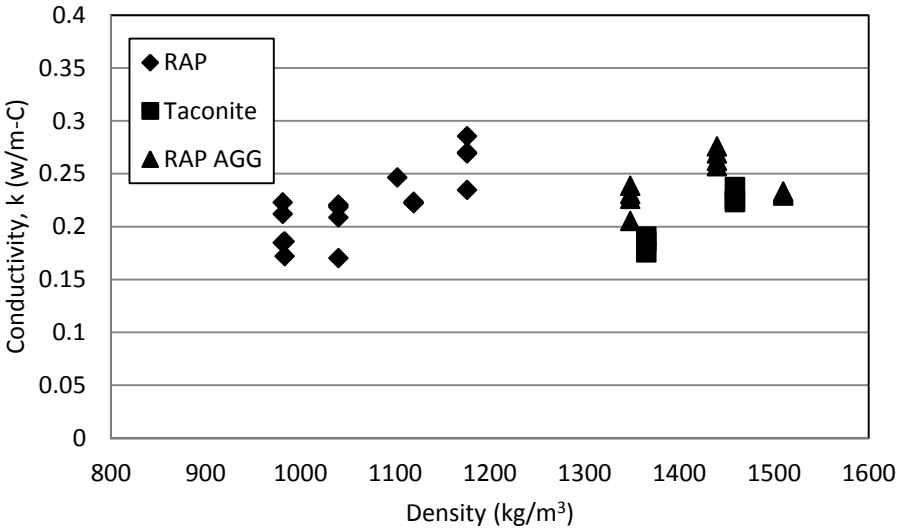

Figure 3.10 Bulk Density vs. Thermal Conductivity

The last trend in the data that was observed was the change in conductivity with the change in air voids. From the bulk density and theoretical maximum specific gravity, G_{mm}, of the RAP particles, the air voids inside of the specimen could be calculated. Plotting the air voids against thermal conductivity produces Figure 3.11. The trend is that the conductivity decreases as the amount of air inside of the specimen increases, which is to be expected.

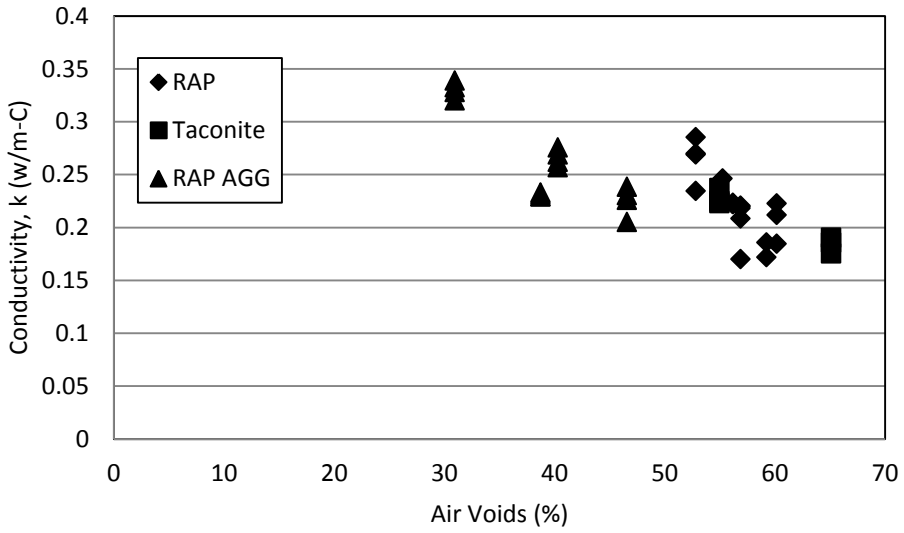

Figure 3.11 Thermal Conductivity vs. Percentage of Air

Statistical analysis was run on the data gathered through experimentation. For the variables considered, particle size, density, and air voids were continuous variables. A correlation matrix, shown in Table 3.1, reveals correlations with air voids and density. Since Density is a correlated variable, it will be omitted from the analysis.

Table 3.1 Correlation Matrix for Lab Testing

	Particle Size	Density	Air Voids
Particle Size	1	-0.078	0.002
Density	-0.078	1	-0.78
Air Voids	0.002	-0.78	1

Simple linear regression was run on the remaining variables, Particle Size, Air Voids, and Particle Type. A full first order model with interaction terms was fit to explain the variation in the data set. Then, a backwards selection of significant variables using AIC criterion was employed. AIC was chosen because it returns a good balance between the fit of a model while penalizing

excessive complexity. The results of the linear regression can be seen in Table 3.2. For the chosen model, all of the variables tested as significant at the 1 percent significance level. Lastly, the regression equation was able to explain approximately 78 percent of the variation in the laboratory testing.

Table 3.2 Linear Regression Results for Particle Laboratory Data

Coefficients:	Estimate	Std. Error	t value	Pr(>|t|)	
(Intercept)	0.592	0.062	9.626	4.16E-11	***
RAP Aggregate (factor)	-0.071	0.031	-2.313	2.71E-02	*
Taconite (factor)	0.033	0.015	2.18	3.65E-02	*
Particle Size(mm)	0.003	0.002	2.067	4.66E-02	*
Air Voids (%)	-0.007	0.001	-6.552	1.92E-07	***
RAP Aggregate:Particle Size	-0.001	0.005	-0.153	8.79E-01	
Taconite:Particle Size	-0.008	0.004	-2.057	4.76E-02	*

Signif. Codes: 0 '***' 0.001 '**' 0.01'*'

Residual Standard Error: 0.02006 on 33 degrees of freedom
Multiple R-Squared: 0.8109, Adjusted R-squared: 0.7765
F-statistic: 23.59 on 6 and 33 Df, p-value: 1.27E-10

The results of the asphalt binder testing can be seen in Table 3.3. There is a slight increase in the thermal conductivity of the oven-aged binder, when compared to the virgin binder, but a decrease when compared to the PAV aged binder. A stiffer substance is expected to conduct heat better than a soft one, which would explain the shift from Virgin Binder to Oven Aged Binder. The decrease in thermal conductivity for PAV aged binder requires further investigation.

Table 3.3 Measured Thermal Conductivities of Asphalt Binder

	Virgin Binder	Oven Aged Binder	PAV Binder
Average k, W/m·K	0.175	0.194	0.159
Standard Deviation	0.005	0.001	0.005

Reclaimed Asphalt Shingles (RAS) were also tested for thermal conductivity in much the same way as RAP and aggregates. For this testing, the thermal conductivity of the RAS was found to be 0.17 W/m*K. This low thermal conductivity is similar to pure asphalt binder.

3.10 Summary

There are several results from the laboratory testing conducted. First, asphalt binder thermal conductivity was measured using a novel approach developed by Sparrow et al [32]. Next, asphalt binder was aged in a pressure aging vessel to simulate RAP binder. The master curve for PAV aged binder was developed to show the difference between the virgin binder and the aged binder. Thermal conductivity testing showed an increase in thermal conductivity for slightly aged binder when compared to the virgin conductivity, and a decrease in thermal conductivity when compared to PAV binder. Although there were significant differences between the thermal conductivity of the three specimens tested, it is worth noting only a 5% percent difference in exists between the three specimens. It was also shown that RAS has a similar conductivity to that of asphalt binder, which makes sense since RAS is mostly asphalt binder.

Thermal conductivity testing revealed a statistically significant difference between the three types of materials tested. RAP aggregate was the least conductive material tested, while taconite was the most conductive. Because taconite is comprised of metals, it is expected to have a higher thermal conductivity than the other materials tested. As the presence of air voids increased, testing revealed a decrease in thermal conductivity, again this trend is as expected. Lastly, as particle size increased, thermal conductivity also increased. One explanation for this increase is that the larger particles allow head to pass through unobstructed before having to transfer between particles or across an air void.

Based on the results of the thermal conductivity of taconite tailings, taconite tailings used as aggregates could provide favorable thermal properties to asphalt pavement recycling. The taconite conducts heat faster than traditional aggregates, which allows for RAP to be heated at a faster rate. Since it was established in Chapter 2 the amount of time RAP spends inside of the asphalt drum is minimal, transferring heat into the RAP faster would have positive benefits for recycling.

4.0 FINITE-DIFFERENCE MODELING

Recycling aged asphalt pavements into new asphalt pavements is a common practice in the pavement industry. The process involves adding the reclaimed asphalt pavement (RAP) into a super-heated asphalt mixing drum, where the binder contained within the RAP is expected to melt and be incorporated into the new hot mix asphalt (HMA). Since the RAP is added partway through the mixing process, the amount of time spent inside the mixing drum is short and possibly not sufficient for the RAP binder to melt and mix with the new asphalt binder.

To address this issue, a numerical model is developed using the thermal properties of asphalt materials to investigate the melting potential of RAP within an asphalt mixing drum. Through a dimensional analysis, the proposed model allows for the practice-ready calculation of the minimum time needed for any spherical particle to heat to a desired temperature given the initial temperature, ambient temperature, thermal diffusivity, and particle radius. Using the resulting equation, it is shown that there may be cases in which RAP is not sufficiently heated within an asphalt mixing drum.

4.1 Asphalt Particle Heating Model

A model which describes the transfer of heat within the asphalt mixing drum was developed as part of this research. The proposed model accounts for the variability in temperatures between stockpiles and the mixing drum in order to predict the amount of time needed to sufficiently heat a spherical particle of RAP to a desired mixing temperature. The model is presented below. A depiction of the particle is shown in Figure 4.1.

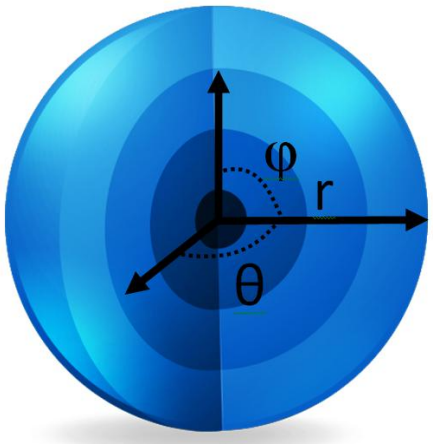

Figure 4.1 Diagram of Particle in Model

The model is used to calculate the time for the center of an assumed spherical RAP particle to reach its recommended mixing temperature, T_m. The key assumptions made are

- The initial temperature of the RAP, T_0, is uniform throughout the particle
- During heating, the surface of the RAP particle is fixed at an assumed drum temperature,T_d
- The RAP is a homogeneous particle with uniform properties, which neglects moisture inside of the particle.

In reality, it is expected that the temperature in the drum will change following RAP addition and that there will not be perfect thermal contact on the RAP surfaces. Thus, for the case when initial drum temperature is taken as the ambient, the calculations of heating times obtained with this model can be viewed as providing a lower bound on the time required for the center of a given RAP particle to reach the desired mixing temperature.

Requiring the middle of the RAP particle to reach the mixing temperature may appear too conservative, since only the surface of the RAP particles is coated with the aged binder. The counter argument to this is that it is important for the entire particle to be raised to the mixing temperature so that the mixture as a whole does not cool below the prescribed mixing temperature (on account of incomplete heating of the RAP particles), creating other problems associated with cold mixes.

Transient heating of a sphere via conduction with no internal heat generation is governed by the Fourier heat equation, which is the governing equation for the model. The Fourier heat equation for spherical geometry is as follows

$$\frac{1}{\alpha}\frac{\partial T}{\partial t} = \frac{1}{r^2}\frac{\partial}{\partial r}\left[r^2\frac{\partial T}{\partial r}\right] \qquad for\ 0 < r < R \tag{1}$$

with

$$T(r, t = 0) = T_0, \qquad T(R = r, t > 0) = T_d \tag{2}$$

where r is the radial coordinate, t is time, R is the radius (m) of the RAP particle and α is the assumed constant thermal diffusivity (m^2/s).

Introducing the following time and space scaling, where the superscript $( )^*$ indicates a variable without dimensions

$$t^* = t\frac{\alpha}{R^2}, \qquad r^* = \frac{r}{R} \tag{3}$$

and defining the dimensionless temperature, T^* as

$$T^* = \frac{T - T_0}{T_d - T_0} \tag{4}$$

the governing equation can be written in the dimensionless form

$$\frac{\partial T^*}{\partial t^*} = \frac{1}{r^{*2}}\frac{\partial}{\partial r^*}\left(r^{*2}\frac{\partial T^*}{\partial r^*}\right) \qquad for\ 0 < r^* < 1 \tag{5}$$

with

$$T^*(r^*, t^* = 0) = 0, \qquad T^*(r^* = 1, t^* > 0) = 1 \tag{6}$$

The objective of solving (4) and (5) is to find the dimensionless time, $t_f{}^*$ at which the solution at $r = 0$ (center of the particle) is

$$T_m^* = T \;\; r^* = 0, t^* = t_f{}^* \;\; = \frac{T_m - T_0}{T_d - T_0} \tag{7}$$

for a given mixing temperature, T_m and $T_0 < T_m < T_d$

This solution was achieved using the MATLAB PDEPE tool (Partial Differential Equation solver for Parabolic and Elliptical functions), employing a mesh independent 40 finite difference steps. Figure 4.2 shows the fitted solution obtained from MATLAB.

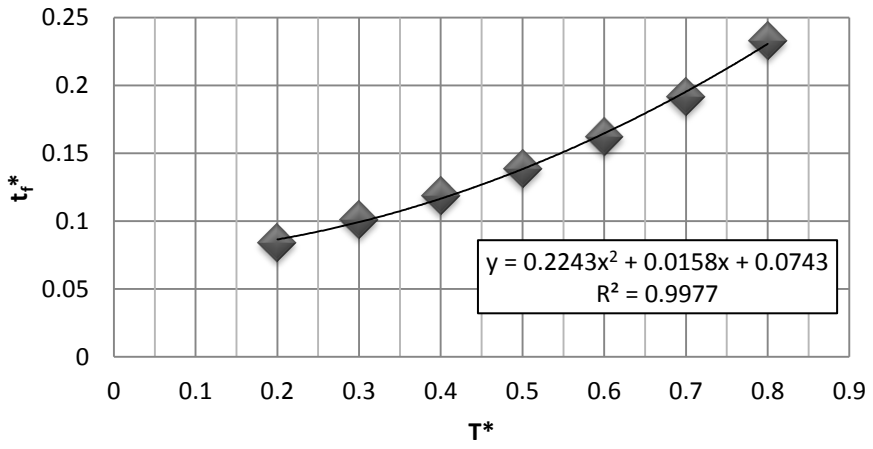

Figure 4.2 Fitted Numerical Solution

For values of $0.2 < T^* < 0.8$ (the expected range of plant conditions), a good fit (R^2 = 0.9977) to the numerical solution of (4) and (5) can be obtained with the following polynomial equation

$$t_f{}^* = 0.2243 \cdot T^{*2} + 0.0158 \cdot T^* + 0.0743 \tag{8}$$

In this way, using the scaling in (3), a single equation for predicting the time(s) for a given particle to reach the mixing temperature is obtained

$$t_f = \frac{R^2}{\alpha}\ 0.2243\ \frac{T_m - T_o}{T_d - T_o}^{\ 2} + 0.158\ \frac{T_m - T_o}{T_d - T_o}\ + 0.743 \tag{9}$$

under the condition that

$$0.2 < \frac{T_m - T_o}{T_d - T_o} < 0.8 \tag{10}$$

Even though it is outside of the precise range of applicability, a simple initial test of the proposed model can be made by estimating the equilibrium time, t_{pr}, that represents the time taken for the particle to reach a uniform temperature, $T_m = T_d$. When this condition is used in (9)the resulting equation for the equilibrium time is given by

$$t_{pr} = \frac{A \cdot R^2}{\alpha} \tag{11}$$

where $A = 0.3144$.

The equation for thermal relation time presented by Ding is shown in (12).

$$t_{pr} = \frac{\rho_s \cdot C \cdot d_p^2}{12 k_p} \tag{12}$$

where the particle density, ρ_s, heat capacity, C, particle diameter,d_p, and thermal conductivity, k_p, are inputs. It can be easily shown that the equation simplifies to (13)

$$t_{pr} = \frac{1}{3} \cdot \frac{R^2}{\alpha} \tag{13}$$

and takes the form of (13) where $A = 0.3333$, which is very close to the previously calculated value for equilibrium time. This provides added confidence in the model proposed by this method.

4.2 Model Verification

Two methods for model verification were employed to check the derivation of the particle heating equation. First, the classic solution of the Heisler-Gröber chart was compared against the model solutions. The Heisler-Gröber chart shows good agreement with the proposed model. Secondly, commercial finite element software was used to predict the time needed to heat a spherical particle with assumed thermal properties to a prescribed inner temperature. The results of the finite element software were then compared to the values predicted by the proposed particle heating equation. Again, the proposed equation has good agreement with the commercial software.

4.2.1 Heisler-Gröber Chart Verification

From the first term of a Fourier series expansion, Heisler-Gröber produced a series of charts to solve the center temperature of both infinite plates and spheres [34]. The Heisler-Gröber chart for spherical geometry is shown in Figure 4.3 below. On the abscissa axis is the Fourier number (Fo), plotted against the dimensionless mid-plane temperature. Plotted on the chart are a number of different Biot numbers for which the chart is applicable.

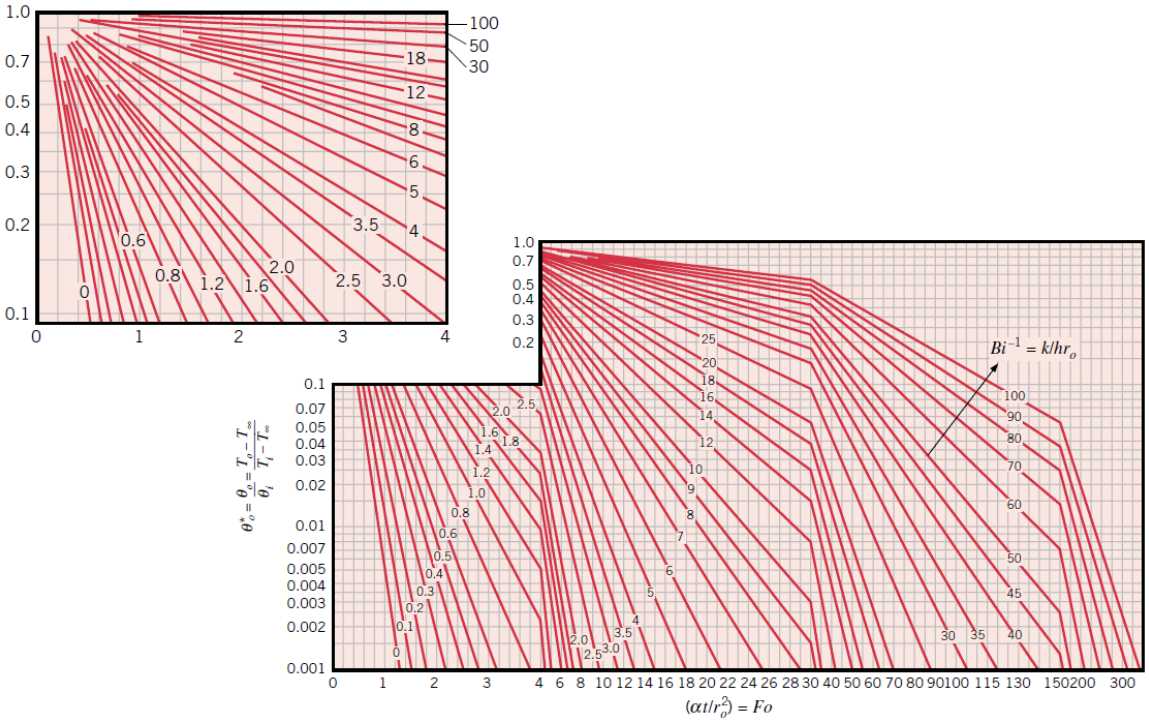

Figure 4.3 Heisler-Gröber Chart, Solved for a Sphere ([34])

One of the main assumtions of the particle heating model was that the surface of the sphere was fixed to the temperature of the drum. That is to say, this assumption implies a case of perfect conduction between the sphere and the environment. For the assumption of perfect conduction, the Biot number for the case of the sphere presented above is equal to infinity. The Heisler-Gröber chart plots inverse Biot number, and in cases with a Biot number of infinity, the corresponding inverse is zero. Shown on Figure 4.4 in blue, are the lines corresponding to the case presented in an ANSYS simulation for a ½-inch diameter sphere with a starting temperature of 20°C, drum temperature of 315°C, desired melting temperature of 121°C, and thermal diffusivity of 5.0410^{-7} m^2/sec. For the particle heating model to be correct the predicted time needed to heat the particle is 7.92 seconds. On the Heisler-Gröber shown below, the dimensionless mid-plane temperature of 0.657 and dimensionless Fourier number of 0.099, which correspond to the above described conditions, were plotted. The intersection of those two lines falls directly on the inverse Biot number line corresponding to zero, which matches the predictions given by the proposed particle heating model.

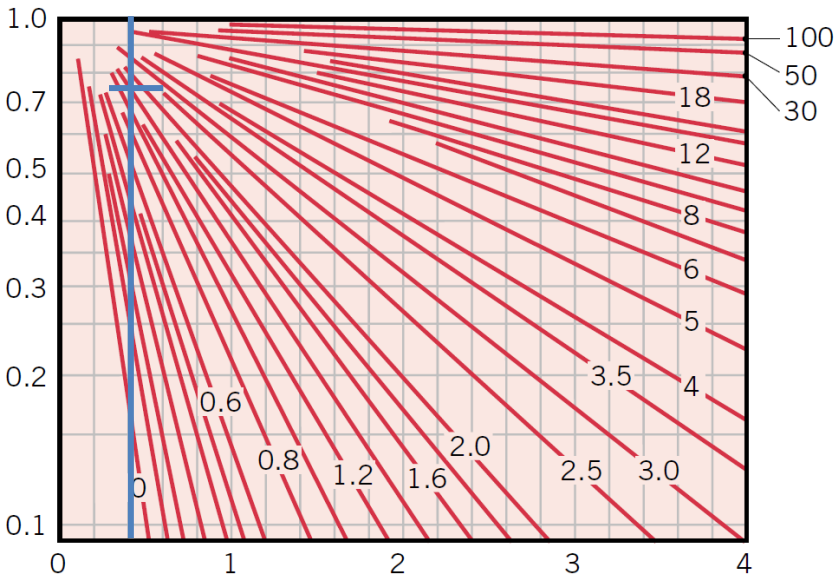

Figure 4.4 Heisler-Gröber Chart Solution ([34])

4.2.2 FEM Model Verification

A sphere was modeled in ANSYS, as shown in Figure 4.5, where homogeneous thermal properties were assumed. A uniform temperature was applied to the surface of the sphere, and the model was run for a specified amount of time, as predicted by the derived equation.

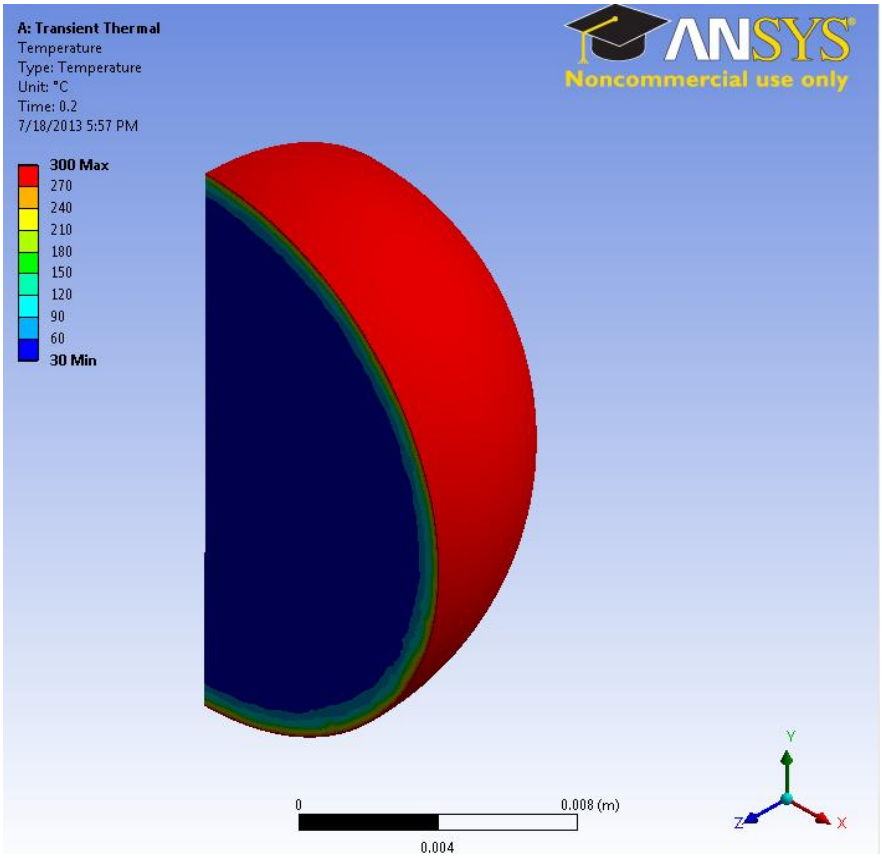

Figure 4.5 Homogeneus Particle in ANSYS

With an assumed melting temperature of 121°C, the finite-element model was run for two test cases against the proposed equation. The finite element loop was terminated once the middle temperature reached the desired melting temperature, and the elapsed time steps could be compared against the predicted time given in the equation. These predictions are shown in Table 4.1. As shown, the FEM times have good agreement with the predicted time for the middle of a spherical particle to reach a desired melting temperature.

Table 4.1 Comparison of Predicted Heating Times to FEM Heating Times

	Trial 1		Trial 2	
	Equation	ANSYS	Equation	ANSYS
Particle Diameter	1/2 inch	1/2 inch	3/4 Inch	3/4 Inch
Starting Temperature (°C)	20	20	30	30
Drum Temperature (°C)	315	315	300	300
Melting Temperature (°C)	121	121	121	121
Time to heat (seconds)	7.92	7.99	17.66	18.41

Because of the difficulty in ending a finite element run at a desired time, this verification looks at the temperature at the center of the sphere at the ends of the two time steps on either side of the predicted time. Linear interpolation was used to estimate the time the particle was heated to 121 °C. Figure 4.6 shows the last time step in the FEM simulation to illustrate that there are thermal gradients present within the sphere of reclaimed asphalt pavement and that the temperature at the center of the sphere has indeed reached the desired melting temperature.

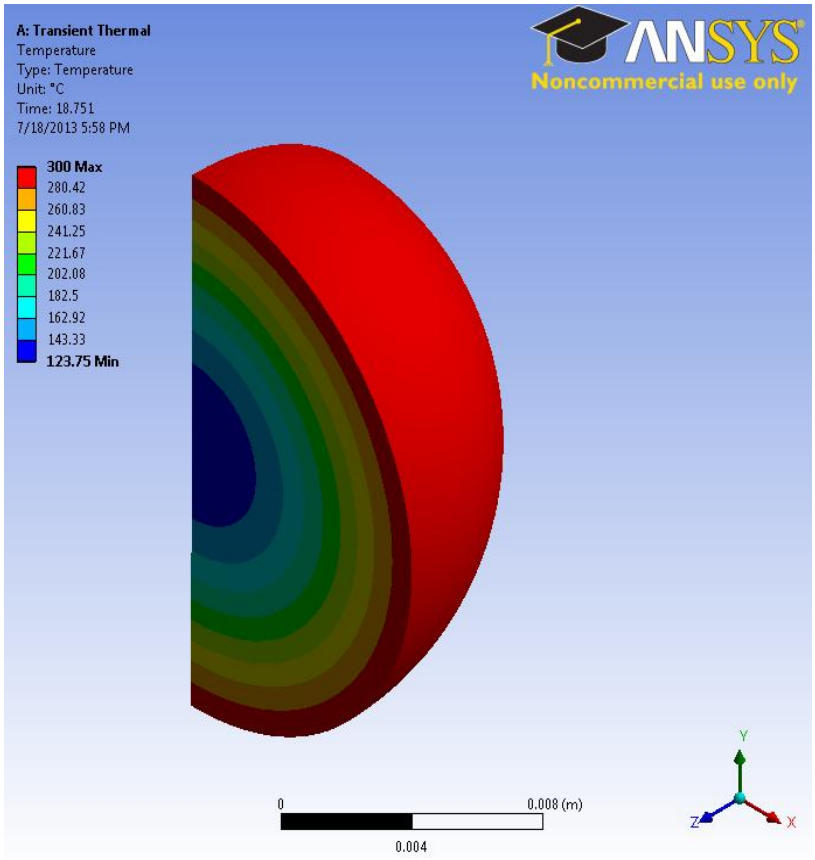

Figure 4.6 Gradient Temperature Inside FEM Sphere

4.3 Model Application

Over the past few years, due to economic and environmental benefits, higher percentages of RAP have been used in pavement projects. To explore the impact that the higher percentages of RAP have on drum mixtures, assumed properties were reported in Table 4.2. As noted above, a number of assumptions were made in the derivation of the model. In particular it was assumed that the RAP particle is completely surrounded by superheated aggregate at the highest expected temperature for the duration of the heating. Since the aggregate mixing in an asphalt drum takes place beyond the burner, the maximum temperature during mixing is the temperature assumed for the superheated aggregates, which is around 315°C (600°F). This temperature will serve as the upper bound for heating in the sense that it represents the most heat to which the particles will be subjected and thus, when used in the model, it will provide a lower limit on the required time to reach the mixing temperature.

A lower-bound temperature surrounding the RAP particles (upper limit on the heating time) can be obtained as follows: the lower bound assumes a perfectly insulated system for mixing, within which heat is conserved during the mixing between the superheated aggregates and the RAP. This means that the system will equilibrate to the temperature obtained at the lower limit. Then, using the lowest possible temperature, equation (9) can be used to find the longest time needed to heat the system. Assuming a perfectly insulated system, the following equation can be used,

$$H_a + H_r = \rho_a \cdot T_a \cdot C_a \cdot Vol_a + \rho_r \cdot T_r \cdot C_r \cdot Vol_r \quad \textbf{(14)}$$

where H is the total energy in the system (kJ), ρ is the material density (kg/m^3), T is the material temperature (K), C is the heat capacity (kJ/kg·K), and the subscripts a and r refer to superheated aggregates and RAP, respectively. Although the energy conservation equation (14) is independent of time, it gives a conservative estimate for the lowest temperatures to be experienced during mixing. This lower limit takes into account possible heat transfer occurring outside of the drum, provided the RAP is stored in a well-insulated vessel.

The assumptions made for (14) are found in Table 4.2. Solving the equation for the combined energy, $(H_a + H_r)$, the resulting temperature is 238°C (~465°F). Thus, two conditions have been found that will provide the bounds for the model estimates of required mixing time, a fixed superheated temperature for the aggregates at 315°C (~600°F) and an estimated equilibrium

temperature of the aggregate RAP mixture at 240°C (~465°F). Both temperatures are well above the recommended HMA mixing temperature of around 150°C (~300°F). If the percentage of RAP is increased, or the superheated temperature is decreased, there may be insufficient heat in the system to melt the RAP [35].

Table 4.2 Lower Bound Assumptions

Aggregate		
Parameter	Value	Reference
Density (kg/m^3)	2650	[36]
Temperature (°C (°F))	315 (~600)	[8]
Heat Capacity (kJ/(kg·K))	0.84	[37]
Volume, Volaggregate (%)	80	Assumed
RAP		
Parameter	Value	Reference
Density (kg/m^3)	2243	[38]
Temperature (°C (°F))	20 (68)	Assumed Outdoor Temperature
Heat Capacity (kJ/(kg·K))	1.4	[10]
Volume (%)	20	1-Volaggregate

If the same values for the material parameters are kept, it is found that when 48% RAP is used, the combined equilibrium temperature drops below the recommended mixing range to 148°C (298°F). This is because of the assumption that the virgin aggregates are providing the heat to melt the RAP. As less virgin aggregates are used, there is less energy available for RAP melting, and eventually there is not enough energy left in the system to provide sufficient melting. However, when (14) is used in conjunction with (9), inputs that are tailored to a specific asphalt plant can be entered into the model to better gage the ability of the asphalt plant to provide enough heat to ensure reheating of the RAP.

With the model developed, it is possible to come up with a range of scenarios in which the RAP particle heating can be analyzed. In the base scenario, RAP was modeled with a diameter of 19 mm (3/4 inch), initial temperature of 20°C (68°F), and thermal diffusivity of 5.04

x 10^{-7} m^2/second. Additionally, the mixing drum's default temperature is 315°C (600°F), and the melting temperature for RAP binder is assumed to be 150°C (302°F). Figure 4.7 shows the effect that model parameters have on the time needed to heat the center of the RAP to mixing temperature.

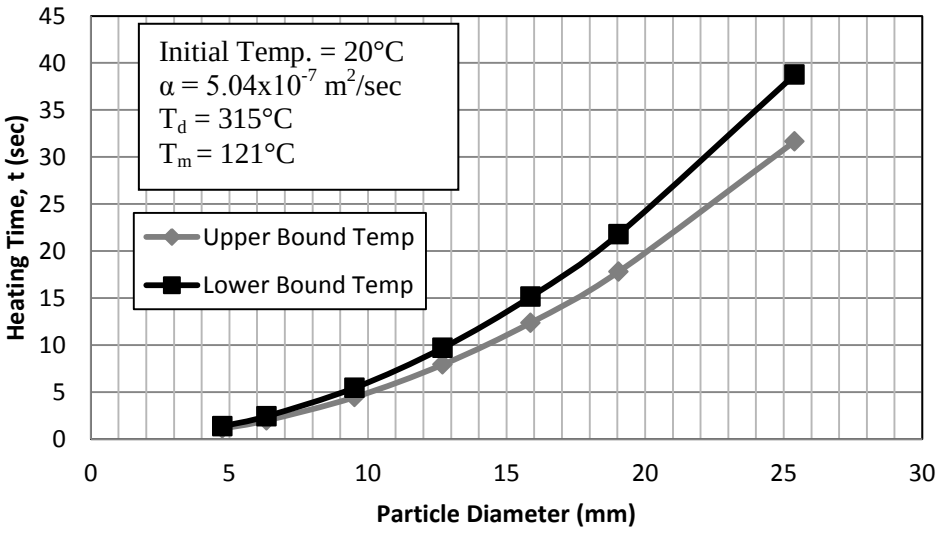

(a) The Effects of Varying Particle Diameter on RAP Heating Time

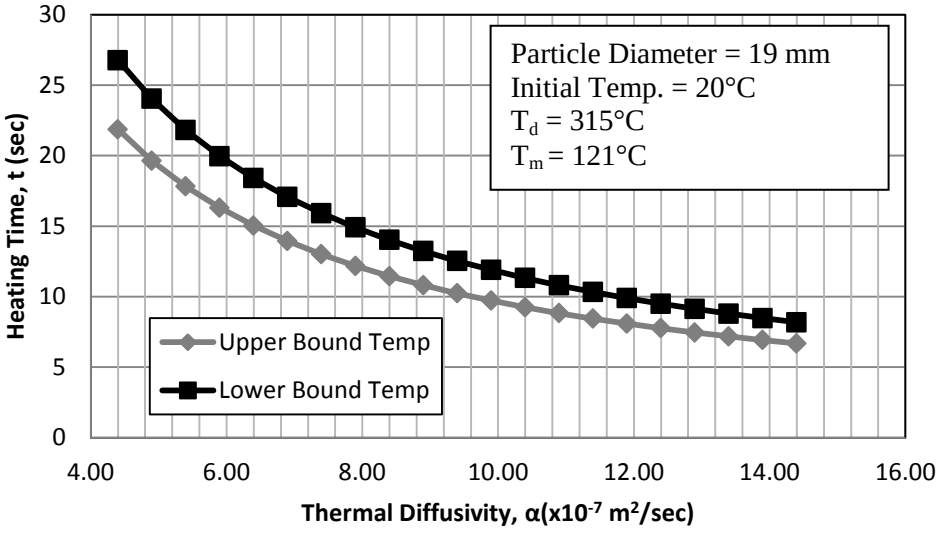

(b) The Effects of Varying Thermal Diffusivity, α on RAP Heating Time

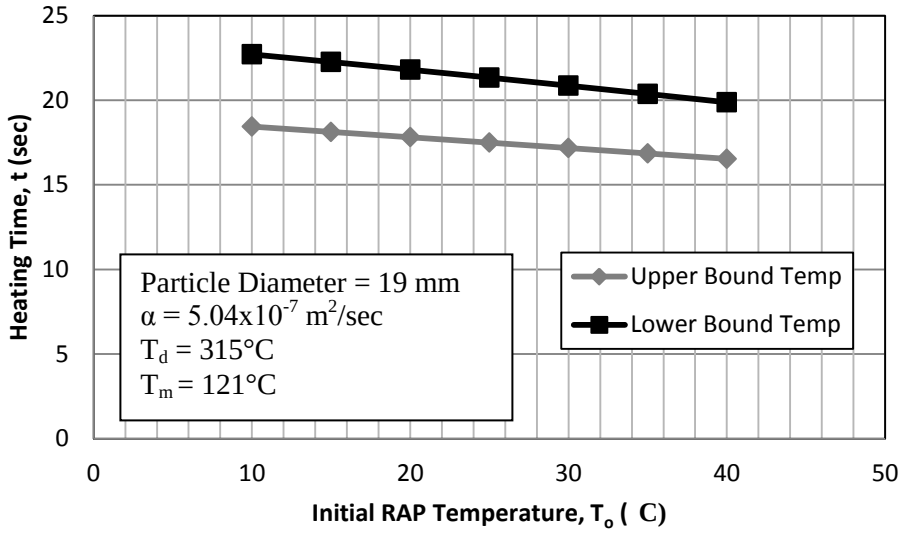

(c) The Effects of Varying Initial RAP Temperature on RAP Heating Time

Figure 4.7 The Effects of Varying Model Inputs on RAP Heating Time

From Figure 4.7 (a) and (b), it can be seen that the two factors with the most influence on the time to heat RAP are the particle diameter and the thermal diffusivity. The trends seen from varying each parameter are not surprising: as the size of the particle increases, the time required to heat it also increases. Also, as the thermal diffusivity or initial RAP temperature increases, the time needed to heat will decrease. The importance of this model lies is in the ability to determine which configuration of parameters results in a required heating time that is beyond what is currently achieved at most asphalt plants. While changing thermal diffusivity is not possible, knowing the effect of particle size on the amount of necessary heating time can also provide valuable insight on RAP crushing operations. However, having accurate values for thermal diffusivity would be beneficial. The results in Figure 4.7 (c) show the effects of initial RAP temperature on the amount of necessary heating time. These results can be used to implement RAP preheating systems, such as solar heating or recirculation of plant byproduct heat. Thus, there are several practical applications of the model developed in this work.

The variation in required heating time when more RAP is added can be seen in Figure 4.8. The upper-bound temperature will remain constant; however, as more RAP is added, there is less energy in the system from superheated aggregates, which increases the time needed to heat the RAP. Increasing the percentage of RAP beyond 40 percent brings the equation beyond the limits expressed in (10)

therefore, the drum temperature would need to be increased to stay within the applicable limits. Lack of such adjustments can deteriorate the quality of final mix.

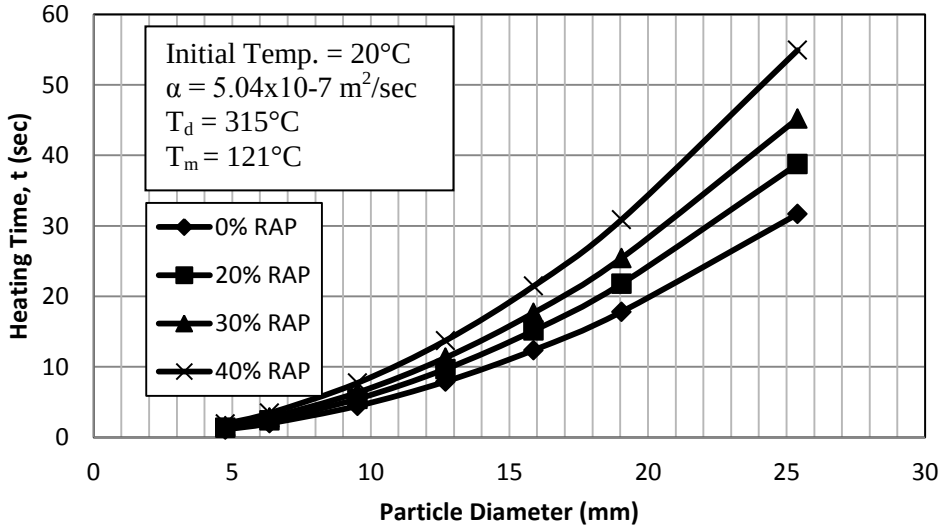

Figure 4.8 Heating Time at Lower Bound Temperatures

From the above figure, it can be seen the effects of increasing the percentage of RAP become more dramatic if the RAP contains larger particles. At small particle sizes, around 10mm, there is almost no change in the time required to heat the RAP. Conversely, if the RAP contains large particles, the heating time becomes unattainable for most plant configurations.

This model is intended to serve as a guideline for a quality control check for asphalt plants producing asphalt mixes with RAP. Since this model makes several assumptions to provide a simple equation for required time to heat RAP, there is some level of uncertainty in its ability to accurately predict internal temperatures. In the future, this model could be expanded to incorporate changes in moisture content of the RAP and account for a non-homogeneous external heating. The external heating being a constant temperature implies the particle is floating in air during the time it is passing through the mixing drum. It does not account for collisions between other particles and the drum wall, which would change the surrounding temperatures as a function of time and space. By use of a probabilistic approach, this model can be expanded to include the effects of both particle to particle contact and the heated air contained within the drum. The contribution from alternative aggregates, such as taconite tailings, may affect the particle-to-particle heat transfer inside the model.

4.4 Summary

The ability of an asphalt mixing drum to completely heat RAP particles is commonly based on empirical results. In order to further investigate the time needed to heat RAP, the heat transfer between RAP and superheated virgin aggregates was modeled using finite difference techniques. The finite difference model led to the derivation of a simple algebraic equation that can be used to predict the minimum time needed for any particle to reach a specified internal temperature, given the initial temperature, surrounding temperature, particle radius and material thermal properties. This model has significant practical applications, such as predicting preliminary estimates of allowable amount of RAP in the mix, developing strategies for RAP processing in terms of particle size, and exploring RAP pre-heating processes to facilitate the uniform mixing of RAP with virgin components of mix.

The model was used to predict the amount of time it takes a RAP particle within an asphalt drum to heat to an internal mixing temperature. When this model is used in conjunction with the energy conservation equation (9) and (14), the problem becomes bounded by the highest and lowest temperatures experienced by the RAP. Inputting the parameters from a specific asphalt mixing operation allows the user to compare the required heating time predicted from the model with the actual heating time allotted by the plant.

For the default inputs presented here, roughly twenty seconds of heating were required for the RAP to achieve an internal temperature of 150°C (300°F). However, it was demonstrated that changing the equation inputs could increase the heating time to as much as 1.2 minutes. Depending on the asphalt drum type and configuration, there could be an insufficient amount of time to fully incorporate the RAP into the mix. If this is the case, unheated RAP would result in effectively dry mixtures that could prematurely fail – causing an accelerated maintenance schedule and greater economic burden on agencies.

This model is intended to serve as a guideline for a quality control check for asphalt plants using RAP in their mix designs. Since this model makes several assumptions to provide a simple equation for required time to heat RAP, there is some level of uncertainty in its ability to accurately predict internal temperatures. The next step is expanding on the model findings by incorporating the effect the asphalt drum has on particle heating.

5.0 FINITE ELEMENT MODELING OF LABORATORY TESTING

The values for thermal conductivity measured in Chapter 3 are bulk thermal conductivities, that is, the thermal conductivity of a composite material consisting of aggregates and air. In order to obtain the individual material properties, back calculation with numerical modeling was employed. By modeling the experimental set-up, it was possible to vary the properties of the individual particles to replicate the results of the laboratory testing. Many finite element iterations were run using the data gathered from the experiments to extract the particle properties based on the global response of the system. This resulted in known material properties for the individual particles, rather than the bulk properties. Using the thermal conductivities of the individual particles, it was then possible to simulate spherical particles coated in layers of asphalt to obtain the thermal conductivity of the aged asphalt binder contained on the RAP.

5.1 Modelling the Parallel Plate Heating Experiment

Parallel-plate experiments were modeled as a way to back-calculate the individual particle properties from experimentation. Using ANSYS, a subsection of the parallel plate was created for thermal analysis. For the thermal analysis, it was assumed the particles between the parallel-plates were spherical and of uniform size and thermal properties. Taking advantage of thermal symmetry, only a subset of the particles contained between the parallel-plates. By taking a subset of the parallel-plates, it drastically improved the computational efficiency; however it imposes the assumption of steady-state heat transfer between the plates and neglect edge losses. Figure 5.1 shows the orientation of the subset of particles analyzed. For ease of viewing, the subset will be shown rotated as depicted by the Figure.

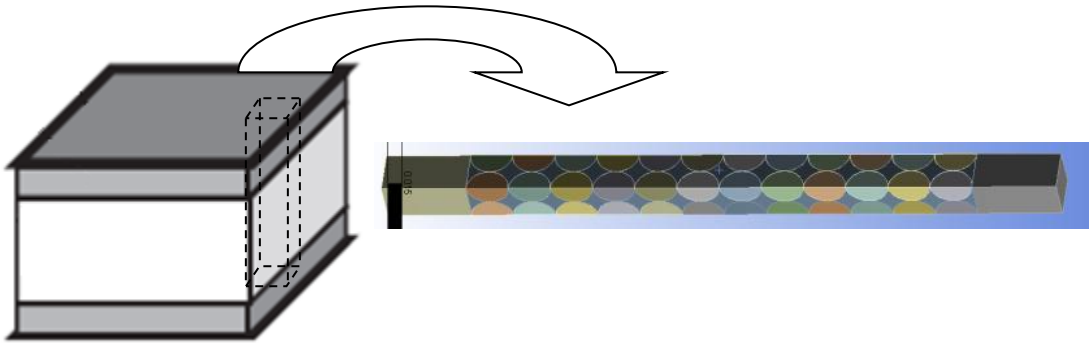

Figure 5.1 Parallel Plate Setup

The top and bottom of the model have been set to represent aluminum, and the space between the spheres is air. During the laboratory testing, reversing the hot side of the plates produced no change in thermal conductivity, which indicated there was no natural convection affecting the results of the testing. Because of this observation, no convection was modeled inside of the air void. The spheres are packed in simple cubic packing. Cubic packing of spheres is known to have 47.65% air voids, which is as close to the measured air voids of 52% from the laboratory testing [39]. Other regular spherical packings increase in density to 74.05%, which is well beyond what was achieved with the laboratory specimens. Below shows the three different diameters of particles modeled. The particle diameters represent three different sieve sizes that were tested in the lab, retained on the No. 8 sieve, retained on the No. 16 sieve, and passing the No. 16 sieve. The diameters chosen to represent each sieve size represent the average particle size of all particles retained on their respective sieve.

Table 5.1 Particle Diameters Simulated

	# 8	# 16	pass #16
Diameter (in)	0.125	0.075	0.025

5.2 Mesh Independence

The model was meshed with a progressively finer mesh in order to reach a state of mesh independence where there was no significant change in the model output. For simple geometries, like that of the aluminum plate, a hexahedral element was chosen, while more complex geometry required tetrahedral elements to mesh the curvature. Figure 5.2 shows an example of the finite element mesh chosen for the No. 8 sieve particles.

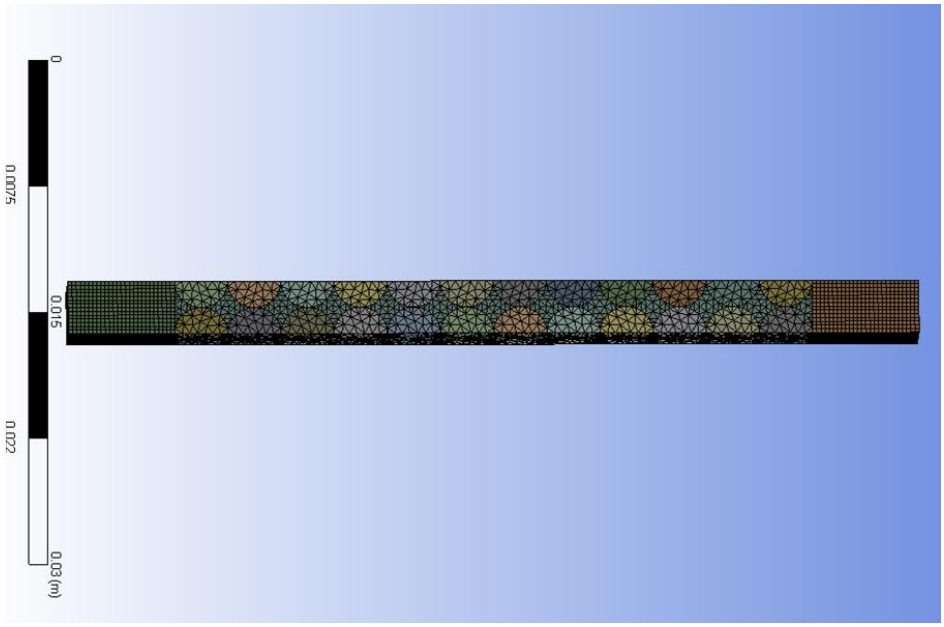

Figure 5.2 Finite Element Mesh

As shown in Figure 5.3, when the mesh was refined, the calculated effective thermal conductivity would change, implying that a state of mesh independence had not been reached. When a sufficient number of nodes was used, there was a negligible difference between results obtained. For the #8 sieve, this negligible difference was realized when a mesh with 200,000 nodes, was compared to a node density of 2.6 million nodes, shown in Figure 5.3. This implies a state of mesh independence has been reached at 200,000 nodes, or an element size of 0.015 inches. Thus the node size of 0.015 inches was maintained for the remainder of the simulations.

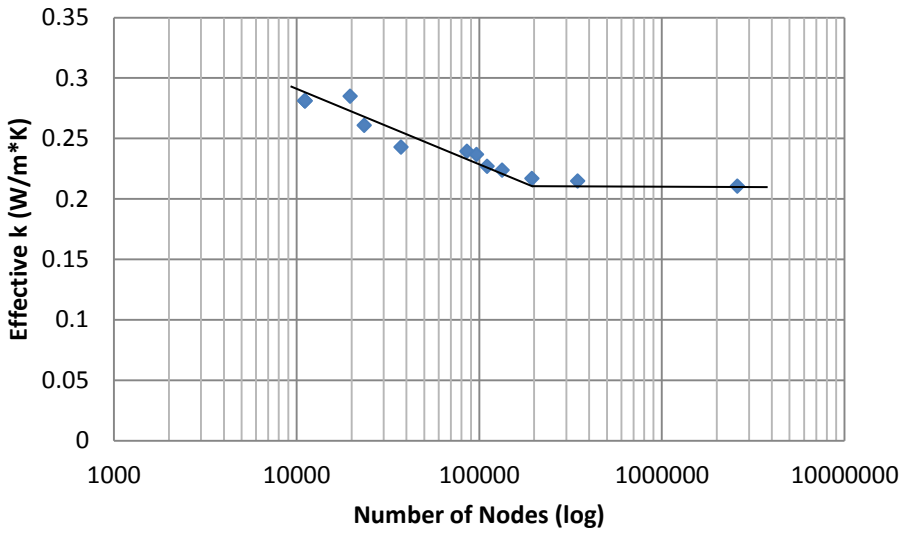

Figure 5.3 Mesh Independence Results

5.3 Simulation of Packed Bed Properties

For the simulations, the top and bottom of the model were set to a constant temperature, which was based on the measurements taken in the laboratory. The simulation was then run until steady state was achieved. At steady state, shown in Figure 5.4 for No. 8 aggregates, the temperature of the model is unchanging with respect to time.

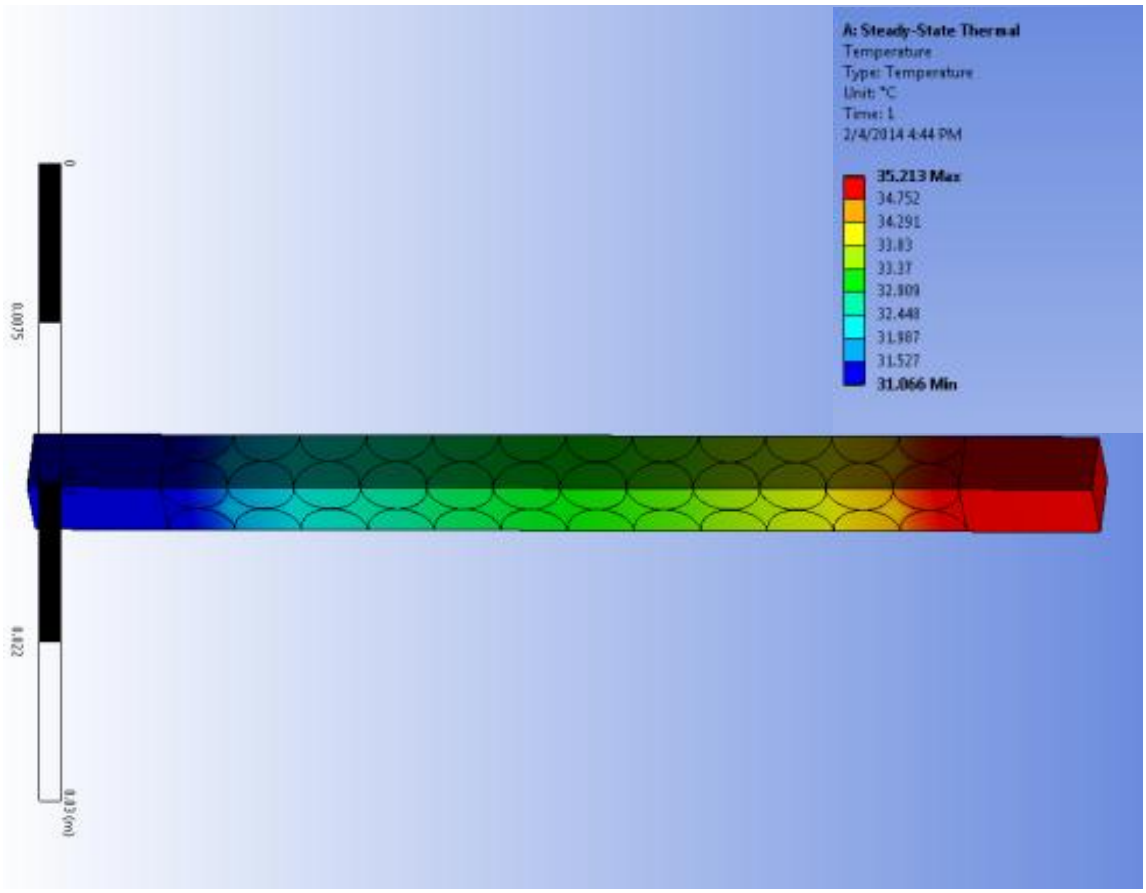

Figure 5.4 Temperature Distribution of the Model

Since the sides of the spheres are assumed adiabatic, due to thermal symmetry, the heat entering and exiting the system must be equal at steady state. Having an unequal flux in a steady-state thermal analysis would lead to an infinite amount of heat energy inside the system, since heat would be collecting inside the system. This state of constant heat flux is shown in Figure 5.5 for No. 8 sized aggregates.

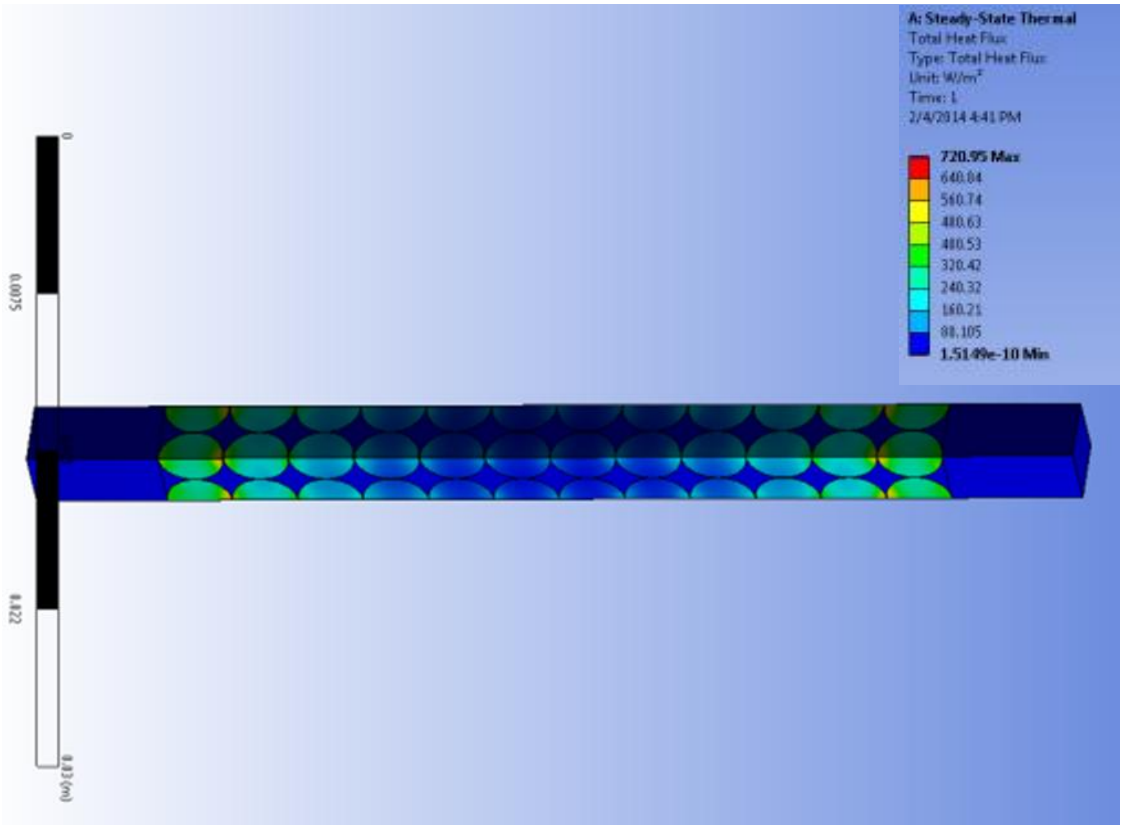

Figure 5.5 Total Heat Flux of the Model

The constant heat flux was then recorded and used in conjunction with the following equation to solve for the bulk thermal conductivity of the system, where q is the heat flux, L is the length between the ends of the plates, and delta T is the thermal gradient imposed on the simulation.

$$\frac{q \cdot L}{\Delta T} = k \qquad (2)$$

A trial and error approach was then employed to determine the thermal conductivity of the particles. Since the conductivity of the aluminum and air are known, and the global effective conductivity of the bulk material were measured, the individual particle conductivity can be varied until the simulated global conductivity matches the experimental conductivity. For example, Figure 5.6 shows the resulting effective, or bulk, conductivities obtained when the individual particle conductivity is varied. In this case, the effective conductivity measured in the laboratory was 0.22 W/m·K, which the ANSYS simulation was able to predict when the asphalt conductivity was set to 2.34 W/m·K.

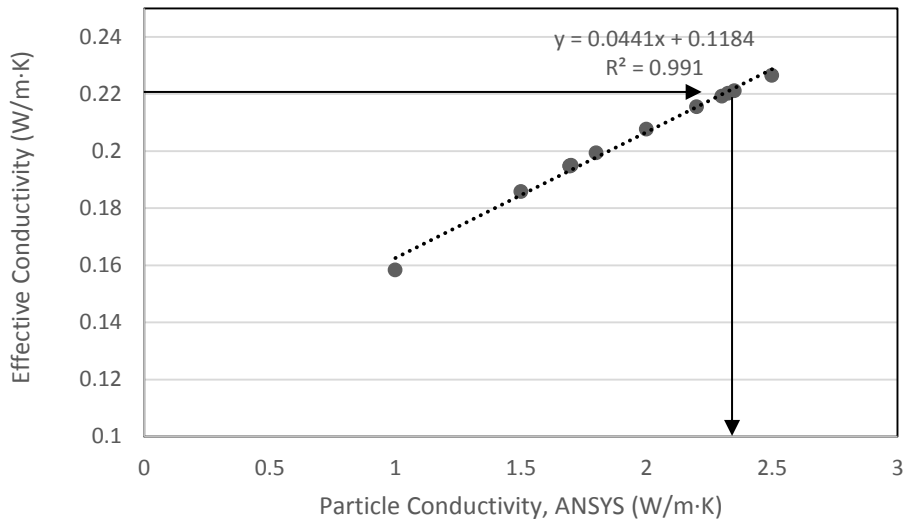

Figure 5.6 Homogeneous Asphalt Particle Thermal Conductivities

The same iterative process was employed to determine the individual conductivity of the RAP aggregates recovered from ignition oven, and pure taconite. This process was repeated for several different sieve sizes as well. Table 5.2 contains a summary of the particle conductivities back calculated using the above described methodology.

Table 5.2 Back Calculated Particle Conductivities (W/m·K)

	RAP	Aggregate	Taconite Tailings
#8	2.325	2.4704	2.6
#16	2.05	2.25	-
Pass #16	1.325	2.6	1.2

One source of error for this approximation may have come in the percentage of air voids present in the particles. As mentioned earlier, the assumption of a simple spherical lattice resulted in an air void distribution of 47.65%. Figure 5.7, shown below is the comparison of the calculated air void contents compared to the simulated 47.65% as represented by the horizontal black line.

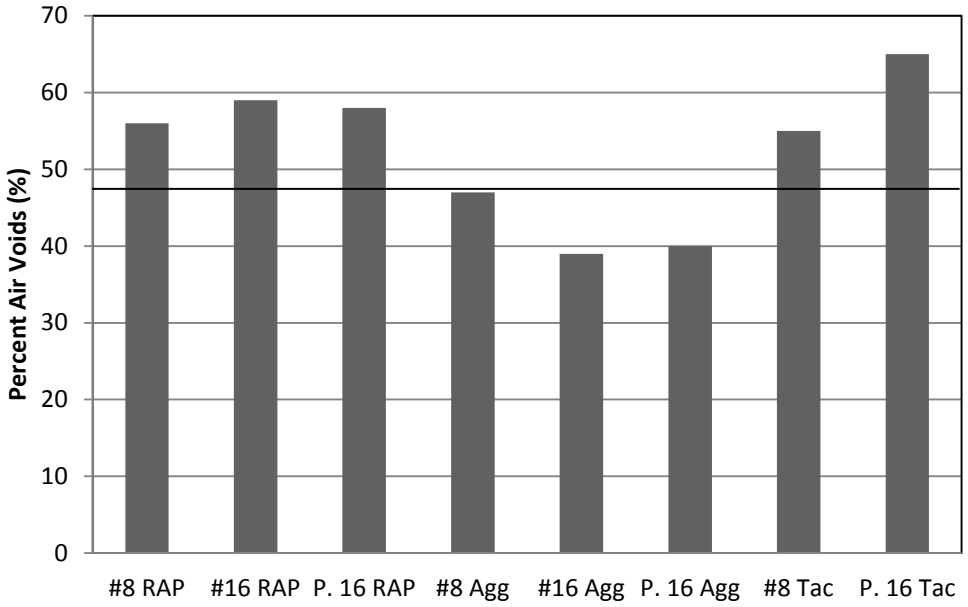

Figure 5.7 Air Voids of Particles Simulated

5.4 Simulation of Asphalt Binder Film Thickness

Knowing the thermal conductivity of a two-material composite and the thermal conductivity of one of the components, a separate simulation was run to determine the thermal conductivity of only the RAP layer surrounding the particles. For this simulation, it is necessary to assume an asphalt binder film thickness. A range of film thicknesses was chosen for the analysis, as measuring the film thickness was not possible. To better illustrate the objectives contained in this section, Figure 5.8 shows a schematic of the known conductivities and variables used in this phase of simulation.

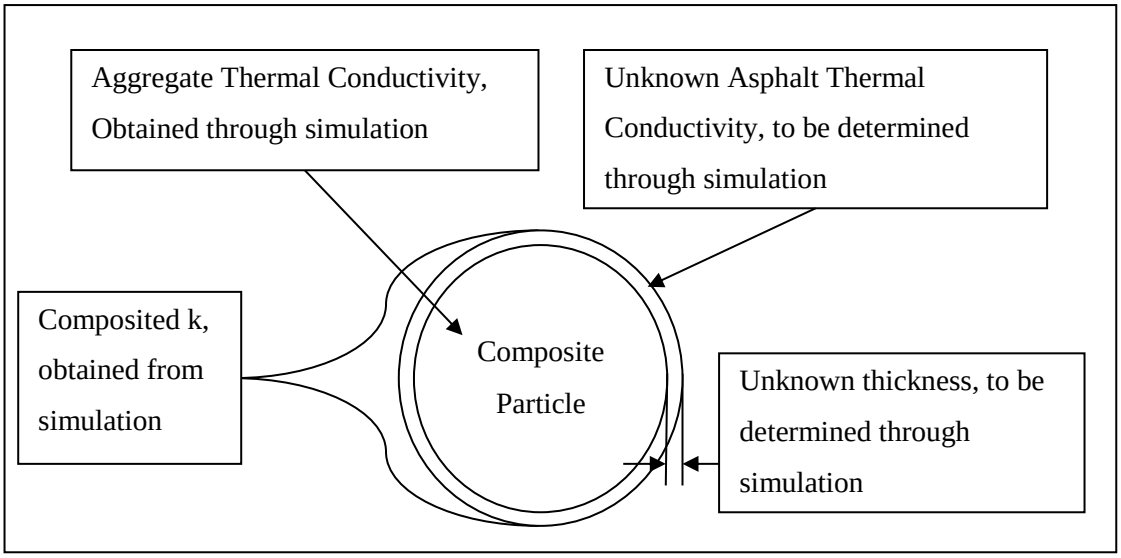

Figure 5.8 Schematic of Composite Sphere

A single sphere was used for this simulation, since it was not necessary to a bulk scenario as the individual particle thermal conductivities has been determined. Figure 5.9 shows the model used for the composite sphere analysis. The picture shown has a 10 micron coating of asphalt over a #8 sieve particle (.125" dia). Due to non-manifold geometry errors within ANSYS, it was necessary to take the single sphere, quadrisected it and rotate it so that the adiabatic edge of the solution boundary could be reproduced.

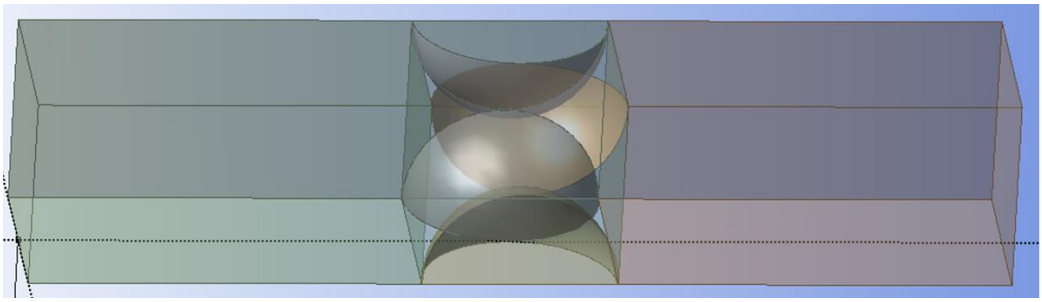

Figure 5.9 Composite Sphere Picture

The same method of back calculation of thermal conductivity that was used to determine the particle conductivities of the packed beds was employed to determine the conductivity of the asphalt layer in the case of the composite aggregate coated in asphalt binder. Since the film thickness was unknown, several different thicknesses, ranging from 5 microns to 15 microns were modeled. Working with one thickness at a time, the asphalt binder conductivity was varied to

produce the effective thermal conductivity of the RAP particles from section 5.3. A steady-state temperature profile is shown in Figure 5.10 for a particle with a 3.175 mm (0.125 inch) diameter and 10 micron (4.0×10^{-4} inch) film coating.

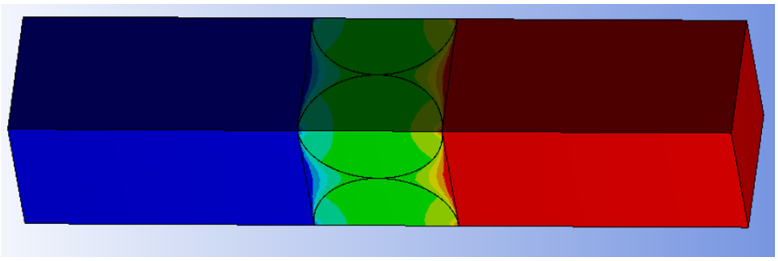

Figure 5.10 Composite Sphere Temperature Profile

Once the conductivity of the aged asphalt binder was found, the film thickness was changed and the determination process was repeated for the new binder thickness. An iterative process was used to determine if the asphalt binder layer thickness had a significant impact on the asphalt binder conductivity. This was done by simulating several different asphalt binder thicknesses and back-calculating the thermal conductivity of the layer for each thickness. Table 5.3 below contains the tabulated results for the different asphalt binder film thicknesses for RAP retained on the No. 8 sieve. It is worth reiterating, for the film thickness portion of this research, only the film thickness and binder conductivity were varied between tests and the aggregate and composite conductivities, which were determined through simulation, were held as constant.

Table 5.3 Simulated Binder Thermal Conductivities

Film thickness (in)	2.00×10^{-4}	3.00×10^{-4}	4.00×10^{-4}	5.00×10^{-4}	6.00×10^{-4}
Film thickness (microns)	5	8	10	12	15
Combined k (W/m·K)	2.47	2.47	2.47	2.47	2.47
Agg k (W/m·K)	2.325	2.325	2.325	2.325	2.325
Binder k (W/m·K)	0.12	0.13	0.17	0.2	0.24

A plot of the thermal conductivity of the asphalt binder, which was determined during the simulation was plotted against the different binder thicknesses. This plot can be seen in Figure 5.11. From section 3.9, the measured thermal conductivity of aged asphalt binder was 0.159 W/m·K and 0.175 W/m·K for virgin binder. Since the exact age of the binder contained in the RAP is unknown, and extimate of 0.168 W/m·K can be set as the target conductivity. Using the figure below, this conductivity corresponds to a binder thickness of approximately 10 microns.

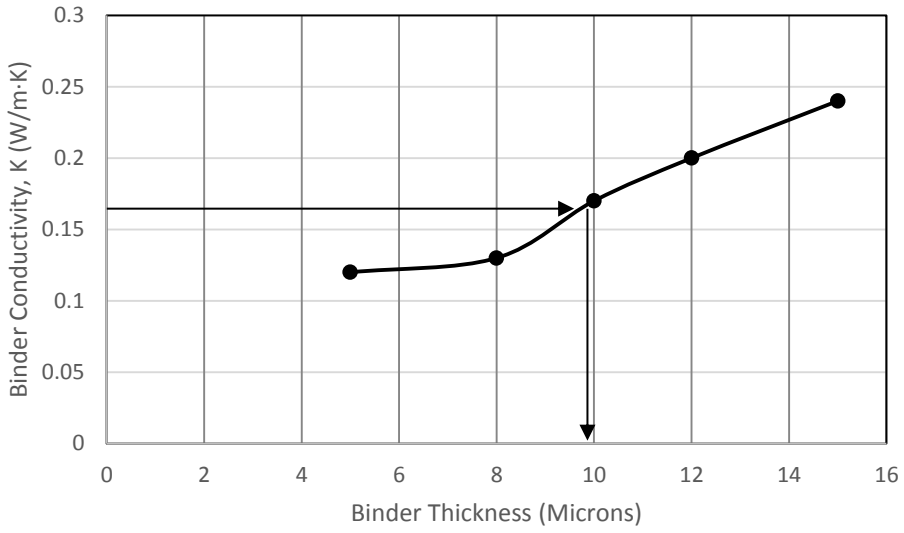

Figure 5.11 Binder Conductivity versus Thickness

Modeling of spheres of different diameters was also performed. The assumption of uniform film thickness was made for the remaining parts of this analysis, since this assumption is commonly made by departments of transportation (DOTs) as a part of their material specification process. Table 5.4 shows the resulting binder thermal conductivities predicted by the ANSYS simulation for different sized particles. For particles smaller than the No. 8 sieve, the binder thermal conductivity required to satisfy the combined composite thermal conductivity is much too small than a typical asphalt binder thermal conductivity.

Table 5.4 Binder Conductivities for Different Particles

	#8 Sieve	#16 Sieve	P. 16 Sieve
Film thickness (in)	4.00×10^{-4}	4.00×10^{-4}	4.00×10^{-4}
Film thickness (microns)	10	10	10
Combined k (W/m·K)	2.47	2.05	1.33
Aggregate k (W/m·K)	2.325	2.25	2.6
Binder k (W/m·K)	0.17	1.00×10^{-4}	1.00×10^{-6}

The aggregate thermal conductivities presented in Table 5.4 are higher than the corresponding combined composite thermal conductivity – which means the aggregates are more conductive than pure asphalt. Furthermore, asphalt binder is known to be less conductive than aggregates, so it is expected the combination of aggregate and binder would result in a conductivity less than the aggregate. However, the amount of binder required to lower the thermal

conductivity to the range measured in the laboratory is significantly higher than what a 10 micron film coating allows.

5.4.1 Verification with Generalized Self-Consistent Model

An analytical solution for a composite sphere surrounded by another sphere has been presented by Park et al. [40]. The paper presents a solution derived from the Generalized Self-Consistent Model (GSCM) and is shown in $k_{eff} = k_b \frac{2\ 1-f_{ba}\ +\ 1+2f_{ba}\ k_{ab}}{2+f_{ba}\ +\ 1-f_{ba}\ k_{ab}}$ (3), where the subscript b refers to the binder and a the aggregate.

$$k_{eff} = k_b \frac{2\ 1-f_{ba}\ +\ 1+2f_{ba}\ k_{ab}}{2+f_{ba}\ +\ 1-f_{ba}\ k_{ab}} \quad \textbf{(3)}$$

The thermal conductivity ratio, k_{ab} is defined as

$$k_{ab} = \frac{k_a}{k_b} \quad \textbf{(4)}$$

The volume fraction of fillers, f_{ba} is defined as follows, where V is the folume

$$f_{ba} = \frac{V_a}{V_b + V_a} \quad \textbf{(5)}$$

Using the GSCM, it is possible to calculate an effective thermal conductivity for concentric spherical particles, such is the case for aggregate coated in asphalt binder. For this application, the aggregate thermal conductivity and effective thermal conductivities presented in Table 5.4 were used. The averaged asphalt binder conductivity measured in Section 3.9 of 1.68 W/m·K was assumed to be the asphalt binder conductivity, and the film thickness was varied until the effective thermal conductivity, keff matched the combined effective thermal conductivity presented in Table 5.4. Table 5.5 presents the asphalt binder thicknesses required to satisfy the thermal conductivities presented. The thicknesses are close for the No. 8 and No. 16 sized particles, however for the smaller particles, the binder thickness implies almost 15% of the particle is asphalt binder in order to satisfy the thermal conductivities obtained.

Table 5.5 Binder Thicknesses Predicted by the GSCM

	#8	#16	<16
Binder Thickness (inches)	5.00×10^{-4}	5.10×10^{-4}	1.35×10^{-4}
fba, Volume Fraction (%)	98.80	97.97	84.66
Binder Thickness (Microns)	12.7	12.954	34.29

5.5 Summary

Based on the laboratory tests presented in Chapter 3, ANSYS simulations of the laboratory tests were presented. The goal of these simulations was to back calculate the individual particle thermal conductivities from the bulk thermal conductivity of a packed bed, which was measured directly. Once the individual particle conductivities were obtained, a second ANSYS simulation was performed on a single particle in order to determine the thickness of the asphalt film on the RAP particles. In addition to calculating the film thickness, the results of the single particle simulations allowed for a comparison of the homogenous PAV aged binder thermal conductivity presented in Section 3.9 to the RAP binder thermal conductivity.

From the simulations conducted in this chapter, a few conclusions can be reached. Using a model for the laboratory testing, the bulk thermal conductivities obtained from experimentation were successfully converted into a material property for the three types of specimens tested. Building on the simulated material properties, a method for determining asphalt binder film thickness was developed. This method consisted of simulating one sphere of aggregate coated with asphalt binder, then back calculating the thermal conductivity of the asphalt layer. The back calculated thermal conductivity of the asphalt binder was then used to estimate the asphalt binder thickness.

For large particles, the back calculated binder thickness was an acceptable thickness, however as smaller particles were tested, the asphalt binder thickness must increase, as shown by ANSYS simulation and with the GSCM. This finding contradicts conventional assumptions of a uniform binder thickness on aggregates.

6.0 FINITE ELEMENT ASPHALT DRUM MODELING

A simulation of an asphalt drum was created in ANSYS in order to gain insight into the heating times of RAP particles for field applications. In order to simplify the modeling, a single particle was modeled inside of an asphalt mixing drum. The simulated particle was subjected to a differential heating regime similar to what would be expected inside of an actual plant. The particle was placed inside of a cylinder, which represents the asphalt mixing drum. The inlet of the cylinder has a variable heat source at the inlet of the drum, rather than simulating a particle cascading through an entire cylinder. This type of simulation heats the particles as though they were moving through a drum mixer, except that it has the added benefit of allowing the particles to remain stationary for the simulation.

6.1 Model Set-Up

Thermal symmetry was employed to increase computational efficiency of the model. Since the flow inside the drum was assumed symmetric in the radial direction, the problem reduces to a two dimensional solution. For ease of modeling, a very thin 3-dimensional wedge-shaped section of the drum was chosen for the drum simulation. The drum was meshed with a combination of quadrilateral and triangular nodes. Areas far away from the particle discontinuity were exclusively quadrilateral nodes, while triangular nodes were employed closer to the particle. Figure 6.1 shows the meshed drum. 484,000 nodes and 267,000 elements make up the dense grid shown. Elements inside of the solid sphere have a mesh size of .01 inches, using tetrahedral elements, while elements that make up the drum employ hexahedral elements with a dimension of 0.05 inches. A residual convergence criterion of 10^{-6} was specified for all simulations conducted.

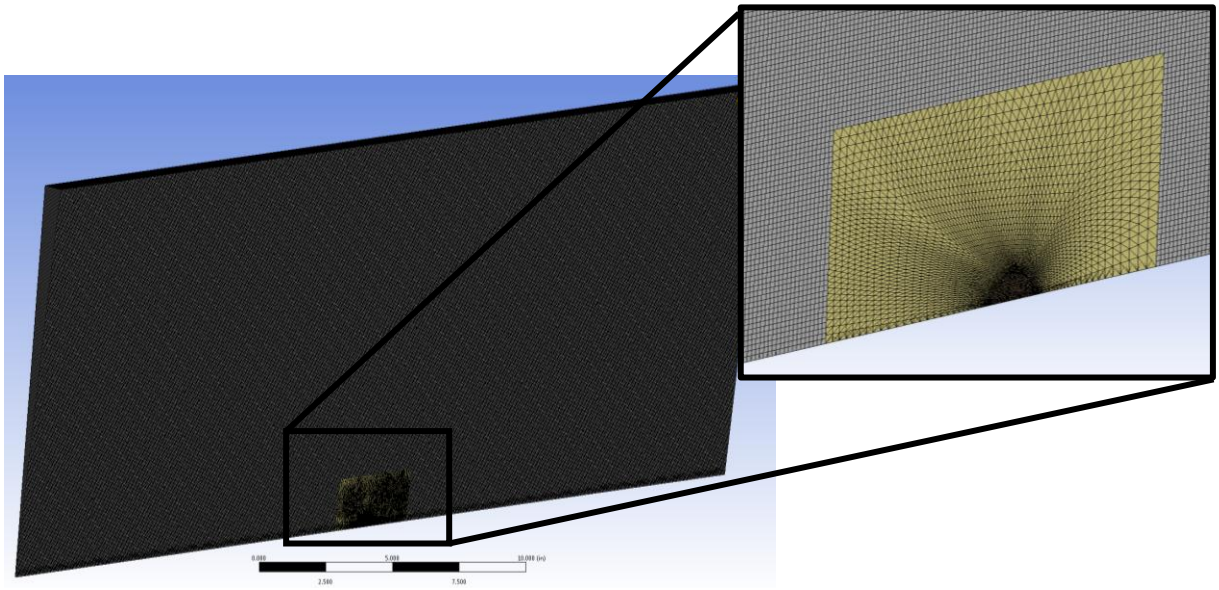

Figure 6.1 Meshed Drum Slice

6.2 Thermal Profiles

The inlet of the asphalt drum had an inlet velocity of 10 m/s, with a fully developed flow velocity profile. The sides of the wedge were thermal symmetry boundaries, meaning any heat or particles leaving one side of the drum was placed on the opposite face. The outlet of the drum was modeled an opening with zero gage pressure. Lastly, the top of the drum was an adiabatic wall. Care was taken to extend the domain of the drum long enough that edge effects from the domain would not affect the drum particle solution. Figure 6.2 shows the thermally defined drum. In the middle of the drum along the bottom edge is the particle of interest. Since the geometry is a wedge, the particle is represented as a half circle.

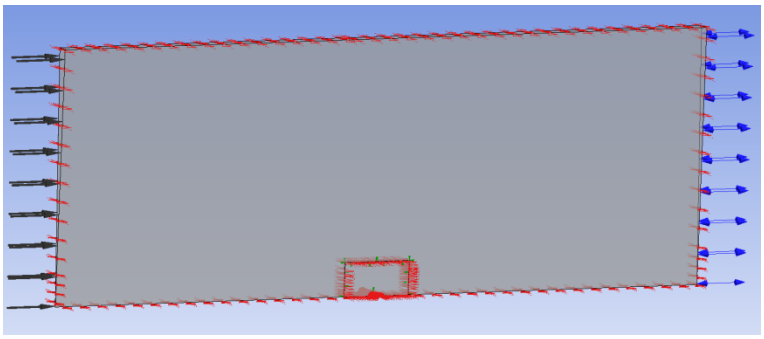

Figure 6.2 Thermally Defined Drum

The temperature of the inlet was set as a linear function of time. The simulation began with the particle at a uniform starting temperature surrounded by the drum at a given starting temperature. For all of the simulations presented, the particle started at a uniform 70°C. Based on findings from Section 4.3, the starting temperature has little effect on the heating time of a particle. A drum outlet temperature of 300°F was used for all simulations. The starting temperature of the drum was varied. A linear temperature profile was used for the inlet temperature, where the maximum temperature is entering at time t=0 and the exit temperature of 300°F was reached at the end of the simulation. Figure 6.3 is a screen shot taken during a drum simulation and is included to show how the drum temperature profile changes with respect to time. The right side of the drum is warmer than the left, while the particle is suspended in the middle along the bottom edge of the simulation domain.

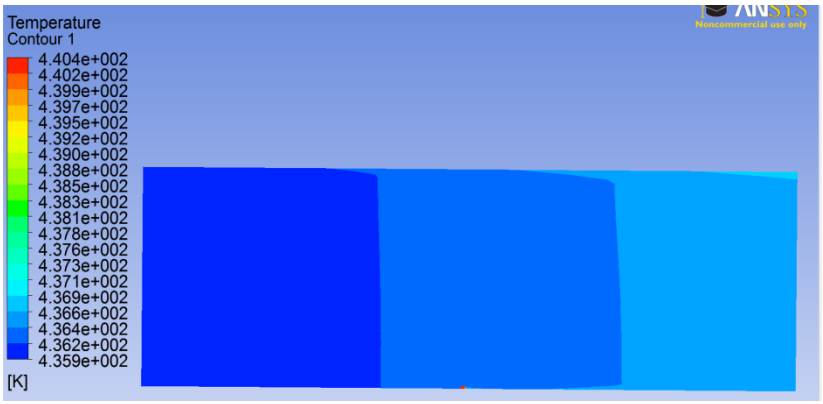

Figure 6.3 Drum Temperature Profile During Simulation

6.3 Explanation of Drum Simulations

The simulations run were for three different heating cases. Case 1 represents plain aggregates inside of the drum. For cases where only aggregates are heated, the starting temperature was set to 500°F. Case 2 is the case where homogenous RAP particles were inside the drum. A third case, Case 3, is for an aggregate particle coated with a 10 micron layer of asphalt. For both Case 2 and Case 3 the initial drum temperature was set to 400°F. Since RAP particles typically enter through a center collar, it is expected that the middle of the drum is cooler than the beginning where pure aggregates would be introduced. In total three different types of materials were simulated, RAP, Taconite and Limestone. Limestone was chosen to represent a generic aggregate that could serve as a contrast to the Taconite. The thermal properties for the three materials are shown in Table 6.1.

Table 6.1 Material Properties Used in Drum Simulation

	RAP	Taconite	Limestone
Density (kg/m^3)	2480	3240	2450
Thermal Conductivity, k (W/m·k)	2.475	3.3	1.3
Heat Capacity, c (J/kg·K)	920	800	908

The following screen shots of simulations are included to justify a state of mesh independence for the simulations, as well as to explain the phenomena taking place during the simulation. Figure 6.4 was taken during a simulation in which the particle has been partially heated by the hot interstitial gasses entering the drum from the left side. It can be seen that the front of the particle, where the air first reaches the particle has begun to heat, while the back of the particle lags behind in temperature. Also worth noting is the cool thermal trail which the particle leaves in the drum.

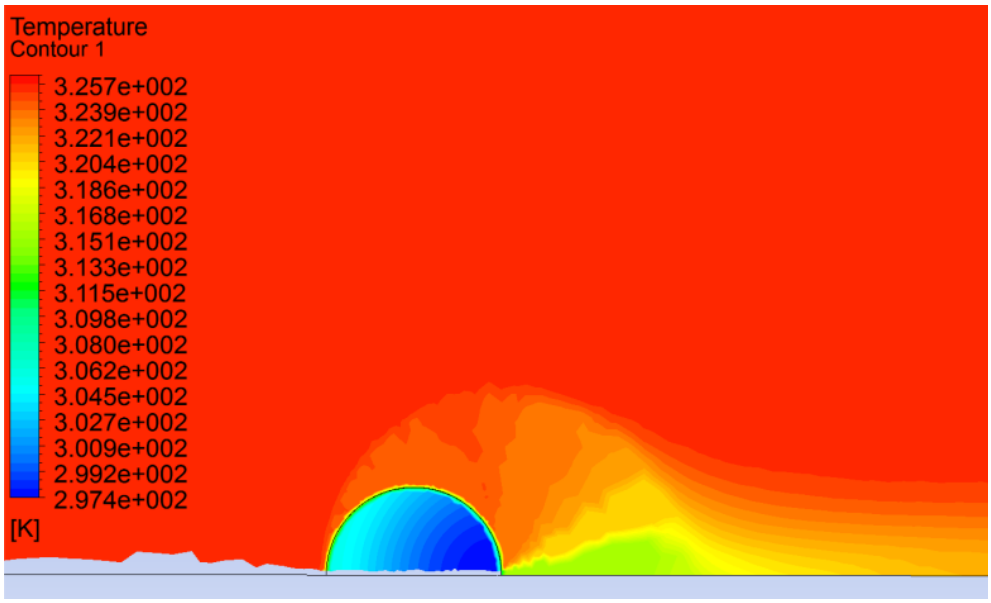

Figure 6.4 1 inch Particle Heating

The same particle is shown in Figure 6.5 with the mesh of the drum shown for illustration. Towards the obstruction in the flow space, an inflation layer was used to concentrate node points towards the particle. This allowed for subtle changes in the temperature and air velocity to be observed without looking pixelated. Lastly, towards the right side of the Figure, the mesh was transitioned into a hexahedral element type, since the mesh was far enough away from the discontinuity at this point to be inconsequential.

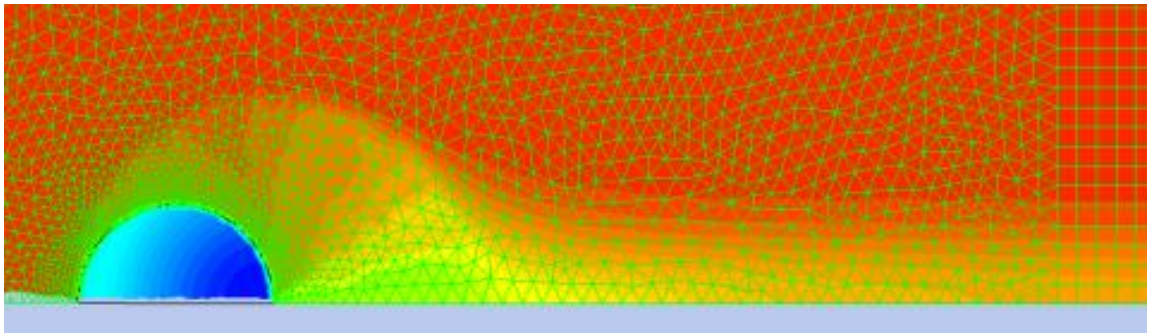

Figure 6.5 1 inch Particle with Drum Mesh Overlain

To observe the meshing of the particle, Figure 6.6 is included. The tetrahedral elements are of uniform size inside of the particle, as the particle was small enough relative to the rest of the model to warrant a densely packed grid. The contour lines seen in the middle of the particle pass through the middle of the elements with some smoothness, which is an indication of a mesh

independent solution, however towards the edge of the particle, some jagged contour lines are present.

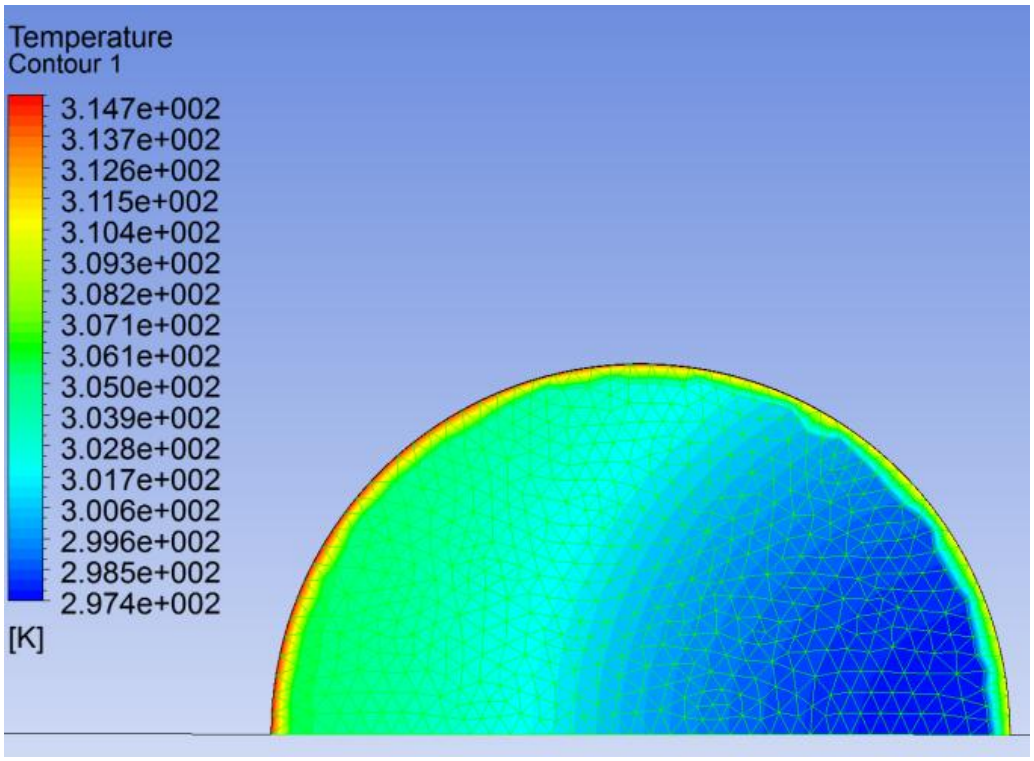

Figure 6.6 1 inch Particle Mesh (Legend Range: 314 K ~= 105°F – 297 K ~= 75°F)

Figure 6.7 is a time lapse of a particle heating inside of the drum over 15 seconds. At time t=0 seconds, the drum, shown in red, is considerably hotter than the aggregate particle. As time progresses in the simulation, the drum will cool – this represents the particle traveling through the asphalt mixing drum, where it is considerably hotter at the inlet than the outlet. Towards the end of the particles stay inside of the drum, it can be seen that the drum and the particle are close to the same temperature.

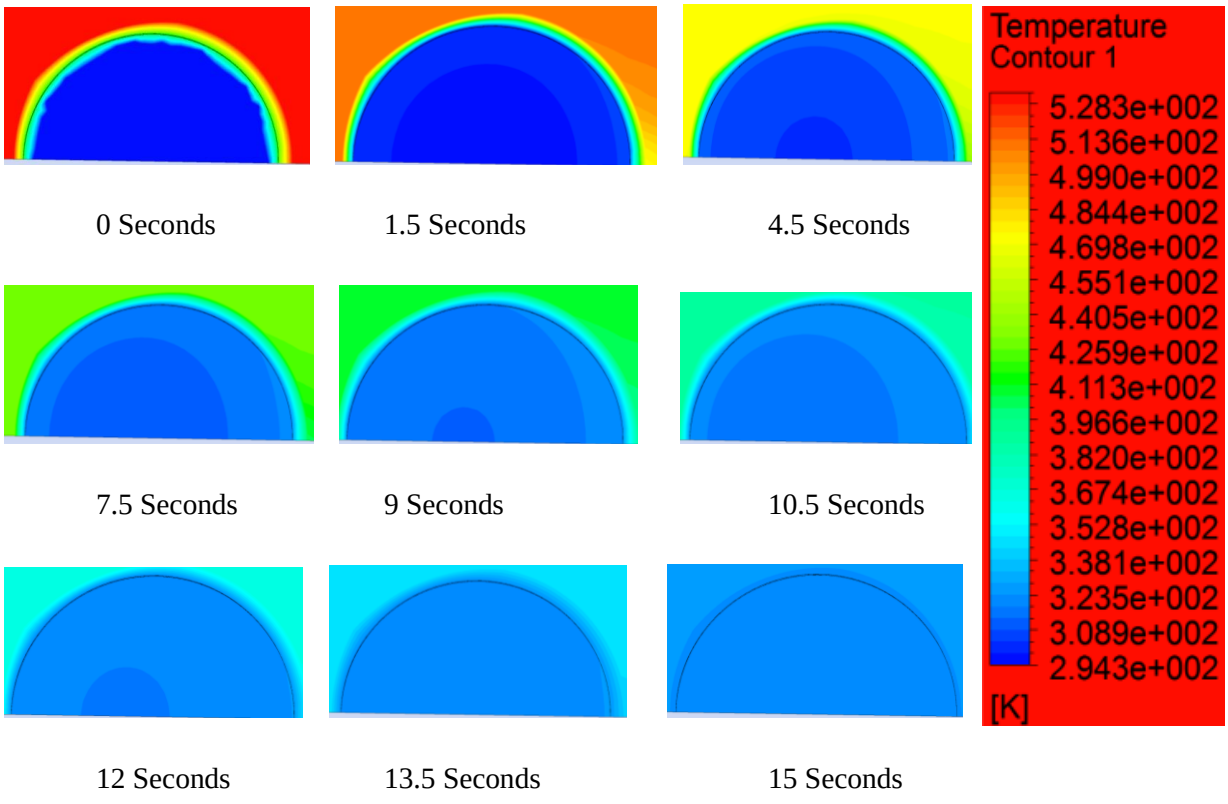

Figure 6.7 Time Lapse of 1/2 inch Particle Heating

In order to compare different simulations, two pieces of information were recorded at each time step, the maximum and minimum particle temperature. When looking at a detailed snapshot in time, as shown on the left of Figure 6.8, it becomes difficult to identify the maximum and minimum temperatures. To remedy this, the contour bins were expanded until the maximum and minimum temperatures could be read from the simulation, as shown on the right of Figure 6.8

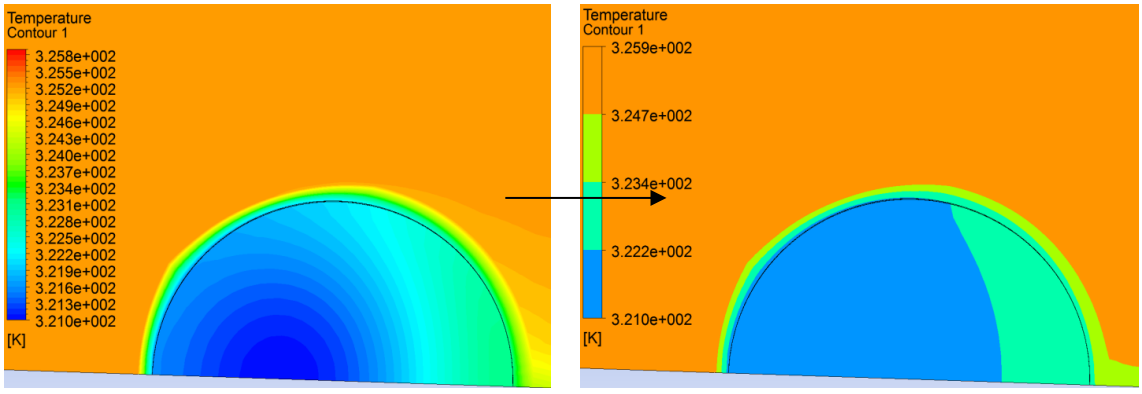

Figure 6.8 Condensing Simulation Data

For simulations with aggregate coated in asphalt, the asphalt layer is relatively thin compared to the rest of the particle. This size discrepancy is best shown in Figure 6.9. The two thin black lines on the right side of the Figure denote the asphalt layer.

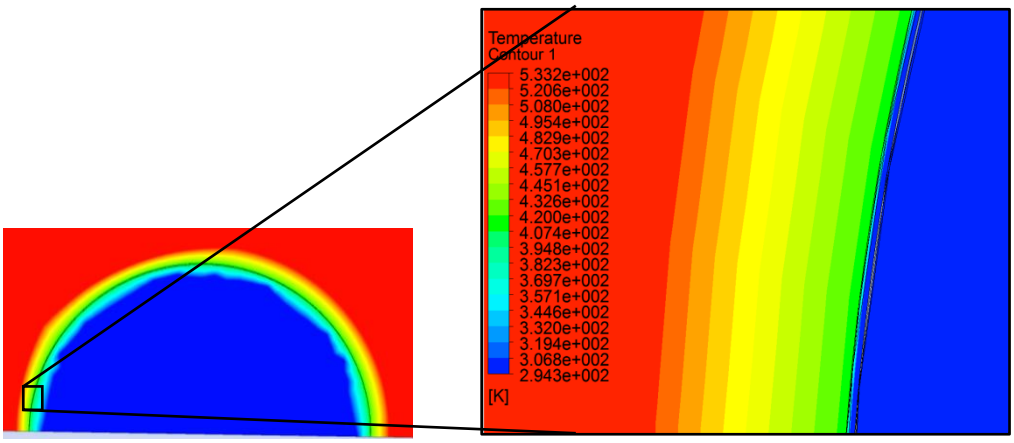

Figure 6.9 1/2 inch Aggregate with 10 Micron Asphalt Layer

For analysis of particles with asphalt coatings, it becomes difficult to decipher the differences in asphalt temperature and aggregate temperature, as shown in Figure 6.10. For identifying the temperatures these layers, a post-processing step of suppressing the vestigial layers became necessary. With the aggregate and drum components suppressed and only the asphalt layer remaining, identifying the temperature became possible.

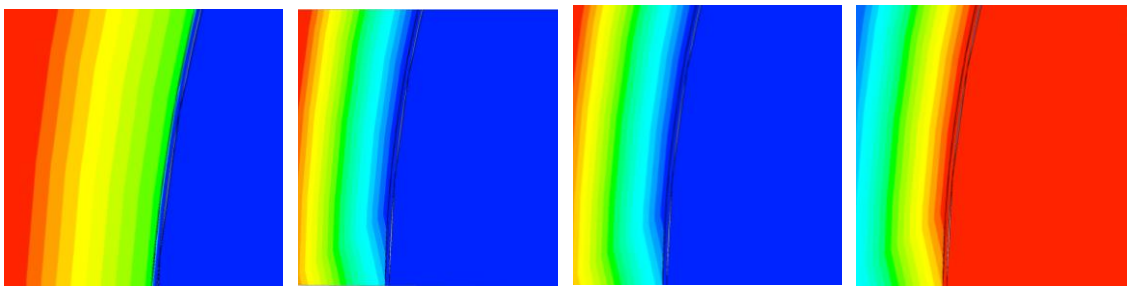

0 Seconds (70°F) 1 Second (208°F) 2 Seconds (327°F) 3 Seconds (332°F)

Figure 6.10 1/2 inch with 10 micron (Asphalt Film Temperature)

6.4 Results

Using the above techniques to process the data from the drum simulations, the minimum, or center, and maximum, or edge, temperatures at each time step were collected and assembled into the following graphs. The first sets of graphs represent the heating for pure aggregate particles. These particles were heated over 30 seconds, with a starting temperature of 500°F and a final temperature of 300°F. Figure 6.11shows the temperature at the center of the two particles. In both cases, after 30 seconds, the particles are heated to approximately 145°F.

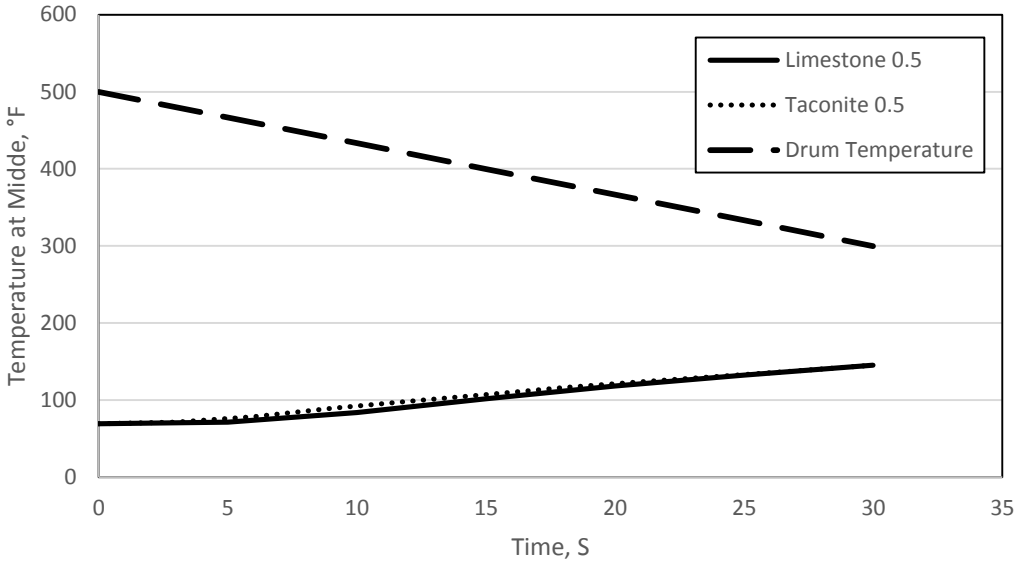

Figure 6.11 1/2 inch Aggregate Heating, Center Temperature Shown

One observable difference is in the edge temperatures of the particles. After 30 seconds, the limestone particle reaches a temperature of 174°F, 18°F hotter than the taconite. This result can be seen in Figure 6.12.

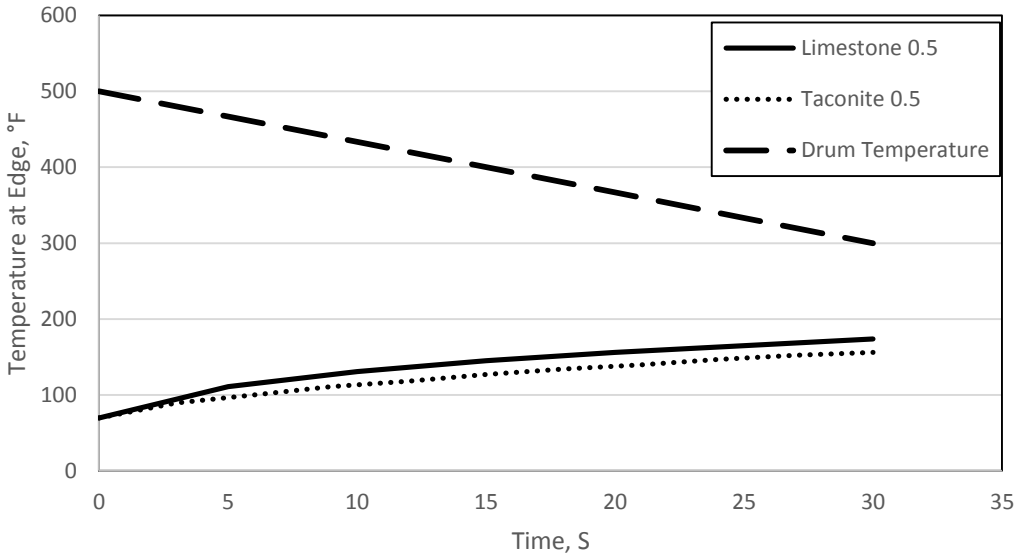

Figure 6.12 1/2 inch Aggregate Heating, Edge Temperature Shown

One observation from the 30 second heating of aggregates was that the drum was still much hotter than the aggregates at the conclusion of the heating time. For the next set of tests, the retention time was increased to 150 seconds. The same thermal constraints of a 500°F starting temperature with a 300°F outlet temperature were imposed. However, the rate at which the drum cools was changed since the length of the simulation has increased.

Figure 6.13 shows the results of the 150 second heating of the aggregates. Two different sizes of particle were simulated, one with a 0.25 inch diameter, and one with a 0.5 inch diameter. The drum temperature is also plotted for reference. Interestingly enough, after 100 seconds inside the drum, the 0.25 inch taconite particle surpasses the drum temperature, almost 30 seconds before the limestone particle does. This shows taconites ability to obtain heat faster than conventional aggregates.

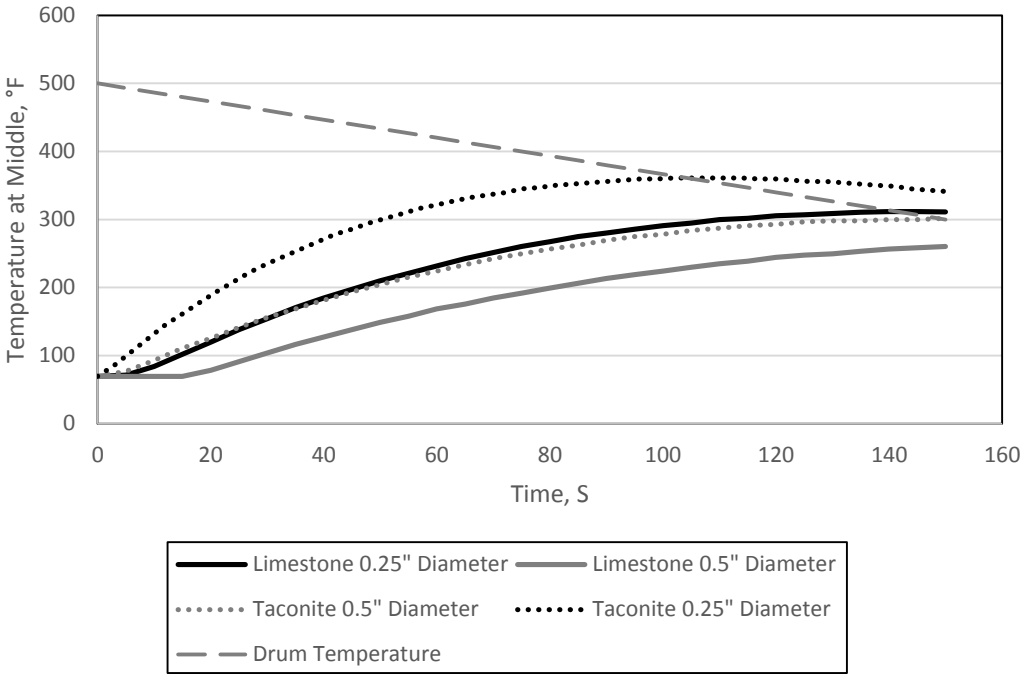

Figure 6.13 150 Second Aggregate Heating, Center Temperature Shown

Similar results for 150 second aggregate heating are presented in Figure 6.14. Again, taconites ability to heat faster than the limestone is showcased in this figure.

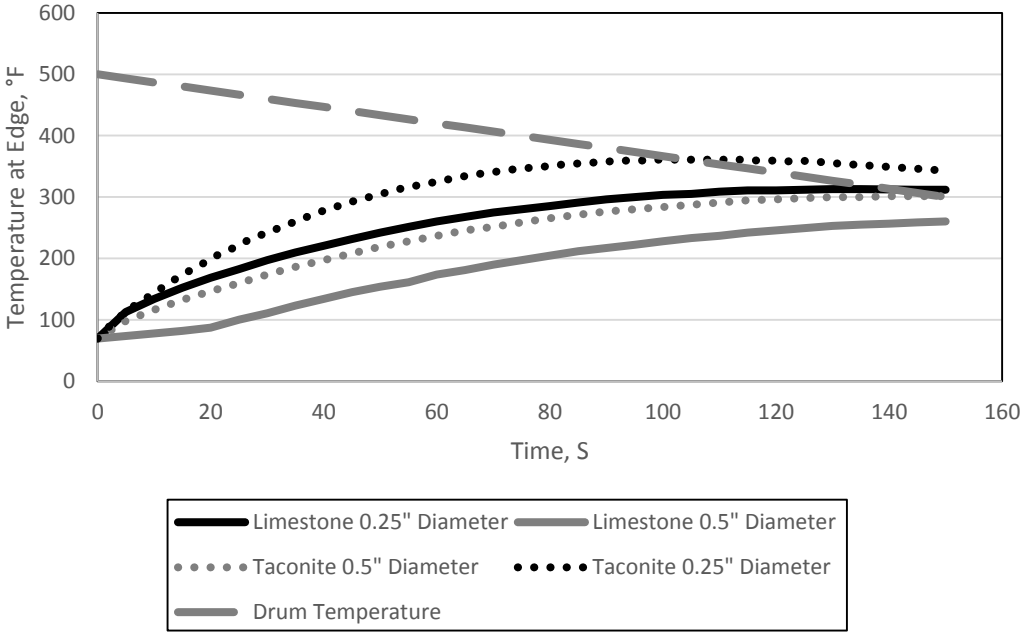

Figure 6.14 150 Second Aggregate Heating, Edge Temperature Shown

For the trials where RAP was simulated, an initial drum temperature of 400°F was used. Based on literature, RAP spends only a short amount of time inside of the asphalt drum, so the following simulations were carried out for 15 seconds, so explore the limits of drum heating on RAP. Figure 6.15 shows the middle temperatures of both 0.25 inch and 0.5 inch diameter particles of RAP being heated inside of a drum. After 15 seconds of heating, the 0.25 inch particle was 45°F hotter at its core than the larger particle.

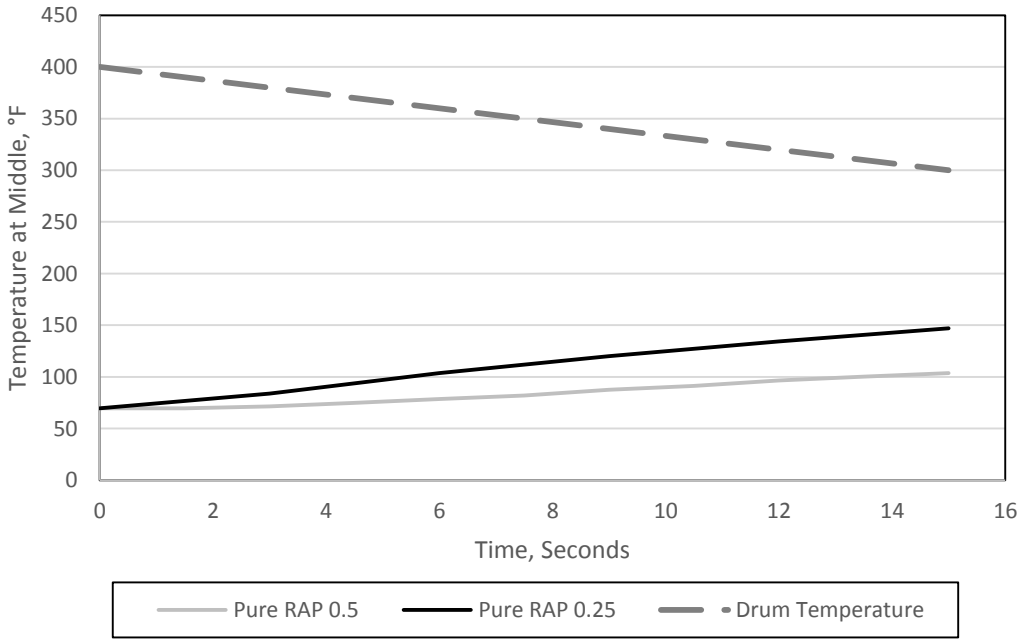

Figure 6.15 Homogenous RAP Heating, Center Temperature Shown

Figure 6.16 depicts the same two particles being heated, except the edge temperatures of the particles are shown. The difference in tempearture between the two particles is now 40°F.

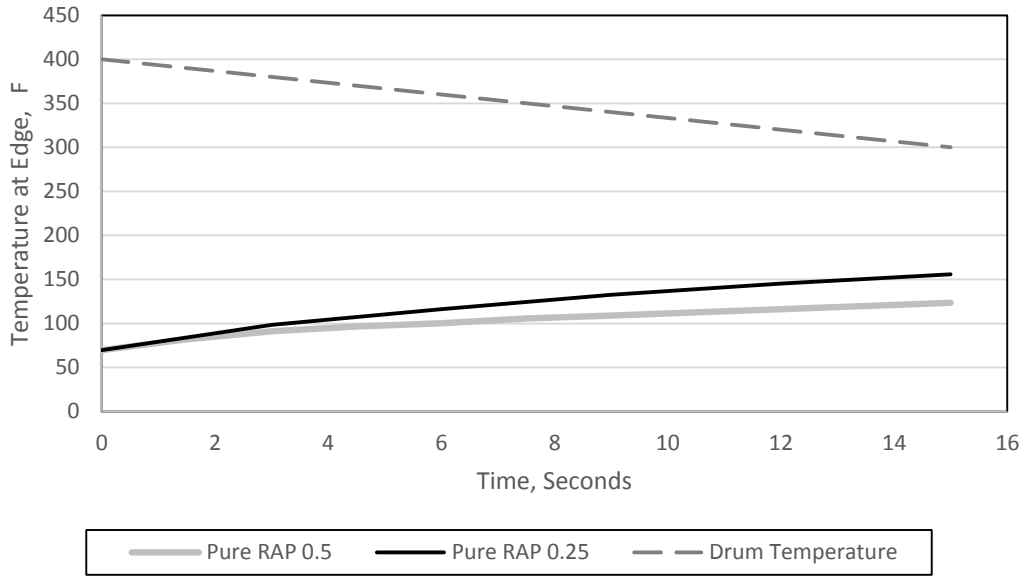

Figure 6.16 Homogenous RAP Heating, Edge Temperature Shown

Two different composite particles were also simulated using the virtual asphalt drum. One composite particle has a taconite aggregate, while the other has a limestone aggregate. For the composite particles, there was no difference in the temperature of the asphalt coating and the edge of the aggregate coating. Results of the half inch particle heating are shown in Figure 6.17. The taconite composite did heat faster than the limestone particle, however, the pure RAP particle was 9°F hotter than the taconite composite after 15 seconds.

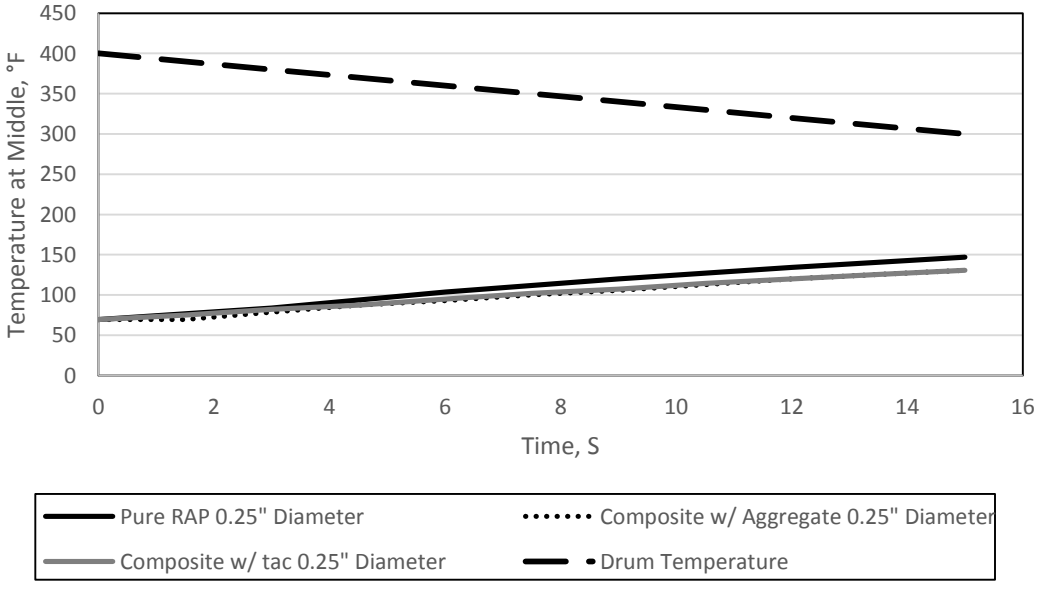

Figure 6.17 0.5 Inch RAP Heating, Center Temperature Shown

Figure 6.18 depicts the same three types of particles being heated as in the previous Figure, except the particle diameters are 0.25 inches instead of 0.5 inches. The same trend of the pure RAP particle being warmer was observed.

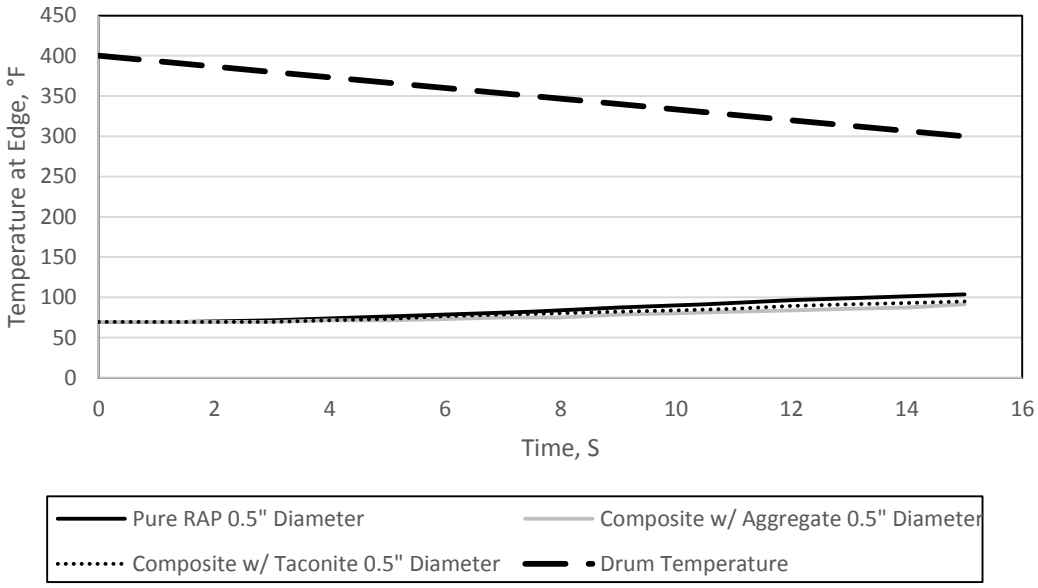

Figure 6.18 0.25 Inch RAP Heating, Center Temperature Shown

6.5 Comparison with Proposed Equation

In order to compare the results obtained using numerical simulation, the proposed equation from Chapter 4 was employed. For RAP, taconite and limestone particles that were simulated in ANSYS, the temperature at the center of each particle after 15 seconds was noted. Using the noted center temperature as the desired center temperature input for the equation, and the remaining inputs could be held constant. Then the time needed for a particle to reach the ANSYS particle temperature was predicted using the equation. For the comparison, a half inch particle diameter was chosen. One difference between the equation and the computer simulation involves a fixed drum temperature assumed with the equation, compared to a constantly decreasing drum temperature used in the simulation. To address this, the drum temperature used in the equation was the simulation drum temperature at 15 seconds. It is worth noting that this assumption provides a conservative prediction time for the equation. The thermal diffusivities used in the model were the same as the ANSYS material properties.

The time predicted by the equation had poor agreement with the ANSYS particles simulated heating times. Table 6.2 shows the results of the comparison of the two methods. The equation consistently under predicts the simulated heating times from the ANSYS simulation. One possible explanation from this under prediction is the differing assumptions used in the two cases. The equation assumes perfect thermal contact between the drum temperature and the particle, while the numerical simulation requires heat to be transmitted into the particle while hot gas passes over the particle. The convective process is not nearly as efficient as the perfect thermal contact assumed by the equation, therefore one would expect the equations predicted times to be less than the heating times simulated in ANSYS.

Table 6.2 Comparison of ANSYS Simulation with Equation Prediction

	RAP	Taconite	Limestone
Thermal Diffusivity (m^2/sec)	1.08×10^{-6}	1.27×10^{-6}	5.84×10^{-7}
Time Predicted with Equation (sec)	3.03	2.5	5.38
Time Simulated with ANSYS (sec)	15	15	15

6.6 Summary

Using ANSYS, a virtual asphalt mixing drum was created. Utilizing thermal symmetry, only a sub section of an entire drum was created. In order to reduce computational time, rather than passing a moving particle through a rotating drum the assumption was made that only the heating due to superheated interstitial would heat the particles inside the drum. With this assumption, it became possible to fix the drum and the particle inside the drum, but allow the inlet temperature of the drum to vary. This would mimic the range of temperatures the particle would experience inside of an actual drum, but save on computational time since mixing would not be simulated.

Three different types of analysis were performed, one on pure aggregates, a second on homogeneous reclaimed asphalt pavement (RAP) particles, and the third on aggregates coated in asphalt, which was referred to as a composite. All of the simulations had a linear drum temperature profile, which started at either 500°F for pure aggregates or 400°F for cases with asphalt. The outlet temperature for all simulations was fixed at 300°F.

The results of the aggregate heating showed that taconite possess more desirable thermal properties for asphalt pavement recycling than conventional aggregates. According to the literature, the heat contained in the aggregates contributes to the heating and melting of the

asphalt binder contained in RAP. Since the taconite becomes hotter faster, this aggregate would carry more heat to the RAP. A secondary benefit of the higher thermal conductivity of the taconite is that the heat contained in the aggregate will be transferred out of the aggregate faster than with traditional aggregates, which may improve the time needed to heat RAP.

Simulations with pure asphalt binder showed that smaller particles were heated faster than larger ones, but in both cases the particles failed to reach the recommended mixing temperature range within 10 seconds of entering the drum. Composite RAP particles with a taconite center were shown to heat faster than particles made of conventional aggregates; however the composite particle failed to heat as fast as a homogenous particle of RAP.

6.7 Recommendations

Although the drum simulation and the particle heating equation produced widely different heating times for the same particles, it is important to distinguish between the intended uses of the two proposed tools. Because of the ease and simplicity at which a rough estimate of heating time can be obtained, the equation serves as a quick method to check the required heating times of a particle fully surrounded by a single temperature. As shown by the comparison earlier in the chapter, the equation does not have good agreement with the ANSYS simulation. This lack of agreement is most likely attributed to the difference in assumptions as to which the simulation and equation were created.

One limitation to this research is that the drum configurations, retention times and temperature profiles were assumed. Future recommendations of this research are to work with industry partners to create simulations based on actual asphalt drum configurations. By modeling existing drum plants, it would be possible to validate the findings of this research.

7.0 Summary, Conclusions and Future Recommendations

It was the aim of this thesis to improve asphalt pavement recycling by producing a simulation that predicts the heating times of reclaimed asphalt pavement (RAP). Those simulations would then be used as a justification for the asphalt recycling process, rather than perpetuating the reliance on empirical trials. In order to properly model RAP, it was necessary to first calculate the thermal conductivity of the recycled material rather than relying on the assumption that thermal properties do not change when asphalt binder ages. The nature of the thermal conductivity testing made it necessary to back-calculate the individual particle thermal conductivities using finite element simulation.

A simple algebraic equation was derived in order to predict the amount of time needed to reheat particles of RAP inside of an asphalt mixing drum. This equation predicts the maximum and minimum retention time needed to ensure proper heating of particles, and will serve as an easy to use tool for asphalt plant operators producing mixtures with RAP.

Using the measured thermal parameters of RAP and aggregates, a drum simulation was created. The simulation modeled both homogenous particles and coated particles of RAP. The drum model developed is easily adaptable to any existing drum configuration, so that any plant with known geometries and operating temperatures can be simulated.

7.1 Summary

Based on a review of the literature, it is apparent that the thermal properties of aged asphalt binder are generally assumed to be the same as virgin asphalt binder. In Chapter 3, this assumption was tested using a simple one-directional laboratory heating set-up. The results of the laboratory testing showed that there is indeed a difference between the thermal conductivity of aged and virgin asphalt binder, but the magnitude of that difference is quite small.

In Chapter 4, a simple algebraic equation for the heating time of a single particle of reclaimed asphalt pavement (RAP), was derived. This equation is intended to be used as a design aid for asphalt producers, at it serves as a quick check to determine if sufficient heating times are available in a particular plant configuration. This equation was verified with both a Heisler-Gröber chart and finite element analysis. The equation was then validated with a surrogate of RAP (as it works for all spherical particles) and showed good agreement with the experimental methods presented, and it can be found in the appendix.

From laboratory tests, the bulk thermal conductivity of RAP, RAP aggregates recovered from the ignition oven, and taconite tailings were measured. These properties were used in the creation of a model that could back calculate the individual particle thermal conductivities, by recreating the experiments performed and using an iterative process to mimic the results of the laboratory testing. From the back calculation, it was possible to come up with thermal conductivities for RAP, and aggregates without the need to report a bulk value.

The material thermal conductivities were then used to simulate a composite RAP particle with aggregate in the middle and surrounded by asphalt. The film thickness of the particle could then be varied until the simulation results for composite aggregates matched the experiment results from laboratory testing. In doing this variation, it was found that the film thickness contained on larger RAP particles was approximately 10 microns. For smaller aggregates, this approach yielded erroneous results, which the author attributes to a fundamental difference in small RAP particles being conglomerates, of dust and binder, rather than a simple sphere coated in asphalt binder. These findings were supported by the GSCM model extended by Park, which directly calculates a thermal conductivity for concentric spheres based on the component thermal conductivity and the volume fraction of each sphere [40].

Next, a virtual asphalt mixing drum was created using ANSYS. Using the assumptions pioneered by Chen and Louge, in which particle contacts do not significantly contribute to heat transfer inside of a rotating drum [26]. Because of the relatively small contact time between the particles, a particle suspended in air was passed through the drum for this analysis. Based on literature of drum retention times for RAP, the drum simulations revealed an insufficient amount of heating time is present for melting RAP particles during recycling. This drum model can easily be tailored to represent almost any commercial drum, and would serve as a more accurate simulation than the algebraic equation presented in Chapter 4.

In addition to the findings of insufficient RAP heating, it was shown that taconite is a superior aggregate for asphalt recycling than conventional aggregates. The main explanation for taconites ability to transfer more heat than the other aggregates simulated is that the increased metal content produces a much higher thermal conductivity, which allows heat to enter the taconite particles faster, and then conduct the stored energy into the RAP more efficiently than other aggregates. Since it was shown that RAP has insufficient heating times, using taconite aggregate may provide additional heat for the melting of the RAP, which could increase recycled content of new asphalt mixes.

7.2 Conclusions

Based on the research presented, the following conclusions can be made:

- The thermal conductivity of RAP binder and virgin binder are different; however, the magnitude of the difference is within 5% different from each other.
- Bulk thermal conductivities of granular material were found to be statistically dependent on Air Voids, Aggregate Type, and Particle Size. There was an inverse relationship between conductivity and air voids, and a direct one with particle size. Taconite tailings were also shown to be more conductive than the other aggregates tested.
- An easy to use algebraic equation predicting the time required to heat any homogenous spherical particle was presented, verified and validated.
- Asphalt binder film thickness was shown to vary between particle sizes, and is not a constant as previously assumed.
- RAP particles cannot be fully reheated to a point where the binder can be mobilized inside of new asphalt mixes because there is not enough time spent inside of the asphalt drum for the particle to heat.
- Taconite aggregates may improve asphalt recycling, as were shown to heat faster than conventional aggregates. This thermal advantage may conduct more heat faster into RAP during mixing

7.3 Future Extensions

Several assumptions were made in the development of this work. Those assumptions could impact the accuracy of the results, and it is recommended that as an extension of this thesis to explore several key assumptions. The moisture content of particles was neglected in both the equation and simulation development. If a particle contains moisture, that moisture must first be driven off before heating beyond the boiling point of water can take place. Anecdotally, this moisture has a great impact on drum heating and it is recommended the effects of particle moisture on heating times be explored. The inclusion of particle contact within the asphalt drum could lead to shorter heating times due to the effects of conduction and convection heating particles. The flame inside of the asphalt drum is considerably hotter than the temperatures used in the simulations presented in this work. Depending on the drum configuration, the effect of radiant heating from the drums' internal combustion should be explored. Lastly, after the hot mix asphalt exits the drum it is stored inside of a heated silo for an undetermined period of time.

During heated storage, additional heat could become available to the particles, as well as other mechanisms such as diffusion of the RAP binder into the mix. Therefore, it is also recommend that the effects storage has on fresh HMA be explored.

Another future recommendation of this thesis is to extend the asphalt drum model by partnering with industry to take measurements from actual asphalt drums. Using field data, the drum model presented can be validated and improved.

8.0 REFERENCES:

1. Institute, T.A., *The Asphalt Handbook: Revised Edition*. Vol. Manual Series No. 4. 1960, College Park, Maryland: The Asphalt Institute.
2. Huang, Y.H., *Pavement Analysis and Design*. 1st ed. 1993, Engelwood Clifs, New Jersey: Prentice Hall.
3. ASTM, *ASTM D 6521 - 08 Standard Practice for Accelerated Aging of Asphalt Binder Using a Pressurized Aging Vessel (PAV)*, in *2008 Annual Book of ASTM Standards*. 2008, ASTM International: West Conshohocken, PA.
4. Ozer, H., et al. *Evaluation of RAP impact on hot-mix asphalt design and performance*. 2009. Minneapolis, MN, United States: Association of Asphalt Paving Technologist.
5. Ma, T., et al. *Estimating allowable RAP in asphalt mixes to meet target low temperature PG requirements*. 2010. Sacramento, CA, United States: Association of Asphalt Paving Technologist.
6. Widyatmoko, I., *Mechanistic-empirical mixture design for hot mix asphalt pavement recycling.* Construction and Building Materials, 2008. **22**(2): p. 77-87.
7. FHWA. *Hot-Mix Asphalt Recycling - Drum Plant*. Chapter 6. Construction Methods And Equipment 2011 July 24, 2012]; Available from: http://www.fhwa.dot.gov/pavement/recycling/98042/06.cfm.
8. Brock, J.D. and J.L. Richmond Sr., *Milling and Recycling*, I. ASTEC, Editor. 2007, ASTEC, INC: Chattanooga, TN.
9. O'Blenis, J.D., *Thermal properties of West Virginia highway materials*, in *Civil Engineering*. 1940, West Virginia University: Morgantown, West Virginia.
10. Highter, W.H. and D.J. Wall, *THERMAL PROPERTIES OF SOME ASPHALTIC CONCRETE MIXES.* Transportation Research Record, 1984: p. 38-45.
11. Mamlouk, M.S., et al., *Determination of thermal properties of asphalt mixtures.* Journal of Testing and Evaluation, 2005. **33**(2): p. 118-126.
12. Mallick, R.B., et al., *Practical method to understand the effect of aggregate drying on the moisture content of hot-mix asphalt.* Transportation Research Record, 2011(2208): p. 90-96.
13. Solaimanian, M. and P. Bolzan, *Analysis of the Integrated Model of Climatic Effects on Pavements*, S.H.R. Program, Editor. 1993, Strategic Highway Research Program: Washington, DC.
14. Tan, S.N., et al., *Determination of thermal properties of pavement materials and unbound aggregates by transient heat conduction.* Journal of Testing and Evaluation, 1997. **25**(1): p. 15-22.
15. Luca, J. and D. Mrawira, *New measurement of thermal properties of superpave asphalt concrete*. Journal of Materials in Civil Engineering, 2005. **17**(1): p. 72-79.
16. Qinwu, X. and M. Solaimanian, *Modeling temperature distribution and thermal property of asphalt concrete for laboratory testing applications.* Construction & Building Materials, 2010. **24**(4): p. 487-97.
17. Holman, J.P., *Heat Transfer*. 1972: McGraw-Hill Inc.
18. Vinson, T.S., V.C. Janoo, and R.C. Haas, *Low Temperature and Thermal Fatigue Cracking*. 1989: Washington,DC,USA.
19. Yoder, E.J. and M.W. Witczak, *Principles of Pavement Design*. 1975: John Wiley & Sons.
20. Mirza, M.W., *Temperature Equilibrium Study for the Development of Complex Modulus (E∗) Protocol*. 2002: Department of Civil and Environmental Engineering, Arizona State University.

21. Johnston, G.H., et al., *Engineering Characteristics of Frozen and Thawing Soils, Permafrost Engineering Design and Construction*. 1981: John Wiley & Sons.
22. Abraham, H., *Asphalts And Allied Substances*. 1920, D.Van Nostrand Company, INC. p. 1031-1032.
23. Henein, H., J.K. Brimacombe, and A.P. Watkinson, *Experimental Study of Transverse Bed Motion in Rotary Kilns.* Metallurgical Transactions B (Process Metallurgy), 1983. **14 B**(2): p. 191-205.
24. Ding, Y.L., et al., *Granular motion in rotating drums: bed turnover time and slumping-rolling transition.* Powder Technology, 2002. **124**(1-2): p. 18-27.
25. Mellmann, J., *The transverse motion of solids in rotating cylinders-forms of motion and transition behavior.* Powder Technology, 2001. **118**(3): p. 251-270.
26. Chen, X. and M. Louge, *Heat transfer enhancement in dense suspensions of agitated solids. Part I: Theory*. International Journal of Heat and Mass Transfer, 2008. **51**(21–22): p. 5108-5118.
27. Chaudhuri, B., F.J. Muzzio, and M.S. Tomassone, *Modeling of heat transfer in granular flow in rotating vessels.* Chemical Engineering Science, 2006. **61**(19): p. 6348-6360.
28. Lisboa, M.H., et al., *A study of particle motion in rotary dryer*. Brazilian Journal of Chemical Engineering, 2007. **24**(3): p. 365-374.
29. Carmichael, T., R.E. Boyer, and L.D. Hokanson, *Modeling Heater Techniques for In-Place Recycling of Asphalt Pavements.* AAPT, 1977. **46-47**: p. 526.
30. LeGuen, L., F. Huchet, and P. Tamagny, *Drying and Heating Modelling of Granular Flow: Application to the Mix-Asphalt Processes.* Journal of Applied Fluid Mechanics, 2011. **4**(2): p. 71-80.
31. Sparrow, E.M., et al., *Novel techniques for measurement of thermal conductivity of both highly and lowly conducting solid media.* International Journal of Heat and Mass Transfer, 2012. **55**(15–16): p. 4037-4042.
32. Sparrow, E.M., et al., *Novel techniques for measurement of thermal conductivity of both highly and lowly conducting solid media.* International Journal of Heat and Mass Transfer, 2012. **55**(15-16): p. 4037-42.
33. Jensen, B., Z. Liang, and A. Schenk, *Tar Sand Post-Processing: Computational simulation of light hydrocarbon removal from oil-bearing sands*, E. Sparrow and J. Gorman, Editors. 2013: University of Minnesota.
34. Lee, H. *ME 4310 Heat Transfer Notes*. 2006.
35. Miro, R., et al., *Evaluation of high modulus mixture behaviour with high reclaimed asphalt pavement (RAP) percentages for sustainable road construction.* Construction & Building Materials, 2011. **25**(10): p. 3854-62.
36. Stetler, L. ***Basic Rock Mechanics***. 2012; Available from: http://webpages.sdsmt.edu/~lstetler/merlot/rock_mechanics.htm.
37. Toolbox, E. *Solids - Specific Heats*. 2012 [cited 2012; Available from: http://www.engineeringtoolbox.com/specific-heat-solids-d_154.html.
38. Aqua-calc. *Concrete, Asphaltdensity in 209 measurement units*. 2012 [cited 2012; Available from: www.aqua-calc.com/page/density-table/substance/Concrete-coma-and-blank-Asphalt.
39. *Beals, M., L. Gross,* and *S. Harrell*. ***CELL AGGREGATION AND SPHERE PACKING***. **UTK Mathematical Life Sciences** 2000; Available from: http://www.tiem.utk.edu/~gross/bioed/webmodules/spherepacking.htm.
40. Park, Y.K., J.-K. Le[e], and J.-G. Kim, *A New Approach to Predict the Thermal Conductivity of Composites with Coated Spherical Fillers and Imperfect Interface.* Materials Transactions, 2008. **49**(4): p. 733-736.

41. Sheridan, P.S. and N.C. Shilton, *Determination of the thermal diffusivity of ground beef patties under infrared radiation oven-shelf cooking*. Journal of Food Engineering, 2002. **52**(1): p. 39-45.
42. Bernard, K., *USDA Revises Recommended Cooking Temperature for All Whole Cuts of Meat, Including Pork, to 145 °F*. 2011.

9.0 APPENDIX A: MODEL VALIDATION

Since the proposed model works for any spherical particle for which the thermal diffusivity is known, a surrogate for RAP particles was used to validate the model assumptions. An analogous scenario to heating of RAP inside of a mixing drum is heating of a meatball inside a fluid of constant temperature. Inside an asphalt drum, there are two heating mechanisms involved in RAP heating: the aggregate contact and the interstitial gasses inside the drum. Since aggregate contacts are constantly cascading, the contact between the particles account for a portion of the heat transferred to the RAP. However, the particles are constantly surrounded by heated gas (fluid) inside the drum, which was represented by the marinara sauce.

With published values of the thermal diffusivity of lean beef, the time required to heat the middle of spheres of beef to 71.1°C (160°F) can be calculated [41]. The desired middle temperature corresponds to the recommended USDA cooking temperature to ensure destruction of pathogens [42]. With the published range of thermal diffusivity for lean beef from 1.94×10^{-7} m^2/sec to 1.29×10^{-7} m^2/sec, an initial homogeneous temperature of room temperature, 20°C (68°F), and a fluid temperature of 87.8°C (190°F), the predicted heating times for changing particle diameters is shown below in Figure 9.1.

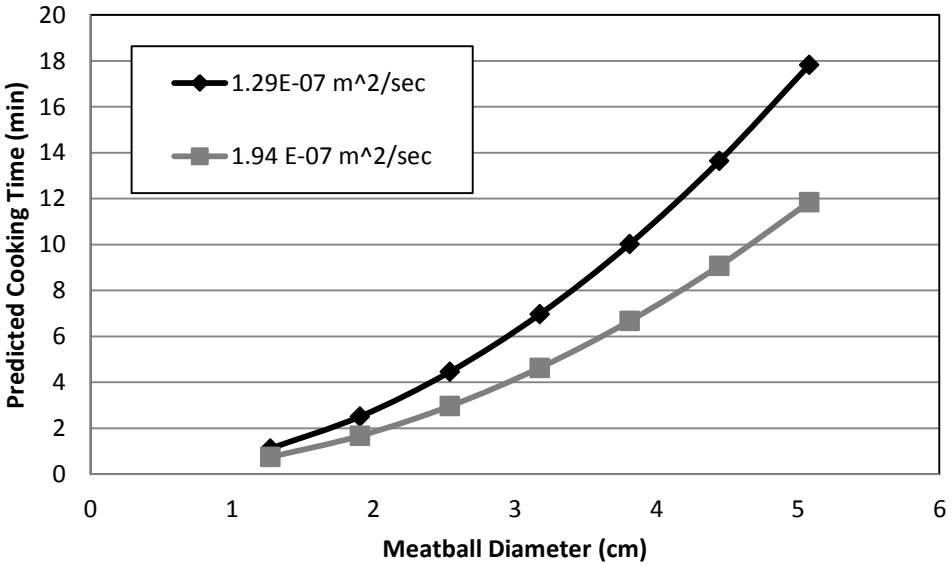

Figure 9.1 Predicted Meatball Heating Times

The experimental procedure consisted of first forming 3.81 cm (1.5 in) balls of lean beef which were conditioned at room temperature. A vessel of marinara sauce was brought to a boil,

and the temperature taken with a probe kitchen thermometer. Pictures of the experimental setup are shown below.

Figure 9.2 Experimental Set-up

One by one, the probe thermometer was inserted into a meatball then placed within the heated fluid. Temperature readings were taken at regular time intervals until the middle of the meatball reached the recommended cooking temperature. Figure 9.3 is a plot of the data obtained from the experiment. During Test 1, the probe came out of the meatball causing the spike in temperature around 1 minute. The probe was reinserted and readings commenced.

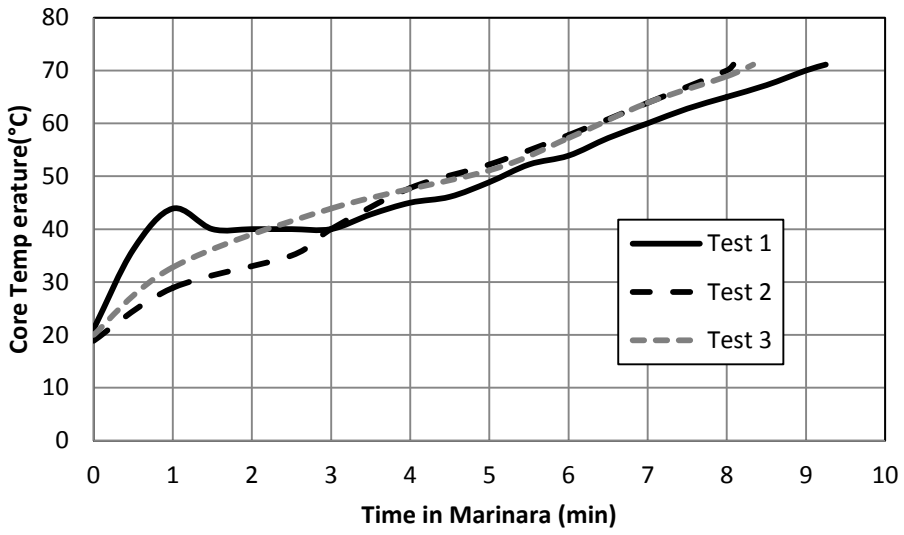

Figure 9.3 Experimental Results

From Figure 9.1 above, the expected cooking time of 3.81 cm (1.5 in) meatballs ranges from 6.67 to 10.02 minutes. As shown above, all of the meatballs tested fall well within this range, taking between 8.08 and 9.25 minutes to cook. Therefore, the proposed model predicted reasonably well a range of heating times for spherical particles of lean beef.

10.0 APPENDIX B: LABORATORY RAW DATA

Thermal Conductivity Data for Particles

Sample No.	Date	Sample Type	Sieve(s)	Weight (g)	Conductivity, k (w/m-C)
1	7/5/2013	RAP Aggregate (Loose, w/ binder)	Minus #16	2308	0.1700
1	7/8/2013	RAP Aggregate (Loose, w/ binder)	Minus #16	2308	0.2084
1	7/9/2013	RAP Aggregate (Loose, w/ binder)	Minus #16	2308	0.2197
1	7/10/2013	RAP Aggregate (Loose, w/ binder)	Minus #16	2308	0.2207
1	7/12/2013	RAP Aggregate (Loose, w/ binder)	Minus #16	2308	0.2182
2	7/14/2013	RAP Aggregate (Loose, w/ binder)	Minus #16	2182	0.1858
2	7/15/2013	RAP Aggregate (Loose, w/ binder)	Minus #16	2182	0.1718
3	7/16/2013	RAP Aggregate (Loose, w/ binder)	#16	2177.5	0.1846
3	7/17/2013	RAP Aggregate (Loose, w/ binder)	#16	2177.5	0.2227
3	7/17/2013	RAP Aggregate (Loose, w/ binder)	#16	2177.5	0.2119
4	7/18/2013	RAP Aggregate (Loose, w/ binder)	#16	2446	0.2463
5	7/25/2013	RAP Aggregate (Loose, w/ binder)	# 8	2484	0.2221
5	7/27/2013	RAP Aggregate (Loose, w/ binder)	# 8	2484	0.2232
5	7/27/2013	RAP Aggregate (Loose, w/ binder)	# 8	2484	0.2222
6	7/31/2013	RAP Aggregate (Loose, w/ binder)	3/8-#4	2609	0.2346
6	8/1/2013	RAP Aggregate (Loose, w/ binder)	3/8-#4	2609	0.2853
6	8/1/2013	RAP Aggregate (Loose, w/ binder)	3/8-#4	2609	0.2691
6	8/2/2013	RAP Aggregate (Loose, w/ binder)	3/8-#4	2609	0.2698
7	8/9/2013	Taconite	#200	3029	0.1756
7	8/12/2013	Taconite	#200	3029	0.1857
7	8/13/2013	Taconite	#200	3029	0.1903
8	8/28/2013	Taconite	#8	3236.5	0.2229
8	8/29/2013	Taconite	#8	3236.5	0.2373
8	8/30/2013	Taconite	#8	3236.5	0.2248

Sample No.	Date	Sample Type	Sieve(s)	Weight (g)	Conductivity, k (w/m-C)
9	9/5/2013	Rap Aggregate (From Ig. Oven)	#8 & #4	2991.5	0.2052
9	9/6/2013	Rap Aggregate (From Ig. Oven)	#8 & #4	2991.5	0.2260
9	9/10/2013	Rap Aggregate (From Ig. Oven)	#8 & #4	2991.5	0.2383
9	9/12/2013	Rap Aggregate (From Ig. Oven)	#8 & #4	2991.5	0.2304
10	10/1/2013	Rap Aggregate (From Ig. Oven)	Minus 16	3195	0.2569
10	10/4/2013	Rap Aggregate (From Ig. Oven)	Minus 16	3195	0.2620
10	10/8/2013	Rap Aggregate (From Ig. Oven)	Minus 16	3195	0.2690
10	10/10/2013	Rap Aggregate (From Ig. Oven)	Minus 16	3195	0.2757
11	10/15/2014	Rap Aggregate (From Ig. Oven)	#16	3349.5	0.2294
11	10/18/2014	Rap Aggregate (From Ig. Oven)	#16	3349.5	0.2315
11	10/23/2014	Rap Aggregate (From Ig. Oven)	#16	3349.5	0.2330
11	10/31/2014	Rap Aggregate (From Ig. Oven)	#16	3349.5	0.2293
12	11/6/2014	Rap Aggregate (From Ig. Oven)	#16-pan	3735.5	0.3279
12	11/8/2014	Rap Aggregate (From Ig. Oven)	#16-pan	3735.5	0.3201
12	11/12/2014	Rap Aggregate (From Ig. Oven)	#16-pan	3735.5	0.3388
12	11/15/2014	Rap Aggregate (From Ig. Oven)	#16-pan	3735.5	0.3325
13	12/4/2013	RAS	Unsieved	1923.5	0.1715
14	1/22/2014	RAS	Unsieved	1827	0.1452
14	1/23/2014	RAS	Unsieved	1827	0.1609
14	1/24/2014	RAS	Unsieved	1827	0.1529
15	1/25/2014	RAS	Unsieved	2081	0.1561
15	1/26/2014	RAS	Unsieved	2081	0.2183
15	1/30/2014	RAS	Unsieved	2081	0.1612
15	2/3/2014	RAS	Unsieved	2081	0.1683

Thermal Conductivity Data for Binder

Sample No.	Date	Sample Type	Sample thickness (m)	Conductivity, k (w/m-C)
1	8/14/2013	PG 58-28 Neat	0.037	0.1808
1	8/15/2013	PG 58-28 Neat	0.037	0.1779
1	8/16/2013	PG 58-28 Neat	0.037	0.1688
1	8/19/2013	PG 58-28 Neat	0.037	0.1734
2	9/12/2014	Oven Aged	0.0381	0.1950
2	9/17/2014	Oven Aged	0.0381	0.1935
2	9/18/2014	Oven Aged	0.0381	0.1936
2	9/20/2014	Oven Aged	0.0381	0.1929
3	2/13/2014	Oven Aged - PAV	0.0341	0.1549
3	2/14/2014	Oven Aged - PAV	0.0341	0.1517
3	2/18/2014	Oven Aged - PAV	0.0341	0.1583
3	2/21/2014	Oven Aged - PAV	0.0341	0.1643
3	2/24/2014	Oven Aged - PAV	0.0341	0.1541
3	2/27/2014	Oven Aged - PAV	0.0341	0.1566
3	3/4/2014	Oven Aged - PAV	0.0341	0.1550
3	3/5/2014	Oven Aged - PAV	0.0341	0.1588
3	3/6/2014	Oven Aged - PAV	0.0341	0.1586
3	3/7/2014	Oven Aged - PAV	0.0341	0.1620
3	3/10/2014	Oven Aged - PAV	0.0341	0.1615
3	3/11/2014	Oven Aged - PAV	0.0351	0.1670
3	3/12/2014	Oven Aged - PAV	0.0351	0.1679
3	3/14/2014	Oven Aged - PAV	0.0341	0.1580

G_{mm} Results for Particles

RAP Aggregate (Loose, w/ binder)				
Size	A Wair	E, W agg+H20	D, W empty	G_{mm}
-16	1000	5268.8	4,683.3	2.41
16	1000	5277.6	4683.3	2.46
8	1000	5292.1	4683.3	2.56
4	1000	5282.1	4683.3	2.49

Taconite				
Size	A Wair	E, W agg+H20	D, W empty	Gmm
200	1000	5007.4	4,263.00	3.91
#8	1500	7631.1	6594	3.24

Rap Aggregate (From Ig. Oven)				
Size	A Wair	E, W agg+H20	D, W empty	Gmm
#4 - #8	2000	7890.9	6,594.00	2.845
#16 - Pan	1000	7278.3	6,594.00	3.17

RAS				
Size	A Wair	E, W agg+H20	D, W empty	Gmm
RAS	1000	7054.3	6,594.00	1.85